

13

Compact Heat Exchangers— Recuperators and Regenerators

13.1	Introduction	13-2
13.2	Recuperator Heat Transfer and Pressure Drop Analysis	13-5
	Thermal Circuit • ϵ -NTU, P -NTU, and MTD Methods • The ϵ -NTU Method • The P -NTU Method • The MTD Method • Fin Efficiency and Extended Surface Efficiency • Pressure Drop Analysis	
13.3	Regenerator Heat Transfer and Pressure Drop Analysis	13-24
	ϵ -NTU ₀ Method for Heat Transfer • Pressure Drop	
13.4	Heat Transfer and Flow Friction Correlations—Single-Phase Flows	13-27
	Dimensionless Groups • Analytical Solutions • Experimental Correlations	
13.5	Heat Transfer and Pressure Drop Correlations—Two-Phase Flows	13-41
	Two-Phase Pressure Drop Correlations • Heat Transfer Correlations for Condensation • Heat Transfer Correlations for Boiling	
13.6	Exchanger Design Methodology	13-45
	Rating Problem for a Single-Phase Crossflow Plate-Fin Exchanger • Sizing Problem for a Single-Phase Crossflow Plate-Fin Exchangers • Rating and Sizing Problem for Condensers and Evaporators	
13.7	Flow Maldistribution	13-53
	Gross Flow Maldistribution • Passage-to-Passage Flow Maldistribution • Manifold-Induced Flow Maldistribution • Viscosity-Induced Flow Maldistribution	
13.8	Fouling in Heat Exchangers	13-59
	Fouling, Its Effect and Mechanisms • Importance of Fouling • Accounting of Fouling in Heat Exchangers • Influence of Operating and Design Variables • Fouling Control and Cleaning Techniques	
13.9	Concluding Remarks	13-64

Ramesh K. Shah

Subros Limited

13.10 Nomenclature.....	13-65
Subscripts	
References	13-68

13.1 Introduction

A heat exchanger is a device to transfer thermal energy (enthalpy) between two or more fluids, between a solid surface and a fluid, or between solid particulates and a fluid at different temperatures and in thermal contact without external heat and work interactions. The fluids may be single compounds or mixtures. Typical applications involve heating or cooling of a fluid stream of concern, evaporation or condensation of single or multicomponent fluid stream, and heat recovery or heat rejection from a system. In other applications, the objective may be to heat, cool, condense, vaporize, sterilize, pasteurize, fractionate, distill, concentrate, crystallize, or control process fluid. In some heat exchangers, the fluids transferring heat are in direct contact. In other heat exchangers, heat transfer between fluids takes place through a separating wall or into and out of a wall in a transient manner. In most heat exchangers, the fluids are separated by a heat transfer surface, and ideally they do not mix. Such exchangers are referred to as *direct transfer type* or simply *recuperators*. In contrast, exchangers in which there is an intermittent flow of heat from the hot to cold fluid—via heat storage and heat rejection through the exchanger surface or matrix—are referred to as *indirect transfer type* or *storage type exchangers*, or simply *regenerators*.¹

A heat exchanger consists of heat exchanging elements, such as a core or a matrix containing the heat transfer surface, and fluid distribution elements such as headers, manifolds, tanks, inlet, and outlet nozzles or pipes, or seals. Usually there are no moving parts in a heat exchanger; however, there are exceptions such as a rotary regenerator, in which the matrix is mechanically driven to rotate at some design speed.

The heat transfer surface is a surface of the exchanger core that is in direct contact with fluids and through which heat is transferred by conduction in a recuperator, and by heat storage and rejection in a regenerator. The portion of the surface which also separates the fluids in a recuperator is referred to as *primary* or *direct surface*. To increase heat transfer area, appendages known as fins may be intimately connected to the primary surface to provide *extended*, *secondary*, or *indirect surface*. Thus, the addition of fins reduces the thermal resistance on that fluid side and thereby increases the net heat transfer from the surface for the same temperature difference. Note that in a regenerator, all heat transfer surface acts as a primary surface.

Heat exchangers may be classified according to transfer process, construction, flow arrangement, surface compactness, number of fluids, and heat transfer mechanisms as shown in Figure 13.1 (Shah 1981; Shah and Muller 1988) or according to the process function as shown in Figure 13.2 (Shah and Muller 1988). Further general description of heat exchangers is provided by Walker (1990); Saunders (1988), and Hewitt (1989).

A gas-to-fluid heat exchanger is referred to as compact heat exchanger if it incorporates heat transfer surface having a surface area density above about $700 \text{ m}^2/\text{m}^3$ ($213 \text{ ft}^2/\text{ft}^3$) or a hydraulic diameter $D_h \leq 6 \text{ mm}$ (0.25 in.) on at least one of the fluid sides that usually has gas flow. It is referred to as a laminar flow (or meso) heat exchanger if the surface area density is above about $3000 \text{ m}^2/\text{m}^3$ ($914 \text{ ft}^2/\text{ft}^3$) or $100 \mu\text{m} \leq D_h \leq 1 \text{ mm}$, and as a micro heat exchanger if the surface area density is above about $15,000 \text{ m}^2/\text{m}^3$ ($4570 \text{ ft}^2/\text{ft}^3$) or $1 \mu\text{m} \leq D_h \leq 100 \mu\text{m}$. A liquid/two-phase heat exchanger is referred to as compact heat exchanger if the surface area density on anyone fluid side is above about $400 \text{ m}^2/\text{m}^3$ ($122 \text{ ft}^2/\text{ft}^3$). A typical process industry shell-and-tube exchanger has a surface area density

¹In vehicular gas turbines, a stationary heat exchanger is usually referred to as a recuperator, and a rotating heat exchanger as a regenerator. However, in industrial gas turbines, by long tradition and from a thermodynamic sense, a stationary heat exchanger is generally referred to as a regenerator. Hence, a gas turbine regenerator could be either a recuperator or a regenerator in a strict sense depending on the application.

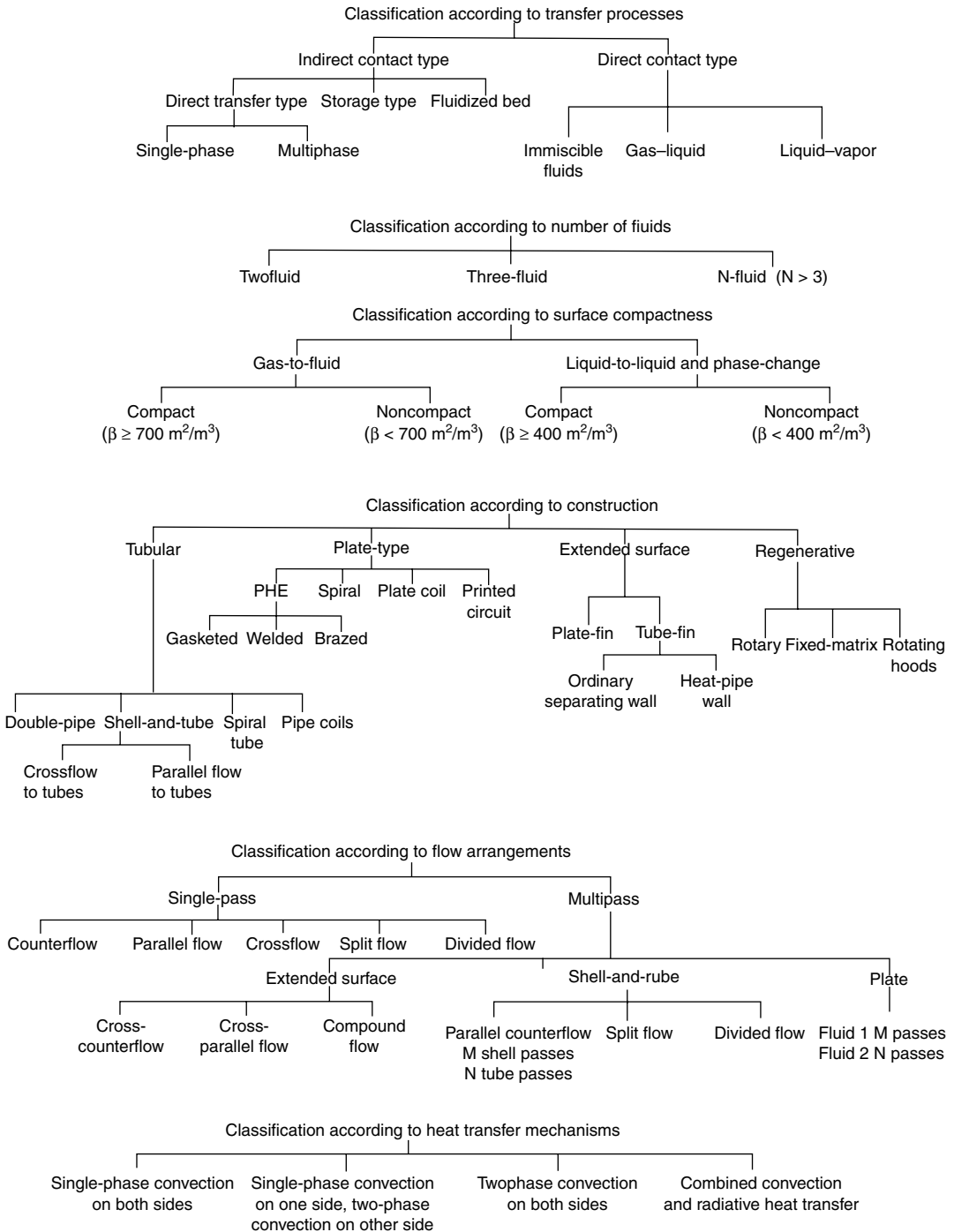


FIGURE 13.1 General classification of heat exchangers. (Modified from Shah, R. K. and Muller, A. C., *Ullmann's Encyclopedia of Industrial Chemistry, Unit Operations II, Vol. B3*. VCH Publishers, Weinheim, Germany, Chap. 2, 1988.)

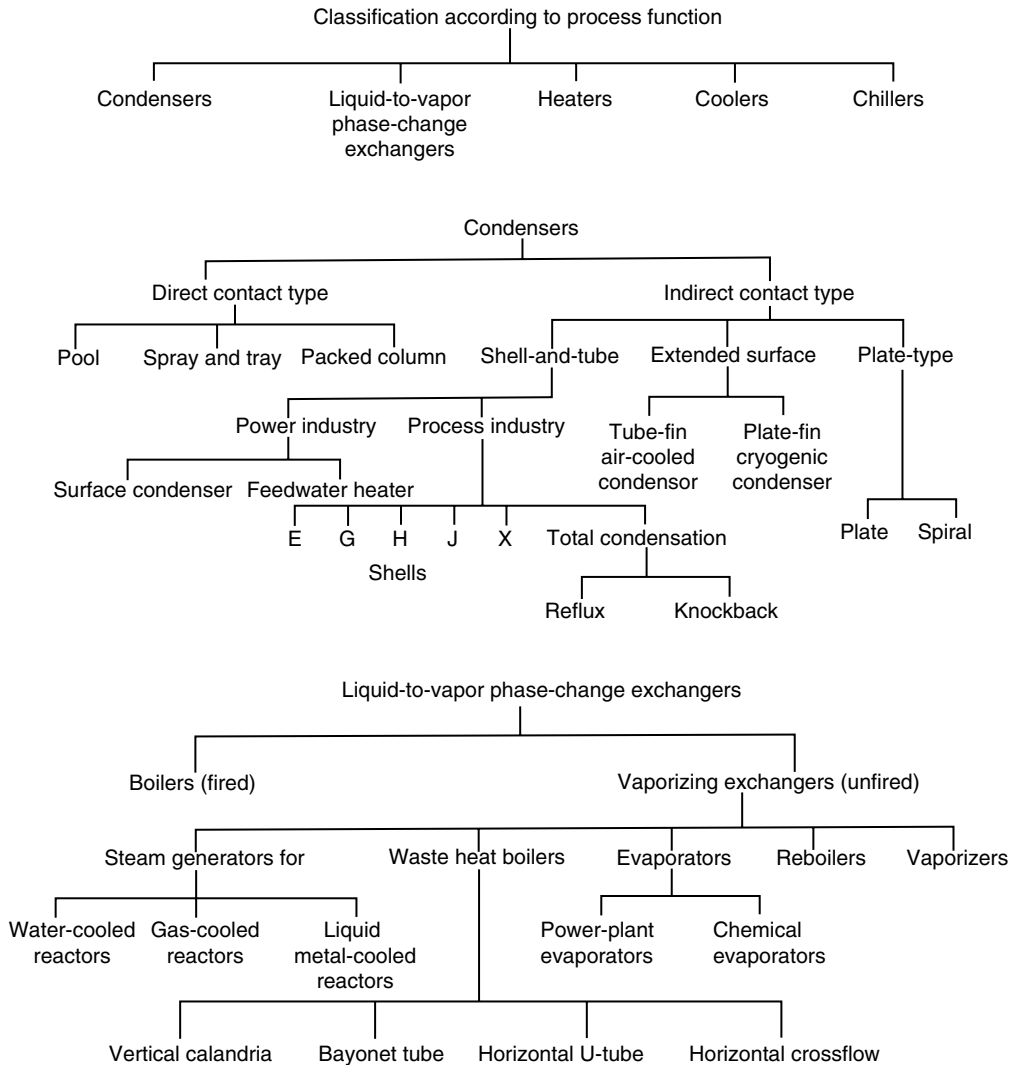


FIGURE 13.2 (a) Classification according to the process functions, (b) classification of condensers, (c) classification of liquid-to-vapor phase-change exchangers. (Modified from Shah, R. K. and Muller, A. C., *Ullmann's Encyclopedia of Industrial Chemistry, Unit Operations II, Vol. B3*. VCH Publishers, Weinheim, Germany, Chap. 2, 1988.)

of less than $100 \text{ m}^2/\text{m}^3$ on one fluid side with plain tubes, and two or three times that with the high-fin-density, low-finned tubing. Plate-fin, tube-fin, and rotary regenerators are examples of compact heat exchangers for gas flows on one or both fluid sides, and gasketed and welded plate heat exchangers are examples of compact heat exchangers for liquid flows.

In this chapter, exchanger heat transfer and pressure drop analysis is presented first. Next, theoretical results/insights and empirical correlations for nondimensional heat transfer and flow friction characteristics of exchanger surfaces are presented. Overall design methodology and step-by-step design procedures for the exchanger rating and sizing problems are then outlined. Finally, flow maldistribution and fouling problems and design considerations are summarized.

There is ever-increasing use of compact heat exchangers for advanced power cycles, and hence the focus in this chapter is on compact heat exchangers. Readers are referred to excellent works of Singh and Soler (1984); Palen (1987); Saunders (1988); Hewitt (1989); Yokell (1990), and Hewitt, Shires, and Bott (1994)

for design information on shell-and-tube and other heat exchangers; Reay (1979) and Hesselgreaves (2001) for compact heat exchangers, and Kakaç and Liu (1998) for single-phase and phase-change heat exchangers. Refer to Shah and Sekulić (2003) for an extensive list of publications on heat exchanger books.

13.2 Recuperator Heat Transfer and Pressure Drop Analysis

In this section, starting with the thermal circuit associated with a two-fluid exchanger, ϵ -NTU, P -NTU, and MTD methods used for an exchanger analysis are presented, followed by the fin efficiency concept and various expressions. Finally, expressions for computation of pressure drop are outlined for various single-phase exchangers.

13.2.1 Thermal Circuit

In order to develop relationships among variables for various exchangers, consider the counterflow exchanger of Figure 13.3 as an example. Two energy conservation differential equations for a two-fluid exchanger with *any* flow arrangement are

$$dq = q''dA = -C_h dT_h = \pm C_c dT_c \tag{13.1}$$

where the \pm sign depends on whether dT_c is increasing or decreasing with increasing dA . The overall rate equation on a local basis is

$$dq = q''dA = U(T_h - T_c)_{\text{local}}dA = U\Delta T dA \tag{13.2}$$

Integration of Equation 13.1 and Equation 13.2 across the exchanger surface area results in

$$q = C_h(T_{h,i} - T_{h,o}) = C_c(T_{c,o} - T_{c,i}) \tag{13.3}$$

and

$$q = UA\Delta T_m = \Delta T_m/R_o \tag{13.4}$$

Here, ΔT_m is the true mean temperature difference dependent on the exchanger flow arrangement and degree of fluid mixing within each fluid stream. The inverse of the overall thermal conductance UA is referred to as the overall thermal resistance R_o as follows (see Figure 13.4).

$$R_o = R_h + R_{h,s} + R_w + R_{c,s} + R_c \tag{13.5}$$

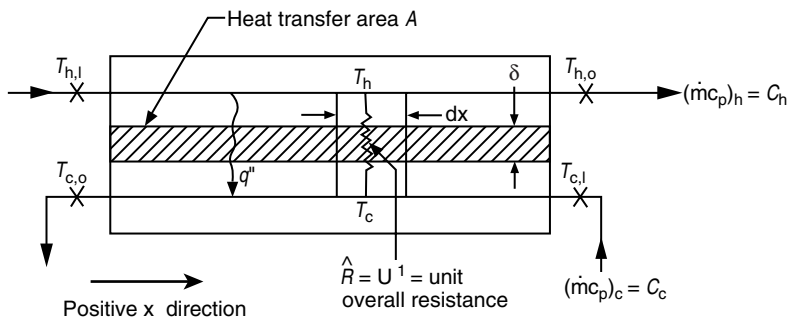


FIGURE 13.3 Nomenclature for heat exchanger variables.

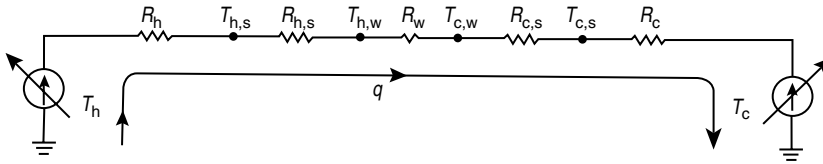


FIGURE 13.4 Thermal circuit for heat transfer in an exchanger.

where the subscripts h, c, s, and w denote hot, cold, scale or fouling, and wall, respectively. In terms of the overall and individual heat transfer coefficients, Equation 13.5 is represented as

$$\frac{1}{UA} = \frac{1}{(\eta_0 hA)_h} + \frac{1}{(\eta_0 h_s A)_h} + R_w + \frac{1}{(\eta_0 h_s A)_c} + \frac{1}{(\eta_0 hA)_c} \tag{13.6}$$

where η_0 is the extended surface efficiency and is related to the fin efficiency η_f , fin surface area A_f and the total heat transfer surface area A as follows:

$$\eta_0 = 1 - \frac{A_f}{A} (1 - \eta_f) \tag{13.7}$$

The wall thermal resistance R_w of Equation 13.5 is given by

$$R_w = \begin{cases} \frac{\delta}{k_w A_w} & \text{for flat walls with a single layer wall} \\ \sum_j \left(\frac{\delta}{k_w A_w} \right)_j & \text{for flat walls with } j \text{ multiple layer wall} \end{cases} \tag{13.8a}$$

and

$$R_w = \begin{cases} \frac{\ln(d_o/d_i)}{2\pi k_w L N_t} & \text{for } N_t \text{ circular tubes with a single layer wall} \\ \frac{1}{2\pi L N_t} \sum_j \frac{\ln(d_{j+1}/d_j)}{k_{w,j}} & \text{for } N_t \text{ circular tubes with } j \text{ multiple layer wall} \end{cases} \tag{13.8b}$$

If there is any contact or bond resistance present between the fin and tube or plate on the hot or cold fluid side, it is included as an added thermal resistance on the right-hand side of Equation 13.5 or Equation 13.6. For a heat-pipe heat exchanger, additional thermal resistances associated with the heat pipe should be included on the right-hand side of Equation 13.5 or Equation 13.6; these resistances are evaporator resistance at the evaporator section of the heat pipe, viscous vapor flow resistance inside the heat pipe (very small), internal wick resistance at the condenser section of the heat pipe, and condensation resistance at the condenser section.

If one of the resistances on the right-hand side of Equation 13.5 or Equation 13.6 is significantly higher than the other resistances, it is referred to as the *controlling resistance*. A reduction in the controlling thermal resistance will have much more impact in reducing the exchanger surface area A requirement compared to the reduction in A due to the reduction in other thermal resistances.

UA of Equation 13.6 may be defined in terms of hot or cold fluid side surface area or wall conduction area as

$$UA = U_h A_h = U_c A_c = U_w A_w \tag{13.9}$$

When R_w is negligible, $T_{w,h} = T_{w,c} = T_w$ of Figure 13.4 is computed from

$$T_w = \frac{T_h + [(R_h + R_{h,s})/(R_c + R_{c,s})]T_c}{1 + [(R_h + R_{h,s})/(R_c + R_{c,s})]} \tag{13.10}$$

When $R_{w,h} = R_{w,c} = 0$, Equation 13.10 reduces to

$$T_w = \frac{T_h/R_h + T_c/R_c}{1/R_h + 1/R_c} = \frac{(\eta_0 hA)_h T_h + (\eta_0 hA)_c T_c}{(\eta_0 hA)_h + (\eta_0 hA)_c} \tag{13.11}$$

13.2.2 ϵ -NTU, P -NTU, and MTD Methods

If we consider the fluid outlet temperatures or heat transfer rate as dependent variables, they are related to independent variables/parameters of Figure 13.3 as follows.

$$T_{h,o}, T_{c,o}, \text{ or } q = \phi\{T_{h,i}, T_{c,i}, C_h, C_c, U, A, \text{ flow arrangement}\} \tag{13.12}$$

Six independent and three dependent variables of Equation 13.12 for a given flow arrangement can be transferred into two independent and one dependent dimensionless groups; three different methods are presented in Table 13.1 based on the choice of three dimensionless groups. The relationship among three dimensionless groups is derived by integrating Equation 13.1 and Equation 13.2 across the surface area for a specified exchanger flow arrangement. Such expressions are presented later, in Table 13.3, for industrially most important flow arrangements. Now we will briefly describe the three methods.

13.2.3 The ϵ -NTU Method

In this method, the heat transfer rate from the hot fluid to the cold fluid in the exchanger is expressed as

$$q = \epsilon C_{\min}(T_{h,i} - T_{c,i}) \tag{13.13}$$

TABLE 13.1 General Functional Relationships and Dimensionless Groups for ϵ -NTU, P -NTU, and LMTD Methods

ϵ -NTU Method	P -NTU Method
$q = \epsilon C_{\min}(T_{h,i} - T_{c,i})$	$q = P_1 C_1 T_{1,i} - T_{2,i} $
$\epsilon = \phi(\text{NTU}, C^*, \text{ flow arrangement})$	$P_1 = \phi(\text{NTU}, R_1, \text{ flow arrangement})$
$\epsilon = \frac{C_h(T_{h,i} - T_{h,o})}{C_{\min}(T_{h,i} - T_{c,i})} = \frac{C_c(T_{c,o} - T_{c,i})}{C_{\min}(T_{h,i} - T_{c,i})}$	$P = \frac{T_{1,o} - T_{1,i}}{T_{2,i} - T_{1,i}}$
$\text{NTU} = \frac{UA}{C_{\min}} = \frac{1}{C_{\min}} \int U dA$	$\text{NTU}_1 = \frac{UA}{C_1} = \frac{ T_{1,o} - T_{1,i} }{\Delta T_m}$
$C^* = \frac{C_{\min}}{C_{\max}} = \frac{(\dot{m}c_p)_{\min}}{(\dot{m}c_p)_{\max}}$	$R = \frac{C_1}{C_2} = \frac{T_{2,i} - T_{2,o}}{T_{1,o} - T_{1,i}}$
MTD method ^a	
$Q = UAF \Delta T_{lm}$	
$\text{LMTD} = \Delta T_{lm} = \frac{\Delta T_1 - \Delta T_2}{\ln(\Delta T_1/\Delta T_2)}$	
$\Delta T_1 = T_{h,i} - T_{c,o} \quad \Delta T_2 = T_{h,o} - T_{c,i}$	
$F = \phi(P, R, \text{ flow arrangement})$	
$F = \frac{\Delta T_m}{\Delta T_{lm}}$	
P and R are defined in the P -NTU method	

^a Although P , R , and NTU are defined on Fluid 1 side. It must be emphasized that all the results of the P -NTU and MTD methods are valid if the definitions of P , NTU , and R are consistently based on C_h , C_c , C_h , or C_c .

Here, the exchanger effectiveness ε is an efficiency factor. It is a ratio of the actual heat transfer rate from the hot fluid to the cold fluid in a given heat exchanger of any flow arrangement to the maximum possible heat transfer rate q_{\max} thermodynamically permitted by the second law of thermodynamics. The q_{\max} is obtained in a *counterflow* heat exchanger (recuperator) of *infinite surface area* operating with the fluid flow rates (heat capacity rates) and fluid inlet temperatures equal to those of an actual exchanger (constant fluid properties are idealized). Refer to Shah and Sekulić (2003) for further details. As noted in Table 13.1, the exchanger effectiveness ε is a function of NTU and C^* in this method. The number of transfer units NTU is a ratio of the overall conductance UA to the smaller heat capacity rate C_{\min} . NTU designates the dimensionless “heat transfer size” or “thermal size” of the exchanger. Other interpretations of NTU are given by Shah (1983); Shah and Sekulić (2003). The heat capacity rate ratio C^* is simply a ratio of the smaller to the larger heat capacity rate for the two fluid streams. Note that $0 < \varepsilon < 1$, $0 < \text{NTU} < \infty$ and $0 \leq C^* \leq 1$.

13.2.4 The P-NTU Method

This method represents a variant of the ε -NTU method. The ε -NTU relationship is different depending on whether the shell fluid is the C_{\min} or C_{\max} fluid in the (stream asymmetric) flow arrangements commonly used for shell-and-tube exchangers. In order to avoid possible errors and confusion, an alternative is to present the temperature effectiveness P as a function of NTU and R , where P , NTU, and R are defined consistently for either Fluid 1 side or Fluid 2 side; in Table 13.1, they are defined for the Fluid 1 side (regardless of whether that side is hot or cold fluid side), and Fluid 1 side is clearly defined for each flow arrangement in Table 13.3; it is the shell side in a shell-and-tube exchanger. Note that

$$q = P_1 C_1 |T_{1,i} - T_{2,i}| = P_2 C_2 |T_{2,i} - T_{1,i}| \quad (13.14)$$

$$P_1 = P_2 R_2 \quad \text{or} \quad P_2 = P_1 R_1 \quad (13.15)$$

$$\text{NTU}_1 = \text{NTU}_2 R_2 \quad \text{or} \quad \text{NTU}_2 = \text{NTU}_1 R_1 \quad (13.16)$$

$$R_1 = \frac{1}{R_2} \quad \text{or} \quad R_2 = \frac{1}{R_1} \quad (13.17)$$

13.2.5 The MTD Method

In this method, the heat transfer rate from the hot fluid to the cold fluid in the exchanger is given by

$$q = \text{UAF} \Delta T_{\text{lm}} \quad (13.18)$$

Here, the log-mean temperature difference correction factor F is a ratio of mean (actual) temperature difference (MTD) to the log-mean temperature difference (LMTD), where

$$\text{LMTD} = \Delta T_{\text{lm}} = \frac{\Delta T_1 - \Delta T_2}{\ln(\Delta T_1 / \Delta T_2)} \quad (13.19)$$

Here, ΔT_1 and ΔT_2 are defined as

$$\Delta T_i = \begin{cases} T_{h,i} - T_{c,o} & \Delta T_2 = T_{h,o} - T_{c,i} & \text{for all flow arrangements except for parallel flow} \\ T_{h,i} - T_{c,i} & \Delta T_2 = T_{h,o} - T_{c,o} & \text{for parallel flow exchanger} \end{cases} \quad (13.20)$$

The LMTD represents a true mean temperature difference for a counterflow arrangement under the idealizations listed next. Thus, the LMTD correction factor F represents a degree of departure for the

MTD from the counterflow LMTD; it does not represent the effectiveness of a heat exchanger. It depends on two dimensionless groups P_1 and R_1 or P_2 and R_2 for a given flow arrangement.

The relationships among the dimensionless groups of the ϵ -NTU, P -NTU, and MTD methods are presented in Table 13.2. The closed-form formulas for industrially important exchangers are presented in terms of P_1 , NTU_1 , and R_1 in Table 13.3. These formulas are valid under the following idealizations.

1. The heat exchanger operates under steady-state conditions, that is, constant fluid temperatures (at the inlet and within the exchanger) independent of time.
2. Heat losses to the surroundings are negligible.
3. There are no thermal energy sources and sinks in the exchanger walls or fluids, such as electric heating, chemical reaction, or nuclear processes.
4. In counterflow and parallel flow exchangers, the temperature of each fluid is uniform over every flow cross section. From the temperature distribution point of view, in crossflow exchangers each fluid is considered mixed or unmixed at every cross section depending on the surface geometries used. For a multipass exchanger, the foregoing statements apply to each pass depending on the basic flow arrangement of the passes; the fluid is considered mixed or unmixed between passes.
5. Either there are no phase changes in the fluid streams flowing through the exchanger or the phase changes (condensation or boiling) occur under one of the following conditions: (a) phase change occurs at a constant temperature for a single component fluid at constant pressure; the effective specific heat for the phase-changing fluid is infinity in this case, and hence $C_{\max} \rightarrow \infty$. (b) The temperature of the phase-changing fluid varies linearly with heat transfer during the condensation or boiling. In this case, the effective specific heat is constant and finite for the phase-changing fluid.
6. The specific heat of each fluid is constant throughout the exchanger so that the heat capacity rate on each fluid side is treated as constant.
7. The velocity and temperature at the entrance of the heat exchanger on each fluid side are uniform.
8. For an extended surface exchanger, the overall extended surface temperature effectiveness η_0 is considered uniform and constant.
9. The individual and overall heat transfer coefficients are constant throughout the exchanger, including the case of phase-changing fluid in idealization 5.

TABLE 13.2 Relationships between Dimensionless Groups of the P -NTU and MTD Methods and Those of the ϵ -NTU Method

$$P_1 = \frac{C_{\min}}{C_1} \epsilon = \begin{cases} \epsilon & \text{for } C_1 = C_{\min} \\ \epsilon C^* & \text{for } C_1 = C_{\max} \end{cases}$$


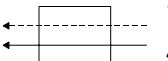
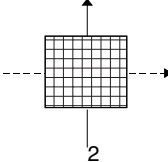
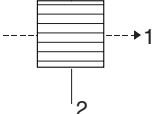
$$R_1 = \frac{C_1}{C_2} = \begin{cases} C^* & \text{for } C_1 = C_{\min} \\ 1/C^* & \text{for } C_1 = C_{\max} \end{cases}$$

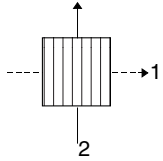
$$NTU_1 = NTU \frac{C_{\min}}{C_1} = \begin{cases} NTU & \text{for } C_1 = C_{\min} \\ NTU C^* & \text{for } C_1 = C_{\max} \end{cases}$$

$$F = \frac{NTU_{cf}}{NTU} = \frac{1}{NTU(1-C^*)} \ln \frac{1-C^*\epsilon}{1-\epsilon} \xrightarrow{C^*=1} \frac{\epsilon}{NTU(1-\epsilon)}$$

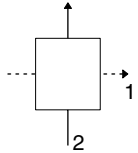
$$F = \frac{1}{NTU_1(1-R_1)} \ln \left[\frac{1-R_1 P_1}{1-P_1} \right] \xrightarrow{R_1=1} \frac{P_1}{NTU_1(1-P_1)}$$

TABLE 13.3 P_1 -NTU₁ Formulas and Limiting Values of P_1 for $R_1 = 1$ and $NTU_1 \rightarrow \infty$ for Various Exchanger Flow Arrangements

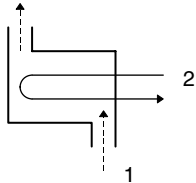
Flow Arrangement	Eq. No.	General Formula ^a	Value for $R_1 = 1$	Value of $NTU_1 \rightarrow \infty$
 Counterflow exchanger, stream symmetric ^b	1.1.1	$P_1 = \frac{1 - \exp[-NTU_1(1 - R_1)]}{1 - R_1 \exp[-NTU_1(1 - R_1)]}$	$P_1 = \frac{NTU_1}{1 + NTU_1}$	$P_1 \rightarrow 1$ for $R_1 \leq 1$
	1.1.2	$NTU_1 = \frac{1}{(1 - R_1)} \ln[(1 - R_1 P_1)/(1 - P_1)]$	$NTU_1 = \frac{P_1}{1 - P_1}$	$P_1 \rightarrow 1/R_1$ for $R_1 \geq 1$ $NTU_1 \rightarrow \infty$
	1.1.3	$F = 1$	$F = 1$	$F = 1$
 Parallel flow exchanger, stream symmetric	1.2.1	$P_1 = \frac{1 - \exp[-NTU_1(1 + R_1)]}{1 + R_1}$	$P_1 = \frac{1}{2} [1 - \exp(-2NTU_1)]$	$P_1 \rightarrow \frac{1}{1 + R_1}$
	1.2.2	$NTU_1 = \frac{1}{1 + R_1} \ln \left[\frac{1}{1 - P_1(1 + R_1)} \right]$	$NTU_1 = \frac{1}{2} \ln \left[\frac{1}{1 - 2P_1} \right]$	$NTU_1 \rightarrow \infty$
	1.2.3	$F = \frac{(R_1 + 1) \ln[1 - R_1 P_1 / (1 - P_1)]}{(R_1 - 1) \ln[1 - P_1(1 + R_1)]}$	$F = \frac{2P_1}{(P_1 - 1) \ln(1 - 2P_1)}$	$F \rightarrow 0$
 Single-pass crossflow exchanger, both fluids unmixed, stream symmetric	2.1	$P_1 = 1 - \exp(-NTU_1)$ $- \exp[-(1 + R_1)NTU_1]$ $\times \sum_{n=1}^{\infty} \frac{1}{(n + 1)!} R_1^n$ $\times \sum_{j=1}^n \frac{(n + 1 - j)}{j!} (NTU_1)^{n+j}$	Same as Equation 2.1 with $R_1 = 1$	$P_1 \rightarrow 1$ for $R_1 \leq 1$ $P_1 \rightarrow \frac{1}{R_1}$ for $R_1 \geq 1$ $P_1 \approx \exp \left[\frac{NTU_1^{0.22}}{R_1} (e^{-P_1 NTU_1^{0.28}} - 1) \right]$
	2.2.1	$P_1 = [1 - \exp(-KR_1)]/R_1$ $K = 1 - \exp(-NTU_1)$	$P_1 = 1 - \exp(-K)$	$P_1 \rightarrow \frac{1 - \exp(-R_1)}{R_1}$
	2.2.2	$NTU = \ln \left[\frac{1}{1 + (1/R_1) \ln(1 - R_1 P_1)} \right]$	$NTU_1 = \ln \left[\frac{1}{1 + \ln(1 - P_1)} \right]$	$NTU_1 \rightarrow \infty$
 Single-pass crossflow exchanger, Fluid 1 unmixed, Fluid 2 mixed	2.2.3	$F = \frac{\ln[(1 - R_1 P_1)/(1 - P_1)]}{(R_1 - 1) \ln[1 + (1/R_1) \ln(1 - R_1 P_1)]}$	$F = \frac{P_1}{(P_1 - 1) \ln[1 + \ln(1 - P_1)]}$	$F \rightarrow 0$
	2.3.1	$P = 1 - \exp(-K/R_1)$	$P = 1 - \exp(-K)$	$P_1 \rightarrow 1 - \exp(-1/R_1)$



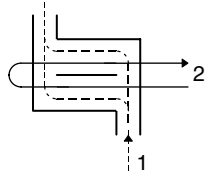
Single-pass crossflow exchanger, Fluid 1 mixed, Fluid 2 unmixed



Single-pass crossflow exchanger, both fluids mixed, stream symmetric



1-2 TEMA E shell-and-tube exchanger, shell fluid mixed, stream symmetric



$$K = 1 - \exp(-R_1 NTU_1)$$

$$2.3.2 \quad NTU_1 = \frac{1}{R_1} \ln \frac{1}{(1 + R_1) \ln(1 - P_1)}$$

$$2.3.3 \quad F = \frac{\ln[(1 - R_1 P_1)/(1 - P_1)]}{(1 - 1/R_1) \ln[1 + R_1 \ln(1 - P_1)]}$$

$$2.4 \quad P_1 = \left[\frac{1}{K_1} + \frac{R_1}{K_2} - \frac{1}{NTU_1} \right]^{-1}$$

$$K_1 = 1 - \exp(-NTU_1)$$

$$K_2 = 1 - \exp(-R_1 NTU_1)$$

$$K = 1 - \exp(-NTU_1)$$

$$NTU_1 = \ln \left[\frac{1}{1 + \ln(1 - P_1)} \right]$$

$$NTU_1 \rightarrow \infty$$

$$F = \frac{P_1}{(P_1 - 1) \ln[1 + \ln(1 - P_1)]}$$

$$P_1 \rightarrow \frac{1}{1 + R_1}$$

$$P_1 = \left[\frac{2}{K_1} - \frac{1}{NTU_1} \right]^{-1}$$

$$P_1 \rightarrow \frac{1}{1 + R_1}$$

$$3.1.1 \quad P_1 = \frac{2}{1 + R_1 + E \coth(E NTU_1 / 2)}$$

$$P_1 = \frac{1}{1 + \coth(NTU_1 / \sqrt{2}) / \sqrt{2}}$$

$$P_1 \rightarrow \frac{2}{1 + R_1 + E}$$

$$E = [1 + R_1^2]^{1/2}$$

$$3.1.2 \quad NTU_1 = \frac{1}{E} \ln \left[\frac{2 - P_1(1 + R_1 - E)}{2 - P_1(1 + R_1 + E)} \right]$$

$$NTU_1 = \ln \left[\frac{2 - P_1}{2 - 3P_1} \right]$$

$$NTU_1 \rightarrow \infty$$

$$3.1.3 \quad F = \frac{E \ln[(1 - R_1 P_1)/(1 - P_1)]}{(1 - R_1) \ln \left[\frac{2 - P_1(1 + R_1 - E)}{2 - P_1(1 + R_1 + E)} \right]}$$

$$F = \frac{P_1 / (1 - P_1)}{\ln[(2 - P_1)/(2 - 3P_1)]}$$

$$F \rightarrow 0$$

$$3.2 \quad P_1 = \frac{1}{R_1} \left[1 - \frac{(2 - R_1)(2E + R_1 B)}{(2 + R_1)(2E - R_1 B)} \right]$$

$$P_1 = \frac{1}{2} \left[1 - \frac{1 + E^{-2}}{2(1 + NTU_1)} \right]$$

$$P_1 \rightarrow \frac{2}{2 + R_1} \text{ for } R_1 \leq 2$$

$$E = \exp(NTU_1)$$

$$\text{for } R_1 = 2$$

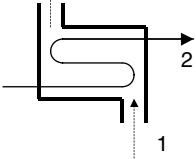
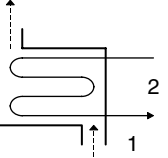
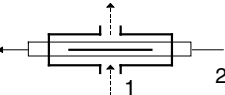
$$B = \exp(-NTU_1 R_1 / 2)$$

$$\text{Same as 1-1 J shell, Equation 3.10}$$

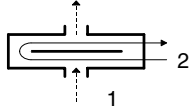
$$P_1 \rightarrow \frac{1}{R_1} \text{ for } R_1 \geq 2$$

(continued)

TABLE 13.3 (Continued)

Flow Arrangement	Eq. No.	General Formula ^a	Value for $R_1 = 1$	Value of $NTU_1 \rightarrow \infty$
1-2 TEMA E shell-and-tube exchanger, shell fluid divided into two streams individually mixed 	3.3	$P_1 = \frac{1}{R_1} \left[1 - \frac{C}{AC + B^2} \right]$ $A = X_1(R_1 + \lambda_1)(R_1 - \lambda_2)/2\lambda_1 - X_3\delta$ $- X_2(R_1 + \lambda_2)(R_1 - \lambda_1)/2\lambda_2 + 1/(1 - R_1)$ $B = X_1(R_1 - \lambda_2) - X_2(R_1 - \lambda_1) + X_3\delta$ $C = X_2(3R_1 + \lambda_1) - X_1(3R_1 + \lambda_2) + X_3\delta$ $X_i = \exp(\lambda_i NTU_1/3)/2\delta, \quad i = 1, 2, 3$ $\delta = \lambda_1 - \lambda_2$ $\lambda_1 = -\frac{3}{2} + \left[\frac{9}{4} + R_1(R_1 - 1) \right]^{1/2}$ $\lambda_2 = -\frac{3}{2} - \left[\frac{9}{4} + R_1(R_1 - 1) \right]^{1/2}$ $\lambda_3 = R_1$	Same as Equation 3.3 with $R_1 = 1$	$P_1 \rightarrow 1$ for $R_1 \leq 1$ $P_1 \rightarrow \frac{1}{R_1}$ for $R_1 \geq 1$
1-3 TEMA E shell-and-tube exchanger, shell and tube fluids mixed, one parallel flow and two counterflow passes 	3.4	$P_1 = 4[2(1 + R_1) + DA + R_1B]^{-1}$ $A = \coth(D NTU_1/4)$ $B = \tanh(R_1 NTU_1/4)$ $D = [4 + R_1^2]^{1/2}$	$P_1 = 4[4 + \sqrt{5}A + B]^{-1}$ $A = \coth(\sqrt{5}NTU_1/4)$ $B = \tanh(NTU_1/4)$	$P_1 \rightarrow \frac{4}{2(1 + 2R_1) + D - R_1}$
1-4 TEMA E shell-and-tube exchanger, shell and tube fluids mixed	3.5	Equation 2.4 applies in this limit with $n \rightarrow \infty$	Same as for Equation 2.4	Same as for Equation 2.4
1-4 TEMA E shell-and-tube exchanger, shell and tube fluids mixed with $n \rightarrow \infty$ 	3.6	$P_1 = A + B - AB(1 + R_1) + R_1AB^2$ $A = \frac{1}{1 + R_1} \{1 - \exp[-NTU_1(1 + R_1)/2]\}$ $B = \frac{1 - D}{1 - R_1D}$	Same as Equation (3.6) with $B = NTU_1/(2 + NTU_1)$ for $R_1 = 1$	$P_1 \rightarrow 1$ for $R_1 \leq 1$ $P_1 \rightarrow \frac{1}{R_1}$ for $R_1 \geq 1$

1-1 TEMA G shell-and-tube exchanger, tube fluid split into two streams individually mixed, shell fluid mixed. Stream symmetric.



3.7

$$D = \exp[-NTU_1(1 - R_1)/2]$$

$$P_1 = (B - \alpha^2)/(A + 2 + R_1 B)$$

$$A = -2R_1(1 - \alpha^2)/(2 + R_1)$$

$$B = [4 - \beta(2 + R_1)]/(2 - R_1)$$

$$\alpha = \exp[-NTU_1(2 + R_1)/4]$$

$$\beta = \exp[-NTU_1(2 - R_1)/2]$$

$$P_1 = \frac{1 + 2NTU_1 - \alpha^2}{4 + 4NTU_1 - (1 - \alpha^2)}$$

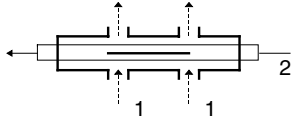
$$\text{for } R_1 = 2$$

$$\alpha = \exp(-NTU_1)$$

$$P_1 \rightarrow \frac{2 + R_1}{R_1^2 + R_1 + 2} \text{ for } R_1 \leq 2$$

$$P_1 \rightarrow \frac{1}{R_1} \text{ for } R_1 \geq 2$$

Overall counterflow 1-2 TEMA G shell-and-tube exchanger. Shell and tube fluids mixed in each pass at a cross section.



3.8

$$P_1 = E[1 + (1 - BR_1/2)(1 - AR_1/2 + ABR_1)] - AB(1 - BR_1/2)$$

Same as Equation (3.8) with $B = NTU_1/(2 + NTU_1)$ for $R_1 = 2$

$$A = \frac{1}{1 + R_1/2} \{1 - \exp[-NTU_1(1 + R_1/2)/2]\}$$

$$B = (1 - D)/(1 - R_1 D/2)$$

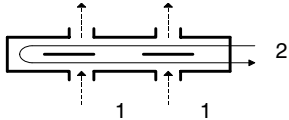
$$D = \exp[-NTU_1(1 - R_1/2)/2]$$

$$E = (A + B - ABR_1/2)/2$$

$$P_1 \rightarrow \frac{4(1 + R_1) - R_1^2}{(2 + R_1)^2} \text{ for } R_1 \leq 2$$

$$P_1 \rightarrow \frac{1}{R_1} \text{ for } R_1 \geq 2$$

1-1 TEMA H shell-and-tube exchanger, tube fluid split into two streams individually mixed, shell fluid mixed.



3.9

$$P_1 = \frac{1}{R_1} \left[1 - \frac{(1 - D)^4}{B - 4G/R_1} \right]$$

Same as Equation 3.11 with $H = NTU_1 + 1$ and $E = NTU_1/2$ for $R_1 = 4$

$$B = (1 + H)(1 + E)^2$$

$$G = (1 - D)^2(D^2 + E^2) + D^2(1 + E)^2$$

$$H = [1 - \exp(-2\beta)]/(4/R_1 - 1)$$

$$E = [1 - \exp(-\beta)]/(4/R_1 - 1)$$

$$D = [1 - \exp(-\alpha)]/(4/R_1 + 1)$$

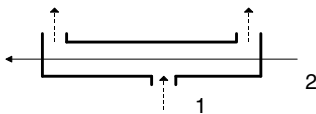
$$\alpha = NTU_1(4 + R_1)/8$$

$$\beta = NTU_1(4 - R_1)/8$$

$$P_1 \rightarrow \left[R_1 + \frac{(4 - R_1)^3}{(4 + R_1)R_1^2 + 16} \right]^{-1}$$

$$P_1 \rightarrow \frac{1}{R_1} \text{ for } R_1 \geq 4$$

Overall counterflow 1-2 TEMA H shell-and-tube exchanger, shell and tube fluids mixed in each pass at a cross section



3.10

$$P_1 = \frac{1}{R_1} \left[1 - \frac{(2 - R_1)(2A + R_1 B)}{(2 + R_1)(2A - R_1/B)} \right]$$

$$P_1 = \frac{1}{2} \left[1 - \frac{1 + A^2}{2(1 + NTU_1)} \right]$$

$$\text{for } R_1 = 2$$

$$P_1 \rightarrow \frac{2}{2 + R_1} \text{ for } R_1 \leq 2$$

$$P_1 \rightarrow \frac{1}{R_1} \text{ for } R_1 \geq 2$$

1-1 TEMA J shell-and-tube exchanger, shell and tube fluids mixed

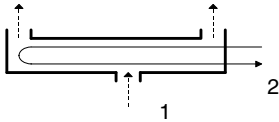
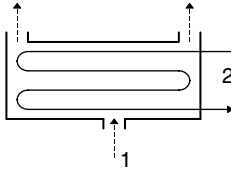
$$A = \exp(NTU_1)$$

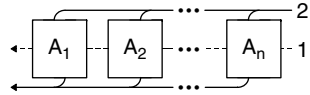
$$B = \exp(-NTU_1 R_1/2)$$

Same as Equation 3.2

(continued)

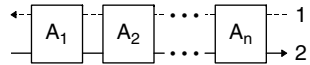
TABLE 13.3 (Continued)

Flow Arrangement	Eq. No.	General Formula ^a	Value for $R_1=1$	Value of $NTU_1 \rightarrow \infty$
 <p>1-2 TEAM J shell-and-tube exchanger, shell and tube fluids mixed; the same; the same results of Fluid 2 reversed</p>	3.11	$P_1 = \left[1 + \frac{R_1}{2} + \lambda B - 2\lambda CD \right]^{-1}$ $B = (A^\lambda + 1)/(A^\lambda - 1)$ $C = \frac{A(1 + \lambda)/2}{\lambda - 1 + (1 + \lambda)A^\lambda}$ $D = 1 + \frac{\lambda A(\lambda - 1)/2}{A^\lambda - 1}$ $A = \exp(NTU_1)$ $\lambda = (1 - R_1^2/4)^{1/2}$	Same as Equation 3.13 with $R_1=1$	$P_1 \rightarrow \left[1 + \frac{R_1}{2} + \lambda \right]^{-1}$
 <p>1-4 TEMA J shell-and-tube exchanger, shell and tube fluids mixed</p>	3.12	$P_1 = \left[1 + \frac{R_1}{4} \left(\frac{1 + 3E}{1 + E} \right) + \lambda B - 2\lambda CD \right]^{-1}$ $B = \frac{A^\lambda + 1}{A^\lambda - 1}$ $C = \frac{A(1 + \lambda)/2}{\lambda - 1 + (1 + \lambda)A^\lambda}$ $D = 1 + \frac{\lambda A(\lambda - 1)/2}{A^\lambda - 1}$ $A = \exp(NTU_1)$ $E = \exp(R_1 NTU_1/2)$ $\lambda = (1 + R_1^2/16)^{1/2}$	Same as Equation 3.14 with $R_1=1$	$P_1 \rightarrow \left[1 + \frac{3R_1}{4} + \lambda \right]^{-1}$
Limit of 1-n TEMA J shell-and-tube exchangers for $n \rightarrow \infty$. Shell and tube fluids mixed, stream symmetric	3.13	Equation 2.4 applies in this limit	Same as for Equation 2.4	Same as for Equation 2.4



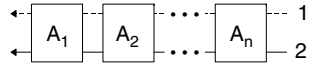
Parallel coupling of n exchangers. Fluid 2 split arbitrarily into n streams

4.1.1	$P_1 = 1 - \prod_{i=1}^n (1 - P_{1, A_i})$	Same as Equation 4.1.1	Same as Equation 4.1.1
4.1.2	$\frac{1}{R_1} = \sum_{i=1}^n R_{1, A_i}$	$1 = \sum_{i=1}^n R_{1, A_i}$	Same as Equation 4.1.2
4.1.3	$NTU_1 = \sum_{i=1}^n NTU_{1, A_i}$	Same as Equation 4.1.3	$NTU_1 \rightarrow \infty$
4.2.1	$P_1 = \frac{\prod_{i=1}^n (1 - R_1 P_{1, A_i}) - \prod_{i=1}^n (1 - P_{1, A_i})}{\prod_{i=1}^n (1 - R_1 P_{1, A_i}) - R_1 \prod_{i=1}^n (1 - P_{1, A_i})}$	$P_1 = \frac{\sum_{i=1}^n \frac{P_{1, A_i}}{1 - P_{1, A_i}}}{1 + \sum_{i=1}^n \frac{P_{1, A_i}}{1 - P_{1, A_i}}}$	Same as Equation 1.2.1 counterflow



Series coupling of n exchangers, overall counterflow arrangement, stream symmetric if all A_i are steam symmetric

4.2.2	$R_1 = R_{1, A_i} \quad i = 1, \dots, n$	$1 = R_{1, A_i}, \quad i = 1, \dots, n$	Same as Equation 4.2.2
4.2.3	$NTU_1 = \sum_{i=1}^n NTU_{1, A_i}$	Same as Equation 4.2.3	Same as Equation 4.2.3
4.2.4	$F = \frac{1}{NTU_1} \sum_{i=1}^n NTU_{1, A_i} F_{A_i}$	Same as Equation 4.2.4	Same as Equation 4.2.4



Series coupling of n exchangers, overall parallel flow arrangement; stream symmetric if all A_i are stream symmetric

4.3.1	$P = \frac{1}{1 + R_1} \left\{ 1 - \prod_{i=1}^n [1 - (1 + R_1) P_{1, A_i}] \right\}$	$P_1 = \frac{1 - \prod_{i=1}^n [1 - 2P_{1, A_i}]}{2}$	Same as Equation 4.3.1
4.3.2	$R_1 = R_{1, A_i} \quad i = 1, \dots, n$	$1 = R_{1, A_i} \quad i = 1, \dots, n$	Same as Equation 4.3.2
4.3.3	$NTU_1 = \sum_{i=1}^n NTU_{1, A_i}$	Same as Equation 4.3.3	$NTU_1 \rightarrow \infty$

In this table all variables except P_1 , R_1 , NTU_1 , and F are local or dummy variables not necessarily related to similar ones defined in nomenclature and the text.

Reprinted from Shah, R. K. and Muller, A. C., *Ullmann's Encyclopedia of Industrial Chemistry, Unit Operations II, Vol. B3*. VCH Publishers, Weinheim, Germany, Chap. 2, 1988. With permission.

^a All the formulas in this table are based on the Fluid 1 side. They can be converted to the Fluid 2 side using the following relations: (1) for stream symmetric exchangers, change P_1 , NTU_1 and R_1 to P_2 , NTU_2 and R_2 . (2) For stream asymmetric exchangers, convert P_1 - NTU_1 - R_1 , expressions to P_2 - NTU_2 - R_2 expressions using the following relationships: $P_1 = P_2 R_2$, $NTU_1 = NTU_2 R_2$, and $R_1 = 1/R_2$.

^b For those flow arrangements where "stream symmetric" is not explicitly mentioned, they are asymmetric.

10. The heat transfer surface area, A is distributed uniformly on each fluid side. In a multipass unit, heat transfer surface area is distributed uniformly in each pass, although different passes can have different surface areas.
11. For a plate-baffled shell-and-tube exchanger, the temperature rise per baffle pass is small compared to the overall temperature rise along the exchanger; that is, the number of baffles is large. Thus, the shell fluid is treated as mixed at its every flow cross section.
12. The fluid flow rate is uniformly distributed through the exchanger on each fluid side in each pass. No stratification, flow bypassing, or flow leakages occur in any stream. The flow condition is characterized by the bulk (or mean) velocity at any cross section.
13. Longitudinal heat conduction in the fluid and the wall is negligible.
14. Wall thermal resistance is distributed uniformly in the entire heat exchanger.

Idealizations 1–4 are necessary in a theoretical analysis of steady-state heat exchangers. Idealization 5 essentially restricts the analysis to single-phase flow on both fluid sides or on one fluid side with a dominating thermal resistance. For two-phase flows on both fluid sides, many of the foregoing idealizations are not valid, since mass transfer in phase change results in variable properties and variable flow rates of each phase, and the heat transfer coefficients vary significantly. As a result, the heat exchanger cannot be analyzed using the theory presented here.

If idealization 6 is not valid, divide the exchanger into small segments until the specific heats can be treated as constant. Idealizations 7 and 8 are primarily important for compact heat exchangers and will be discussed, respectively, in Sections on Flow Maldistribution, and Fin Efficiency and Extended Surface Efficiency.

Idealization 9 has been discussed in detail by Shah (1993). The overall heat transfer coefficient can vary because of variations in local heat transfer coefficients due to two effects: (1) change in heat transfer coefficients in the exchanger as a result of changes in the fluid properties or radiation due to rise or drop of fluid temperatures, and (2) change in heat transfer coefficients in the exchanger due to developing thermal boundary layers; this is referred to as the *length effect*. The first effect due to fluid property variations (or radiation) consists of two components: (i) distortion of velocity and temperature profiles at a given flow cross section due to fluid property variations; this effect is usually taken into account by the so-called property ratio method, with the correction scheme of Equation 13.103 and Equation 13.104, and (ii) variations in the fluid temperature along the axial and transverse directions in the exchanger depending on the exchanger flow arrangement; this effect is referred to as the *temperature effect*. The resultant axial changes in the overall mean heat transfer coefficient can be significant; the variations in U_{local} could be nonlinear depending on the type of the fluid. The effect of varying U_{local} can be taken into account by evaluating U_{local} at a few points in the exchanger and subsequently integrating U_{local} values by Simpson or Gauss method (Shah 1993). The temperature effect can increase or decrease mean U slightly or significantly depending on the fluids and applications. The length effect is important for developing laminar flows for which high heat transfer coefficients are obtained in the thermal entrance region. However, in general, it will have less impact on the overall heat transfer coefficient because the other thermal resistances in series in an exchanger may be controlling. The length effect reduces then overall heat transfer coefficient compared to the mean value calculated conventionally (assuming uniform mean heat transfer coefficient on each fluid side). It is shown that this reduction is up to about 14% for the worst case (Shah 1993).

Idealization 10 is generally true for individual passes due to the manufacturing considerations. However, in a multipass unit, it is possible to have different surface areas in different passes due to the design considerations. This effect has been investigated by Roetzel and Spang (1987, 1989) for 1-2, 1-3, and 1-2N TEMA E exchangers, by Spang, Xuan, and Roetzel (1991) for 1-N split flow TEMA G exchangers, by Xuan, Spang, and Roetzel (1991) for 1-N divided flow TEMA J exchangers, and by Bačić, Romie, and Herman (1988) for two-pass cross-counterflow exchangers.

For Idealization 11, Shah and Pignotti (1997) have shown that the following are the specific number of baffles beyond which the influence of the finite number of baffles on the exchanger effectiveness is not

significantly larger than 2%: $N_b \geq 10$ for the 1-1 TEMA E counterflow exchanger; $N_b \geq 6$ for the 1-2 TEMA E exchanger for $NTU_s \leq 2$, $R_s \leq 5$; $N_b \geq 9$ for the 1-2 TEMA J exchanger for $NTU_s \leq 2$, $R_s \leq 5$; $N_b \geq 5$ for the 1-2 TEMA G exchanger for $NTU_s \leq 3$, all R_s ; $N_b \geq 11$ for the 1-2 TEMA H exchanger for $NTU_s \leq 3$, all R_s .

If any of these idealizations are not valid for a particular exchanger application, the best solution is to work directly with either Equation 13.1 and Equation 13.2 or their modified forms by including a particular effect, and to integrate them over a small exchanger segment (i.e., conduct finite difference type analysis) in which all of the idealizations are valid.

13.2.6 Fin Efficiency and Extended Surface Efficiency

Extended surfaces have fins attached to the primary surface on one or both fluid sides of a two-fluid or a multfluid heat exchanger. Fins can be of a variety of geometries—plain, wavy, or interrupted, and can be attached to the inside, outside, or both sides of circular, flat, or oval tubes, or parting sheets. Fins are primarily used to increase the surface area (when the heat transfer coefficient on that fluid side is relatively low) and consequently to increase the total heat transfer rate. In addition, enhanced fin geometries also increase the heat transfer coefficient compared to that for a plain fin. Fins may also be used on the high heat transfer coefficient fluid side in a heat exchanger primarily for structural strength purpose (for example, for high-pressure water flow through a flat tube) or to provide a thorough mixing of a highly viscous liquid (such as for laminar oil flow in a flat or a round tube). Fins are attached to the primary surface by brazing, soldering, welding, adhesive bonding, or mechanical expansion, or they are extruded or integrally connected to the tubes. Major categories of extended surface heat exchangers are plate-fin (Figure 13.5) and tube-fin (Figure 13.6). Note that shell-and-tube exchangers sometimes employ individually finned tubes—low finned tubes (similar to Figure 13.6a but with low height fins; Shah 1985).

The concept of fin efficiency takes into account the reduction in temperature potential between the fin and the ambient fluid due to conduction along the fin and convection from or to the fin surface depending on fin cooling or heating situation. The *fin efficiency* is defined as the ratio of the actual heat transfer rate through the fin base divided by the maximum possible heat transfer rate through the fin base that would be obtained if the entire fin were at the base temperature (i.e., its material thermal conductivity were infinite). Since most of the real fins are “thin,” they are treated as one-dimensional

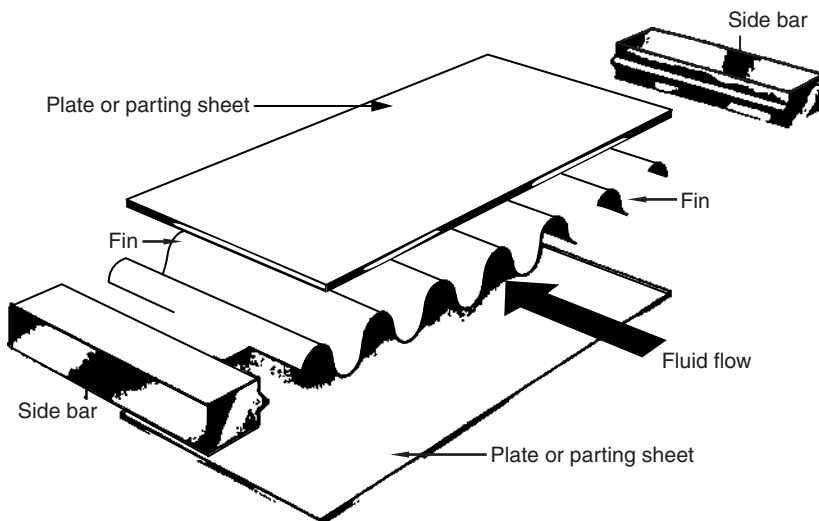


FIGURE 13.5 Basic components of a plate-fin exchanger.

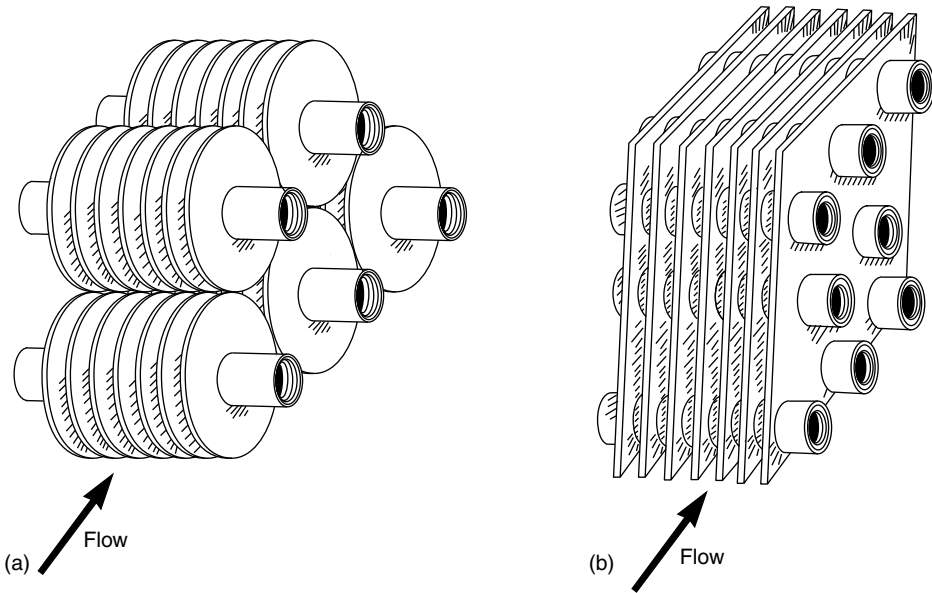


FIGURE 13.6 Types of tube-fin exchangers: (a) individually finned tubes, (b) flat (continuous) fins on an array of tubes; flat fins shown as plain fins, but can be wavy, louvered or interrupted.

(1D) with standard idealizations used for the analysis (Huang and Shah 1992). This 1D fin efficiency is a function of the fin geometry, fin material thermal conductivity, heat transfer coefficient at the fin surface, and the fin tip boundary condition; it is not a function of the fin base or fin tip temperature, ambient temperature, and heat flux at the fin base or fin tip in general. Fin efficiency formulas for some common fins are presented in Table 13.4 (Shah 1985).

The fin efficiency for flat plain fins on inline and staggered tube arrangements is obtained by the sector method. The smallest representative segment of the fin of Figure 13.7c is divided into two parts, OAB and OBC; the OAB part (having the subtended angle θ_0) is then divided into m equal angle ($\Delta\theta = \theta_0/m$) segments. Similarly, the OBC part (having the subtended angle ϕ_0) is then divided into n equal angle ($\Delta\phi = \phi_0/n$) segments. The outer radius of each circular sector is determined by equating the area of the sector with the area of the equivalent annular sector (Kundu and Das 2000). Thus for the inline tube arrangement of Figure 13.7a and c, it is given by

$$r_{e,i} = \frac{X_t}{2} \left(\frac{\tan(i\Delta\theta) - \tan[(i-1)\Delta\theta]}{\Delta\theta} \right)^{1/2} \quad r_{e,j} = \frac{X_\ell}{2} \left(\frac{\tan(j\Delta\phi) - \tan[(j-1)\Delta\phi]}{\Delta\phi} \right)^{1/2} \quad (13.21a)$$

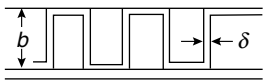
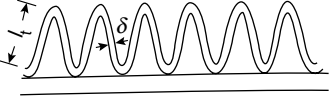
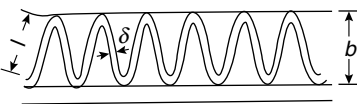
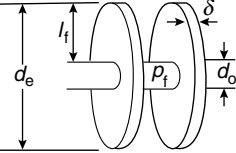
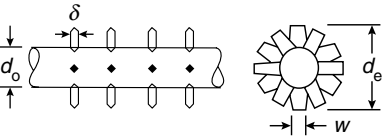
The smallest representative segment of the staggered tube arrangement of Figure 13.7b is shown in Figure 13.7d, which is divided into two parts, OAD and ODF; and ODF is divided into two equal parts ODE and OEF as shown in Figure 13.7d. Here again $r_{e,i}$ and $r_{e,j}$ of i th and j th segments of OAD and ODE are given by

$$r_{e,i} = X_\ell \left(\frac{\tan(i\Delta\theta) - \tan[(i-1)\Delta\theta]}{\Delta\theta} \right)^{1/2} \quad (13.21b)$$

$$r_{e,j} = \frac{[X_\ell^2 + (X_t/2)^2]^{1/2}}{2} \left(\frac{\tan(j\Delta\phi) - \tan[(j-1)\Delta\phi]}{\Delta\phi} \right)^{1/2}$$

The fin efficiency of each sector is then determined by the circular fin of constant cross section of Table 13.4. Once η_f for each sector is determined, η_f for the whole fin is the surface area weighted average

TABLE 13.4 Fin Efficiency Expressions for Plate-Fin and Tube-Fin Geometries of Uniform Fin Thickness

Geometry	Fin efficiency formula
$m_1 = \left[\frac{2h}{k_f \delta_i} \left(1 + \frac{\delta_i}{l_f} \right) \right]^{1/2} \quad E_1 = \frac{\tanh(m_1 l_1)}{m_1 l_1} \quad i = 1, 2, 3, 4$	
 <p>Plain, wavy, or offset strip fin of rectangular cross section</p>	$\eta_f = E_1$ $l_1 = \frac{b}{2} - \delta_1 \quad \delta_1 = \delta$
 <p>Triangular fin heated/cooled from one side</p>	$\eta_f = \frac{h A_1 (T_0 - T_a) \frac{\sinh(m_1 l_1)}{m_1 l_1} q_e}{\cosh(m_1 l_1) \left[h A_1 (T_0 - T_a) + q_e \frac{T_0 - T_a}{T_1 - T_b} \right]}, \quad \delta_1 = \delta$
 <p>Plain, wavy, or louver fin of triangular cross section</p>	$\eta_f = E_1$ $l_1 = \frac{l}{2} \quad \delta_1 = \delta$
 <p>Circular fin</p>	$\eta_f = \begin{cases} a(m l_e)^{-b} & \text{for } \Phi > 0.6 + 2.257(r^*)^{-0.445} \\ \frac{\tanh \Phi}{\Phi} & \text{for } \Phi \leq 0.6 + 2.257(r^*)^{-0.445} \end{cases}$ $a = (r^*)^{-0.246} \quad \Phi = m l_e (r^*) \exp\{0.13 m l_e - 1.3863\}$
 <p>Studded fin Rectangular fin over circular tubes</p>	$b = \begin{cases} 0.9107 + 0.0893 r^* & \text{for } r^* \leq 2 \\ 0.9706 + 0.17125 \ln r^* & \text{for } r^* > 2 \end{cases}$ $m = \left(\frac{2h}{k_f \delta} \right)^{1/2}$ $l_e = l_f + \frac{\delta}{2} r^* = \frac{r_e}{r_o}$ $\eta_f = \frac{\tanh(m l_e)}{m l_e}$ $m = \left[\frac{2h}{k_f \delta} \left(1 + \frac{\delta}{w} \right) \right]^{1/2} \quad l_e = l_f + \frac{\delta}{2} \cdot l_f = \frac{(d_e - d_o)}{2}$
	See the text

of η_{fS} for each sector.

$$\eta_f = \frac{\sum_{i=1}^m \eta_{f,i} A_{f,i} + a \sum_{j=1}^n \eta_{f,j} A_{f,j}}{\sum_{i=1}^m A_{f,i} + a \sum_{j=1}^n A_{f,j}} \quad (13.22)$$

Here, $a = 1$ for inline arrangement (Figure 13.7c) for segment OBC and $a = 2$ for staggered arrangement (Figure 13.7d) for two equal segments ODE and OEF. This approximation improves as the number of sectors $m, n \rightarrow \infty$. However, in reality, only a few sectors m and n will suffice to provide η_f within the

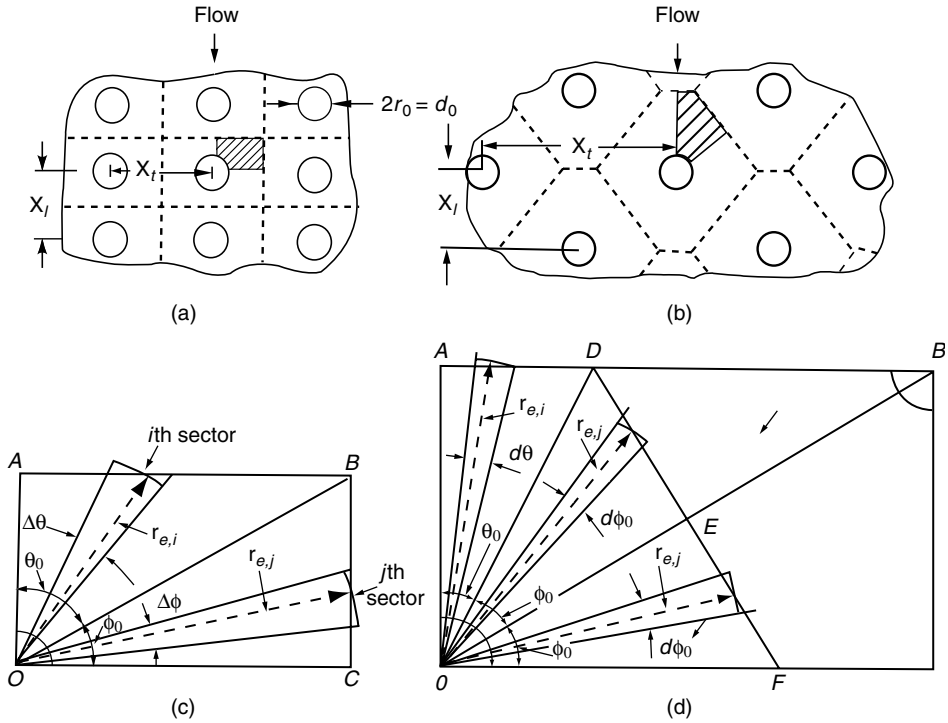


FIGURE 13.7 Flat fin over (a) an inline and (b) staggered arrangement. Smallest representative shaded segment of the fin for (c) an inline and (d) a staggered tube arrangement.

desired accuracy (such as 0.1%). An implicit idealization made in this method is that the heat flow is only in the radial direction, and not in the path of least thermal resistance. Hence, η_f calculated by the sector method will be lower than that for the actual flat fin, a conservative value.

The η_f values of Table 13.4 or Equation 13.22 are not valid in general when the fin is thick, is subject to variable heat transfer coefficients or variable ambient fluid temperature, or has a considerable temperature depression at the base. For a thin rectangular fin of constant cross section, the fin efficiency as presented in Table 13.4 is given by

$$\eta_f = \frac{\tanh(m\ell)}{m\ell} \tag{13.23}$$

where $m = [2h(1 + \delta/\ell_i)/k_f \delta_f]^{1/2}$. For a thick rectangular fin of constant cross section, the fin efficiency (a counterpart of Equation 13.23) is given by (Huang and Shah 1992)

$$\eta_f = \frac{(\text{Bi}^+)^{1/2}}{K\text{Bi}} \tanh \left[K(\text{Bi}^+)^{1/2} \right] \tag{13.24}$$

where $\text{Bi}^+ = \text{Bi}/(1 + \text{Bi}/4)$, $\text{Bi} = h\delta_f/2k_f$, $K = 2\ell/\delta_f$. Equation 13.23 is accurate (within 0.3%) for a “thick” rectangular fin having $\eta_f > 80\%$; otherwise use Equation 13.24 for a thick fin.

The nonuniform heat transfer coefficient h over the fin surface can lead to a significant error in η_f (Huang and Shah 1992) compared to that for a uniform h over the fin surface. However, generally h is obtained experimentally by considering a constant (uniform) value of h over the fin surface and also associated primary surface area. Hence, such experimental h will not introduce significant errors in η_f while designing a heat exchanger, particularly for $\eta_f > 80\%$. However, one needs to be aware of the impact

of nonuniform h on η_f if the heat exchanger test conditions and design conditions are significantly different. Nonuniform ambient temperature has less than a 1% effect on the fin efficiency for $\eta_f > 60\%$ and hence can be neglected. The longitudinal heat conduction effect on the fin efficiency is less than 1% for $\eta_f > 10\%$ and hence can be neglected. The fin base temperature depression increases the total heat flow rate through the extended surface compared to that having no fin base temperature depression, and hence neglecting this effect provides a conservative approach for the extended surface heat transfer. Refer to Huang and Shah (1992) for further details on the foregoing effects and modifications to η_f for rectangular fins of constant cross sections. Refer to Srinivasan and Shah (1995) for fin efficiency of extended surfaces for two-phase flows.

In an extended surface heat exchanger, heat transfer takes place from both the fins ($\eta_f < 100\%$) and the primary surface ($\eta_f = 100\%$). In that case, the total heat transfer rate is evaluated through a concept of *extended surface efficiency* η_0 defined as

$$\eta_0 = \frac{A_p}{A} + \eta_f \frac{A_f}{A} = 1 - \frac{A_f}{A} (1 - \eta_f) \quad (13.25)$$

where A_f is the fin surface area, A_p is the primary surface area, and $A = A_f + A_p$ is the total heat transfer area. In Equation 13.25, heat transfer coefficients over the finned and primary surfaces are idealized to be equal as noted earlier. Note that $\eta_0 \geq \eta_f$ and η_0 is always required for the determination of thermal resistances of Equation 13.5 in heat exchanger analysis.

13.2.7 Pressure Drop Analysis

Usually a fan, blower, or pump is used to flow fluid through individual fluid sides of a heat exchanger. Due to potential initial and operating high cost, low fluid pumping power requirement is highly desired for gases and viscous liquids. The fluid pumping power \mathcal{P} is approximately related to the core pressure drop in the exchanger as (Shah 1985).

$$\mathcal{P} = \frac{\dot{m} \Delta p}{\rho \eta_p} \approx \begin{cases} \frac{1}{2g_c \eta_p} \frac{\mu}{\rho^2} \frac{4L}{D_h} \frac{\dot{m}^2}{D_h A_o} f Re \\ \frac{0.046}{2g_c \eta_p} \frac{\mu^{0.2}}{\rho^2} \frac{4L}{D_h} \frac{\dot{m}^{2.8}}{D_h^{0.2} A_o^{1.8}} \end{cases} \quad (13.26)$$

where η_p is the pump/fan efficiency.

It is clear from Equation 13.26 and Equation 13.26 that the fluid pumping power is strongly dependent on the fluid density ($\mathcal{P} \propto 1/\rho^2$), particularly for low-density fluids in laminar and turbulent flows, and on the viscosity μ in laminar flow. In addition, the pressure drop itself can be an important consideration when blowers and pumps are used for the fluid flow, since they are head limited. Also, for condensing and evaporating fluids, the pressure drop affects the heat transfer rate. Hence, the pressure drop determination in the exchanger is important.

The pressure drop associated with a heat exchanger consists of (1) core pressure drop and (2) the pressure drop associated with the fluid distribution devices, such as inlet and outlet manifolds, headers, tanks, nozzles, ducting, and so on, which may include bends, valves, and fittings. This second Δp component is determined from Idelchik (1994); Miller (1990). The core pressure drop may consist of one or more of the following components depending on the exchanger construction: (i) friction losses associated with fluid flow over heat transfer surface, which usually consists of skin friction, form (profile) drag, and internal contractions and expansions, if any; (ii) the momentum effect (pressure drop or rise due to fluid density changes) in the core, (iii) pressure drop associated with sudden contraction and expansion at the core inlet and outlet, and (iv) the gravity effect due to the change in elevation between the inlet and outlet of the exchanger. The gravity effect is generally negligible for gases. For vertical flow through the exchanger, the pressure drop or rise (“static head”) due to the elevation change is given by

$$\Delta p = \pm \frac{\rho_m g L}{g_c} \quad (13.27)$$

Here, the “+” sign denotes vertical upflow (i.e., pressure drop) and the “-” sign denotes vertical downflow (i.e., pressure rise). The first three components of the core pressure drop are now presented for plate-fin, tube-fin, plate, and regenerative heat exchangers.

13.2.7.1 Plate-Fin Heat Exchangers

For the plate-fin exchanger (Figure 13.5), all three components are considered in the core pressure drop evaluation as follows.

$$\frac{\Delta p}{p_i} = \frac{G^2}{2g_c \rho_i p_i} \left[\underbrace{(1 - \sigma^2 + K_c)}_{\text{entrance effect}} + \underbrace{\left(f \frac{L}{r_h} \rho_i \left(\frac{1}{\rho} \right)_m \right)}_{\text{core friction}} + 2 \underbrace{\left(\frac{\rho_i}{\rho_o} - 1 \right)}_{\text{momentum effect}} - \underbrace{(1 - \sigma^2 - K_e)}_{\text{exit effect}} \frac{\rho_i}{\rho_o} \right] \quad (13.28)$$

where f is the Fanning friction factor, K_c and K_e are flow contraction (entrance) and expansion (exit) pressure loss coefficients, respectively (see Figure 13.8), and σ is a ratio of minimum free flow area to frontal area. K_c and K_e for four different entrance flow passage geometries are presented by Kays and London (1998). The entrance and exit losses are important at low values of σ and L (short cores) and for high values of Re for gases; they are negligible for liquids. The values of K_c and K_e apply to long tubes for which flow is fully-developed at the exit. For partially developed flows, K_c is lower and K_e is higher than that for fully-developed flows. For interrupted surfaces, flow is never fully-developed boundary layer type. For highly interrupted fin geometries, the entrance and exit losses are generally small compared to the core pressure drop and the flow is well mixed; hence, K_c and K_e for $Re \rightarrow \infty$ should represent a good approximation. The mean specific volume v_m or $(1/\rho)_m$ in Equation 13.28 is given as follows: for liquids with any flow arrangement, or for a perfect gas with $C^*=1$ and any flow arrangement (except for parallelflow),

$$\left(\frac{1}{\rho} \right)_m = v_m = \frac{v_i + v_o}{2} = \frac{1}{2} \left(\frac{1}{\rho_i} + \frac{1}{\rho_o} \right) \quad (13.29)$$

where v is the specific volume in m^3/kg .

For a perfect gas with $C^*=0$ and any flow arrangement,

$$\left(\frac{1}{\rho} \right)_m = \frac{\tilde{R}}{p_{\text{avg}}} T_{\text{lm}} \quad (13.30)$$

Here, \tilde{R} is the gas constant for a particular gas in $J/(kg \text{ K})$ (e.g., $\tilde{R}=287.04 \text{ J/kg K}$ for air), $p_{\text{avg}} = (p_i + p_o)/2$, and $T_{\text{lm}} = T_{\text{const}} + \Delta T_{\text{lm}}$, where T_{const} is the mean temperature of the fluid on the other side of the exchanger; the log-mean temperature difference ΔT_{lm} is defined in Table 13.1. The core frictional pressure drop in Equation 13.28 may be approximated as

$$\Delta p \approx \frac{4fLG^2}{2g_c D_h} \left(\frac{1}{\rho} \right)_m \approx \frac{4fLG^2}{2g_c \rho D_h} = f \frac{4L}{D_h} \frac{\rho_m u_m^2}{2g_c} = f \frac{4L}{D_h} \frac{G^2}{2g_c \rho} \quad (13.31)$$

13.2.7.2 Tube-Fin Heat Exchangers

The pressure drop inside a circular tube is computed using Equation 13.28 with proper values of f factors (see equation in Table 13.6 and Table 13.7) and K_c and K_e from Figure 13.8 for circular tubes.

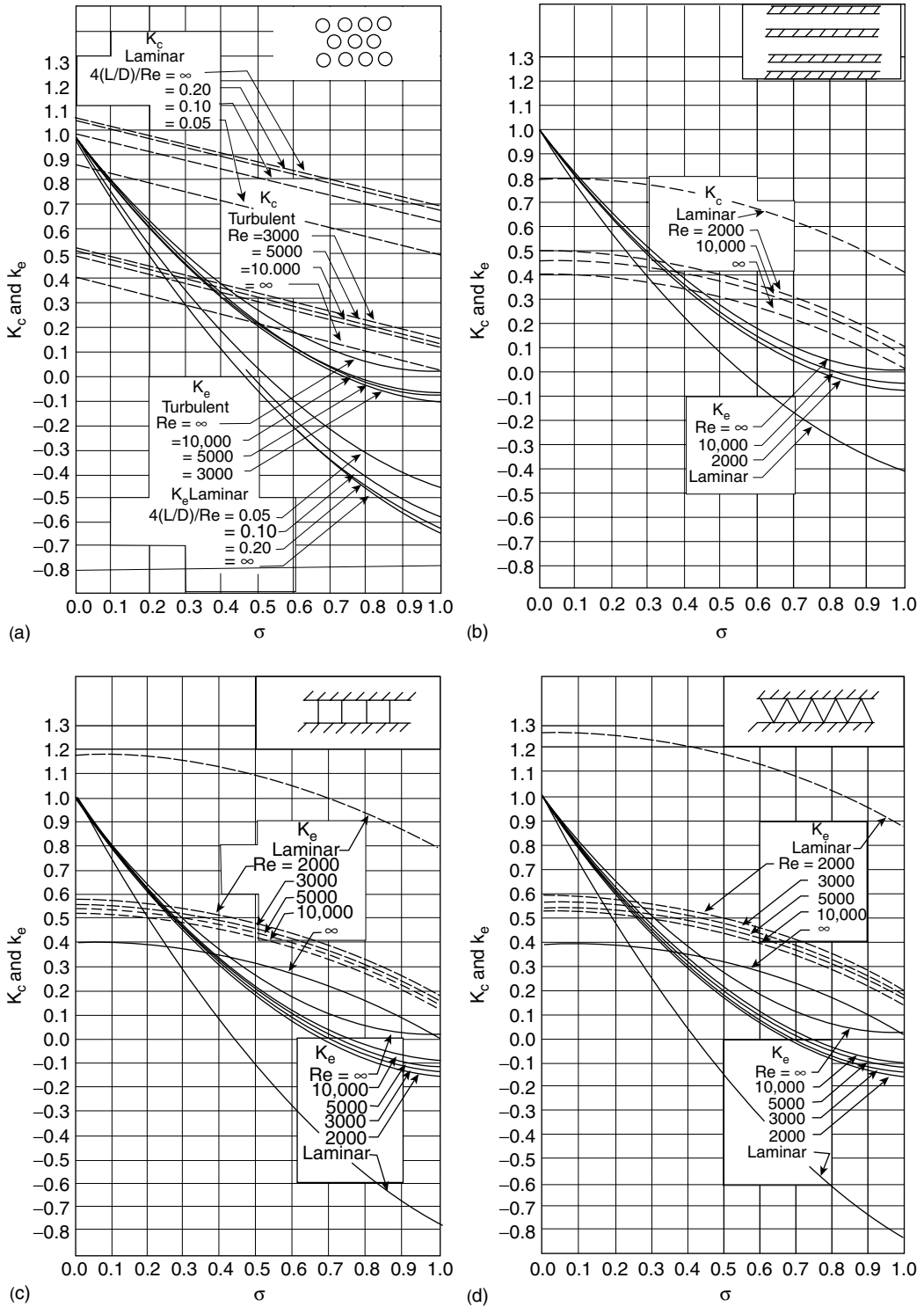


FIGURE 13.8 Entrance and exit pressure loss coefficients: (a) circular tubes, (b) parallel plates, (c) square passages, and (d) triangular passages. For each of these flow passages shown in the inset, the fluid flows perpendicular to the plane of the paper into the flow passages. (From Kays and London 1998. With permission.)

For flat fins on an array of tubes (see Figure 13.6b), the components of the core pressure drop, such as those in Equation 13.28, are the same with the following exception: the core friction and momentum effect take place within the core with $G = \dot{m}/A_0$, where A_0 is the minimum free flow area within the core, and the entrance and exit losses occur at the leading and trailing edges of the core with the associated flow area A'_0 so that

$$\dot{m} = GA_0 = G'A'_0 \text{ or } G'\sigma' = G\sigma \quad (13.32)$$

where σ' is the ratio of free flow area to frontal area at the fin leading edges. The pressure drop for flow normal to a tube bank with flat fins is then given by

$$\begin{aligned} \frac{\Delta p}{p_i} = \frac{G^2}{2g_c \rho_i p_i} \left[f \frac{L}{r_h} \rho_i \left(\frac{1}{\rho} \right)_m + 2 \left(\frac{\rho_i}{\rho_0} - 1 \right) \right] \\ + \frac{G'^2}{2g_c \rho_i p_i} \left[\left(1 - \sigma'^2 + K_c \right) - \left(1 - \sigma'^2 - K_c \right) \frac{\rho_i}{\rho_0} \right] \end{aligned} \quad (13.33)$$

For individually finned tubes as shown in Figure 13.6a, flow expansion and contraction take place along each tube row, and the magnitude is of the same order as that at the entrance and exit. Hence, the entrance and exit losses are generally lumped into the core friction factor. Equation 13.28 for individually (plain and longitudinally) finned tubes then reduces to

$$\frac{\Delta p}{p_i} = \frac{G^2}{2g_c \rho_i p_i} \left[f \frac{L}{r_h} \rho_i \left(\frac{1}{\rho} \right)_m + 2 \left(\frac{\rho_i}{\rho_0} - 1 \right) \right] \quad (13.34)$$

13.2.7.3 Plate Heat Exchangers

Pressure drop in a plate heat exchanger consists of three components: (1) pressure drop associated with the inlet and outlet manifolds and ports, (2) pressure drop within the core (plate passages), and (3) pressure drop due to the elevation change. The pressure drop in the manifolds and ports should be kept as low as possible (generally < 10% of the total pressure drop, but it is found as high as 25%–30% or higher in some designs). Empirically, it is calculated as approximately 1.5 times the inlet velocity head per pass. Since the entrance and exit losses in the core (plate passages) cannot be determined experimentally, they are included in the friction factor for the given plate geometry. The pressure drop (rise) caused by the elevation change for liquids is given by Equation 13.27. Hence, the pressure drop on one fluid side in a plate heat exchanger is given by

$$\Delta p = \frac{1.5 G_p^2 N_p}{2g_c \rho_i} + \frac{4fLG^2}{2g_c D_e} \left(\frac{1}{\rho} \right)_m + \left(\frac{1}{\rho_0} - \frac{1}{\rho_i} \right) \frac{G^2}{g_c} \pm \frac{\rho_m g L}{g_c} \quad (13.35)$$

where $G_p = \dot{m}/(\pi/4)D_p^2$ is the fluid mass velocity in the port, D_p is the port/manifold diameter, N_p is the number of passes on the given fluid side, and D_e is the equivalent diameter of flow passages (usually twice the plate spacing). Note that the third term on the right-hand side of the equality sign of Equation 13.35 is for the momentum effect which is generally negligible for liquids.

13.3 Regenerator Heat Transfer and Pressure Drop Analysis

A regenerator is a storage type heat exchanger in which both fluids flow alternatively through the same flow passages, and hence heat transfer is from the hot gas to the cold gas via thermal energy storage and release through the exchanger surface or matrix wall. For a continuous operation, either the matrix is moved periodically in and out of the fixed gas streams as in a rotary regenerator or the gas flows are diverted through the valves to and from the fixed matrices as in a fixed-matrix regenerator. Seal leakage in

rotary regenerators or valve leakage in fixed-matrix regenerators cannot be avoided and should be kept minimum (less than about 5%) so that its impact on the regenerator performance is minimum. We will focus only on the rotary regenerators because of their use as compact exchangers. Refer to Shah and Sekulić (2003) for further details on rotary and fixed-matrix regenerators.

The heat transfer rate in a regenerator is computed from Equation 13.13 as is for the recuperators.

$$q = \varepsilon C_{\min}(T_{h,i} - T_{c,i}) \quad (13.13b)$$

Two methods have been used for the regenerator design theory: ε -NTU₀ and Λ - Π methods. Also, the most common flow arrangement is counterflow, and parallel flow is also possible. Other flow arrangements of recuperators are not possible due to construction features. We will now briefly describe these methods.

13.3.1 ε -NTU₀ Method for Heat Transfer

Since heat transfer is through the storage in the matrix wall and is of transient nature, it adds two additional dimensionless groups compared to those for the recuperators for the ε -NTU method for recuperators. They are matrix heat capacity rate ratio C_r^* and thermal conductance ratio $(hA)^* = (hA)$ on C_{\min} side divided by (hA) on C_{\max} side. In most practical regenerator uses, the influence of $(hA)^*$ on the regenerator effectiveness is insignificant and is neglected. Hence, the regenerator effectiveness is given by

$$\varepsilon = \phi(\text{NTU}_0, C^*, C_r^*) \quad (13.36)$$

where

$$\text{NTU}_0 = \frac{1}{C_{\min}} \left[\frac{1}{1/(hA)_h + 1/(hA)_c} \right] = \frac{U_0 A}{C_{\min}} \quad (13.37)$$

$$C^* = \frac{C_{\min}}{C_{\max}} \quad (13.38)$$

$$C_r^* = \frac{C_r}{C_{\min}} \quad (13.39)$$

For a counterflow regenerator, the following approximate procedure is proposed by Razelos (1980) to calculate the regenerator effectiveness ε . For the known values of NTU₀, C^* and C_r^* , calculate “equivalent” values of NTU₀ and C_r^* for a balanced regenerator ($C^* = 1$), designated with a subscript m, as follows.

$$\text{NTU}_{0,m} = \frac{2\text{NTU}_0 C^*}{1 + C^*} \quad (13.40)$$

$$C_{r,m}^* = \frac{2C_r^* C^*}{1 + C^*} \quad (13.41)$$

With these values of NTU_{0,m} and $C_{r,m}^*$, obtain the value of ε_r from the following equation.

$$\varepsilon_r = \frac{\text{NTU}_{0,m}}{1 + \text{NTU}_{0,m}} \left[1 - \frac{1}{9(C_{r,m}^*)^{1.93}} \right] \quad (13.42)$$

The regenerator effectiveness ε is then determined from the following equation.

$$\varepsilon = \frac{1 - \exp\{\varepsilon_r(C_r^{*2} - 1)/[2C^*(1 - \varepsilon_r)]\}}{1 - C^* \exp\{\varepsilon_r(C_r^{*2} - 1)/[2C^*(1 - \varepsilon_r)]\}} \quad (13.43)$$

This formula yields regenerator effectiveness within 1% accuracy for $\varepsilon > 80\%$, and lower effectiveness that accuracy is somewhat lower. The following qualitative observations can be made from the ε -NTU₀ results for regenerators:

1. For specified C_r^* and C^* , the heat exchanger effectiveness increases with increasing NTU₀. For all C_r^* and C^* , $\varepsilon \rightarrow 1$ as $\text{NTU}_0 \rightarrow \infty$.
2. For specified NTU₀ and C^* , ε increases with increasing values of C_r^* and asymptotically approaches the value for a counterflow recuperator.
3. For specified NTU₀ and C_r^* , ε increases with decreasing values of C^* . The percentage change in ε is the largest in the lower NTU₀ range, and this percentage change in ε increases with increasing values of C_r^* .
4. For $\varepsilon < 40\%$ and $C_r^* > 0.6$, C^* and C_r^* do not have a significant influence on the exchanger effectiveness.

The ε -NTU₀ results for a parallel flow regenerator are provided in Shah and Sekulić (2003).

The alternative method for regenerator analysis is referred to as Λ -II method as summarized in detail by Shah and Sekulić (2003).

Longitudinal wall heat conduction can become important and can *reduce* the regenerator effectiveness significantly if the regenerator is designed over about 85%. In that case, the effect of longitudinal heat conduction in the wall can be taken into account by the following procedure to compute the regenerator effectiveness.

1. Use the Razelos method to compute NTU_{0,m}, $C_{r,m}^*$ and $\varepsilon_{r,\lambda=0}$ for an equivalent balanced regenerator for known NTU₀ and C^* using Equation 13.40 through Equation 13.42. The ε_r computed from Equation 13.42 is designated as $\varepsilon_{r,\lambda=0}$ here.
2. Compute $\varepsilon_{r,\lambda \neq 0}$ as follows using computed NTU_{0,m} and given λ .

$$\varepsilon_{r,\lambda \neq 0} = \varepsilon_{r,\lambda=0} \left(1 - \frac{C_\lambda}{2 - C^*} \right) \quad (13.44)$$

where

$$C_\lambda = \frac{1}{1 + \frac{\text{NTU}_0(1+\lambda\Phi)}{1+\lambda\text{NTU}_0}} - \frac{1}{1 + \text{NTU}_0} \quad (13.45)$$

and

$$\Phi = \left[\frac{\lambda \text{NTU}_0}{1 + \lambda \text{NTU}_0} \right]^{1/2} \tanh \left[\frac{\text{NTU}_0}{\{\lambda \text{NTU}_0 / (1 + \lambda \text{NTU}_0)\}^{1/2}} \right] \quad (13.46a)$$

$$\approx \left[\frac{\lambda \text{NTU}_0}{1 + \lambda \text{NTU}_0} \right]^{1/2} \quad \text{for } \text{NTU}_0 \geq 3 \quad (13.46b)$$

3. Finally determine ε from Equation 13.43 with ε_r replaced by $\varepsilon_{r,\lambda \neq 0}$ calculated from Equation 13.44. Influence of transverse wall heat conduction may be important for walls of matrix passages either being thick or made up of ceramic materials. In that case, wall thermal resistance term is added to two convective thermal resistances associated with hot and cold fluid flows within the matrix. Also the pressure and carryover leakages in the regenerator can reduce the regenerator effectiveness considerably, and must be taken into account for the desired performance level. Refer to Shah and Sekulić (2003) for the details.

13.3.2 Pressure Drop

For regenerator matrices having cylindrical passages, the pressure drop is computed using Equation 13.28 with appropriate values of f , K_c , and K_e . For regenerator matrices made up of any porous material (such as checkerwork, wire, mesh, spheres, copper wools, etc.), the pressure drop is calculated using Equation 13.34 since the entrance and exit losses are lumped into the friction factor f .

13.4 Heat Transfer and Flow Friction Correlations—Single-Phase Flows

Accurate and reliable surface heat transfer and flow friction characteristics are a key input to the exchanger heat transfer and pressure drop analyses or to the rating and sizing problems (Shah and Sekulić 1998). After presenting the associated nondimensional groups, we will present important analytical solutions and empirical correlations for some important exchanger geometries.

13.4.1 Dimensionless Groups

Heat transfer characteristics of an exchanger surface are presented in terms of the Nusselt number Nu , Stanton number St , or Colburn factor j vs. the Reynolds number Re , dimensionless axial length x^+ , or the Graetz number Gz . Flow friction characteristics are presented in terms of the Fanning friction factor f vs. Re or dimensionless axial length x^+ . These and other important dimensionless groups used in presenting and correlating internal flow forced convection heat transfer are summarized in Table 13.5 with their definitions and physical meanings. Where applicable, the hydraulic diameter D_h is used as a characteristic dimension in all dimensionless groups. A number of different definitions are used in the literature for some of the dimensionless groups; the user should pay particular attention to the specific definitions used in any research paper before using specific results. This is particularly true for the Nusselt number, where many different temperature differences are used in the definition of h , and for f , Re , and other dimensionless groups having characteristic dimensions different from D_h .

13.4.2 Analytical Solutions

Flow passages in most compact heat exchangers are complex with frequent boundary layer interruptions; some heat exchangers (particularly the tube side of shell-and-tube exchangers and highly compact regenerators) have continuous flow passages. The velocity and temperature profiles across the flow cross section are generally fully-developed in the continuous flow passages, whereas they develop at each boundary layer interruption in an interrupted surface and may reach a periodic fully-developed flow. The heat transfer and flow friction characteristics are generally different for fully-developed flows and developing flows. Analytical results for developed and developing flows for simple flow passage geometries follow. For complex surface geometries, the basic surface characteristics are primarily obtained experimentally (Shah and Sekulić 2003); the pertinent correlations are presented in the next subsection.

Analytical solutions for developed and developing velocity/temperature profiles in constant cross section circular and noncircular flow passages are important when no empirical correlations are available, extrapolations are needed for empirical correlations, or in the development of empirical correlations. Fully-developed-laminar-flow solutions are applicable to highly compact regenerator surfaces or highly compact plate-fin exchangers, with plain uninterrupted fins. Developing laminar flow solutions are applicable to interrupted fin geometries and plain uninterrupted fins of “short” lengths, and turbulent flow solutions to not so compact heat exchanger surfaces.

The heat transfer rate in laminar duct flow is very sensitive to the thermal boundary condition. Hence, it is essential to carefully identify the thermal boundary condition in laminar flow. The heat transfer rate in turbulent duct flow is insensitive to the thermal boundary condition for most common fluids

TABLE 13.5 Important Dimensionless Groups for Internal Flow Forced Convection Heat Transfer and Flow Friction, Useful in Heat Exchanger Design


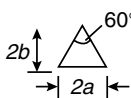
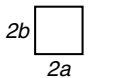
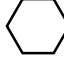
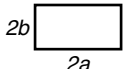

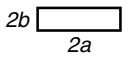
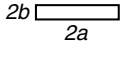
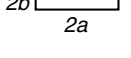
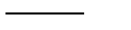
Dimensionless Groups	Definitions and Working Relationships	Physical Meaning and Comments
Reynolds number	$Re = \frac{\rho u_m D_h}{\mu} = \frac{GD_h}{\mu}$	a flow modulus, proportional to the ratio of flow momentum rate (“inertia force”) to viscous force
Fanning friction factor	$f = \frac{\tau_w}{(\rho u_m^2/2g_c)}$ $f = \Delta p^* \frac{r_h}{L} \frac{\Delta p}{(\rho u_m^2/2g_c)} \frac{r_h}{L}$	the ratio of wall shear (skin frictional) stress to the flow kinetic energy per unit volume; commonly used in heat transfer literature
Apparent fanning friction factor	$f_{app} = \Delta p^* \frac{r_h}{L}$	Includes the effects of skin friction and the change in the momentum rates in the entrance region (developing flows)
Incremental pressure drop number	$K(x) = (f_{app} - f_{fd}) \frac{L}{r_h}$	Represents the excess dimensionless pressure drop in the entrance region over that for fully-developed flow
Darcy friction factor	$K(\infty) = \text{constant for } x \rightarrow \infty$ $f_D = 4f = \Delta p^* \frac{D_h}{L}$	four times the Fanning friction factor; commonly used in fluid mechanics literature
Euler number	$Eu = \Delta p^* = \frac{\Delta p}{(\rho u_m^2/2g_c)}$	the pressure drop normalized with respect to the dynamic velocity head; commonly used in the Russian literature
Dimensionless axial distance for the fluid flow problem	$x^+ = \frac{x}{D_h Re}$	the ratio of the dimensionless axial distance (x/D_h) to the Reynolds number; useful in the hydrodynamic entrance region
Nusselt number	$Nu = \frac{h}{k/D_h} = \frac{q'' D_h}{k(T_w - T_m)}$	the ratio of the convective conductance h to the pure molecular thermal conductance k/D_h
Stanton number	$St = \frac{h}{Gc_p} = \frac{Nu}{Pe} = \frac{Nu}{RePr}$	the ratio of convection heat transfer (per unit duct surface area) to amount virtually transferable (per unit of flow cross-sectional area); no dependence upon any geometric characteristic dimension
Colburn factor	$j = St Pr^{2/3} = (Nu Pr^{-1/3})/Re$	a modified Stanton number to take into account the moderate variations in the Prandtl number for $0.5 \leq Pr \leq 10.0$ in turbulent flow
Prandtl number	$Pr = \frac{\nu}{\alpha} = \frac{\mu c_p}{k}$	a fluid property modulus representing the ratio of momentum diffusivity to thermal diffusivity of the fluid
Péclet number	$Pe = \frac{\rho c_p u_m D_h}{k} = \frac{u_m D_h}{\alpha} = RePr$	proportional to the ratio of thermal energy convected to the fluid to thermal energy conducted axially within the fluid; the inverse of Pe indicates relative importance of fluid axial heat conduction
Dimensionless axial distance for the heat transfer problem	$x^* = \frac{x}{D_h Pe} = \frac{x}{D_h Re Pr}$	axial coordinate for describing the thermal entrance region heat transfer results
Graetz number	$Gz = \frac{\dot{m} c_p}{kL} = \frac{PeP}{4L} = \frac{P}{4D_h} \frac{1}{x^*}$ $Gz = \pi/(4x^*)$ for a circular tube	conventionally used in the chemical engineering literature related to x^* as shown when the flow length in Gz is treated as a length variable

Source: From Shah, R. K. and Muller, A. C. Heat exchange. In *Ullmann's Encyclopedia of Industrial Chemistry, Unit Operations II, Vol. B3*. VCH Publishers, Weinheim, Germany, Chap. 2, 1988. With permission.

($Pr \geq 0.7$); the exception is liquid metals ($Pr < 0.03$). Hence, there is generally no need to identify the thermal boundary condition in turbulent flow for all fluids except liquid metals.

Fully-developed-laminar-flow analytical solutions for some duct shapes of interest in compact heat exchangers are presented in Table 13.6 for three important thermal boundary conditions denoted by the subscripts H1, H2, and T (Shah and London 1978; Shah and Bhatti 1987). Here, H1 denotes constant axial wall heat flux with constant peripheral wall temperature, H2 denotes constant axial and peripheral wall heat flux, and T denotes constant wall temperature. The following observations may be made from this table: (1) there is a strong influence of flow passage geometry on Nu and fRe . Rectangular passages approaching a small aspect ratio exhibit the highest Nu and fRe . (2) The thermal boundary conditions have a strong influence on the Nusselt numbers. (3) As $Nu = hD_h/k$, a constant Nu implies the convective heat transfer coefficient h independent of the flow velocity and fluid type (Prandtl number). (4) An increase in h can be best achieved either by reducing D_h or by selecting a geometry with a low aspect ratio rectangular flow passage. Reducing the hydraulic diameter is an obvious way to increase exchanger compactness and heat transfer, or D_h can be optimized using well-known heat transfer correlations based on design problem specifications. (5) Since $fRe = \text{constant}$, $f \propto 1/Re \propto 1/u_m$. In this case, it can be shown

TABLE 13.6 Solutions for Heat Transfer and Friction for Fully-Developed-Laminar-Flow Through Specified Ducts

Geometry ($L/D_h > 100$)	Nu_{H1}	Nu_{H2}	Nu_T	fRe	$\frac{j_{H1}^+ a}{f}$	$K(\infty)^b$	$L_{hy}^+{}^c$
 $\frac{2b}{2a} = \frac{\sqrt{3}}{2}$	3.014	1.474	2.39	12.630	0.269	1.739	0.040
 $\frac{2b}{2a} = \frac{\sqrt{3}}{2}$	3.111	1.892	2.47	13.333	0.263	1.818	0.040
 $\frac{2b}{2a} = 1$	3.608	3.091	2.976	14.227	0.286	1.433	0.090
	4.002	3.862	3.34	15.054	0.299	1.335	0.086
 $\frac{2b}{2a} = \frac{1}{2}$	4.123	3.017	3.391	15.548	0.299	1.281	0.085
	4.364	4.364	3.657	16.000	0.307	1.25	0.056
 $\frac{2b}{2a} = \frac{1}{4}$	5.331	2.94	4.439	18.233	0.329	1.001	0.078
 $\frac{2b}{2a} = \frac{1}{6}$	6.049	2.93	5.137	19.702	0.346	0.885	0.070
 $\frac{2b}{2a} = \frac{1}{8}$	6.490	2.94	5.597	20.585	0.355	0.825	0.063
 $\frac{2b}{2a} = 0$	8.235	8.235	7.541	24.000	0.386	0.674	0.011

^a $j_{H1}/f = Nu_{H1} Pr^{-1/3} / (fRe)$ with $Pr = 0.7$. Similarly, values of j_{H2}/f and j_T/f may be computed.
^b $K(\infty)$ for sine and equilateral triangular channels may be too high (Shah and London 1978); $K(\infty)$ for some rectangular and hexagonal channels is interpolated based on the recommended values in Shah and London (1978).
^c L_{hy}^+ for sine and equilateral triangular channels is too low (Shah and London 1978), so use with caution. L_{hy}^+ for rectangular channels is based on the faired curve drawn through the recommended value in Shah and London (1978). L_{hy}^+ for a hexagonal channel is an interpolated value.
 Source: From Shah and London, 1978. With permission.

that $\Delta p \propto u_m$. Many additional analytical results for fully-developed-laminar-flow ($Re \leq 2000$) are presented by Shah and London (1978); Shah and Bhatti (1987). The entrance effects, flow maldistribution, free convection, property variation, fouling, and surface roughness all affect fully-developed analytical solutions. In order to account for these effects in real plate-fin plain fin geometries having fully-developed flows, it is best to reduce the magnitude of the analytical Nu by at least 10% and to increase the value of the analytical fRe by 10% for design purposes.

The initiation of transition flow (the lower limit of the critical Reynolds number, Re_{crit}) depends on the type of entrance (e.g., smooth vs. abrupt configuration at the exchanger flow passage entrance). For a sharp square inlet configuration, Re_{crit} is about 10%–15% lower than that for a rounded inlet configuration. For most exchangers, the entrance configuration would be sharp. Some information on Re_{crit} is provided by Ghajar and Tam (1994).

Transition flow and fully-developed turbulent flow Fanning friction factors are given by Bhatti and Shah (1987) as

$$f = A + BRe^{-1/m} \quad (13.47)$$

where

$$\begin{aligned} A = 0.0054, \quad B = 2.3 \times 10^{-8}, \quad m = -2/3 \quad & \text{for } 2100 \leq Re \leq 4000 \\ A = 0.00128 \quad B = 0.1143 \quad m = 3.2154 \quad & \text{for } 4000 \leq Re \leq 10^7 \end{aligned}$$

Equation 13.47 is accurate within $\pm 2\%$ (Bhatti and Shah 1987). The transition flow and fully-developed turbulent flow Nusselt number correlation for a circular tube is given by Gnielinski as reported in Bhatti and Shah (1987) as

$$Nu = \frac{(f/2)(Re - 1000)Pr}{1 + 12.7(f/2)^{1/2}(Pr^{2/3} - 1)} \quad (13.48)$$

which is accurate within about $\pm 10\%$ with experimental data for $2300 \leq Re \leq 5 \times 10^6$ and $0.5 \leq Pr \leq 2000$. For higher accuracies in turbulent flow, refer to the correlations by Petukhov et al. reported by Bhatti and Shah (1987); Shah and Sekulić (2003). Churchill (1977) (see also Bhatti and Shah 1987) provides a correlation for laminar, transition, and turbulent flow regimes in a circular tube for $2100 < Re < 10^6$ and $0 < Pr < \infty$.

A careful observation of accurate experimental friction factors for all noncircular smooth ducts reveals that ducts with laminar $fRe < 16$ have turbulent f factors lower than those for the circular tube, whereas ducts with laminar $fRe > 16$ have turbulent f factors higher than those for the circular tube (Shah and Bhatti 1988). Similar trends are observed for the Nusselt numbers. If one is satisfied within $\pm 15\%$ accuracy, Equation 13.47 and Equation 13.48 for f and Nu can be used for noncircular passages with the hydraulic diameter as the characteristic length in f , Nu, and Re ; otherwise, refer to Table 13.7 for more accurate results for turbulent flow.

For hydrodynamically and thermally developing flows, the analytical solutions are boundary condition dependent (for laminar flow heat transfer only) and geometry dependent. The reader may refer to Shah and London (1978); Shah and Bhatti (1987), and Bhatti and Shah (1987) for specific solutions. The hydrodynamic entrance lengths L_{hy} for developing laminar and turbulent flow are given by Shah and Bhatti (1987); Bhatti and Shah (1987) as

$$\frac{L_{hy}}{D_h} = \begin{cases} 0.0565 Re & \text{for laminar flow } (Re \leq 2100) \\ 1.359 Re^{1/4} & \text{for turbulent flow } (Re > 10^4) \end{cases} \quad (13.49)$$

TABLE 13.7 Fully-Developed Turbulent Flow Friction Factors and Nusselt Numbers ($Pr > 0.5$) for Technically Important Smooth-Walled Ducts

Duct Geometry and Characteristic Dimension	Recommended Correlations ^a
$D_h = 2a$	Friction factor correlation for $2300 < Re < 10^7$ [41]: Where $A = 0.0054$, $B = 2.3 \times 10^{-8}$, $m = -2/3$ for $2100 < Re < 4000$ and $= 1.28 \times 10^{-3}$. $B = 0.1143$, $m = 3.2154$ for $4000 < Re < 10^7$ [41]. Nusselt number correlation by Gnielinski for $2300 < Re < 5 \times 10^6$: $Nu = \frac{(f/2)(Re - 1000)Pr}{1 + 12.7(f/2)^{1/2}(Pr^{2/3} - 1)}$
$D_h = 4b$	Use circular duct f and Nu correlations. Predicted f are up to 12.5% lower and predicted Nu are within $\pm 9\%$ of the most reliable experimental results. f factors: (1) substitute D_1 , for D_h in the circular duct correlation, and calculate f from the resulting equation. (2) Alternatively, calculate f from $f = (1.0875 - 0.1125 \alpha^*) f_c$, where f_c is the friction factor for the circular duct using D_h . In both cases, predicted f factors are within $\pm 5\%$ of the experimental results.
$D_h = \frac{4ab}{a+b}$, $\alpha^* = \frac{2b}{2a}$ $\frac{D_l}{D_h} = \frac{2}{3} + \frac{11}{24} \alpha^* (2 - \alpha^*)$	Nusselt numbers: (1) With uniform heating at four walls, use circular duct Nu correlation for an accuracy of $\pm 9\%$ for $0.5 \leq Pr \leq 100$ and $10^4 \leq Re \leq 10^6$. (2) With equal heating at two long walls, use circular duct correlation for an accuracy of $\pm 10\%$ for $0.5 \leq Pr \leq 10$ and $10^4 \leq Re \leq 10^5$. (3) With heating at one long wall only, use circular duct correlation to get approximate Nu values for $0.5 < Pr < 10$ and $10^4 \leq Re \leq 10^6$. These calculated values may be up to 20% higher than the actual experimental values
$D_h = 2\sqrt{3}a = 4b/3$ $D_l = \sqrt{3}a = 2b/3\sqrt{3}$ $D_h = \frac{4ab}{a + \sqrt{a^2 + 4b^2}}$	Use circular duct f and Nu correlations with D_h replaced by D_l , predicted f are within +3% and (11% and predicted Nu within +9% of the experimental values.
$\frac{D_g}{D_h} = \frac{1}{2\pi} \left[3 \ln \cot \frac{\theta}{2} + 2 \ln \tan \frac{\phi}{2} - \ln \tan \frac{\theta}{2} \right]$	Here $\theta = (90^\circ - \phi)/2$. For $0 < 2\phi < 60^\circ$, use circular duct f and Nu correlations with D_h replaced by D_g ; for $2\phi = 60^\circ$, replace D_h by D_l (see above); and for $60^\circ < 2\phi \leq 90^\circ$ use circular duct correlations directly with D_h . Predicted f and Nu are within +9% and 11% of the experimental values. No recommendations can be made for $2\phi > 90^\circ$ due to lack of the experimental data.
$D_h = 2(r_o - r_i)$ $r^* = \frac{r_i}{r_o}$ $\frac{D_l}{D_h} = \frac{1 + r^{*2} + (1 - r^{*2})/\ln r^*}{(1 - r^{*2})^2}$	f factors: (1) substitute D_l for D_h in the circular duct correlation, and calculate f from the resulting equation. (2) Alternatively, calculate f from $f = (1 + 0.0925 r^*) f_c$, where f_c is the friction factor for the circular duct using D_h . In both cases, predicted f factors are within $\pm 5\%$ of the experimental results. Nusselt numbers: In all the following recommendations, use D_h with a wetted perimeter in Nu and Re : (1) Nu at the outer wall can be determined from the circular duct correlation within the accuracy of about $\pm 10\%$ regardless of the condition at the inner wall. (2) Nu at the inner wall cannot be determined accurately using the circular tube correlation regardless of the heating/cooling condition at the outer wall.

^a The friction factor and Nusselt number correlations for the circular duct are the most reliable and agree with a large amount of the experimental data within $\pm 2\%$ and $\pm 10\%$, respectively. The correlations for all other duct geometries are not as good as those for the circular duct on an absolute basis.

Source: From Bhatti, M. S. and Shah, R. K., *Handbook of Single-Phase Convective Heat Transfer*, Kakaç, S. Shah, R. K. and Aung, W. ed. Wiley, New York, 1987. With permission.

13.4.3 Experimental Correlations

Analytical results presented in the preceding section are useful for well-defined constant cross-sectional surfaces with essentially unidirectional flows. The flows encountered in heat exchangers are generally very complex, having flow separation, reattachment, recirculation, and vortices. Such flows significantly affect Nu and f for the specific exchanger surfaces. Since no analytical or accurate numerical solutions are available, the information is derived experimentally; Kays and London (1998) and Webb (1994) present many of the experimental results reported in the open literature. Many of the geometries reported in these references have been fine-tuned, refined and made more compact with the advancement of manufacturing technologies. Hence the j (Nu) and f vs. Re data reported in these references have a limited use now since they cannot be used for accurate performance evaluation/prediction of modern surface geometries. In the following, empirical correlations for only some important surfaces are summarized due to space limitations.

13.4.3.1 Bare Tubebanks

Zukauskas (1987) has presented extensive experimental results for flow normal to inline and staggered plain and finned tube bundles in graphical form. Comprehensive pressure drop correlations for flow normal to inline and staggered *plain* tube bundles have been developed by Gaddis and Gnielinski (1985) and recast in terms of the Hagen number by Martin (2002) as follows.

$$Hg = \begin{cases} Hg_{\text{lam}} + Hg_{\text{turb},i} \left[1 - \exp \left(1 - \frac{Re_d + 1000}{2000} \right) \right] & \text{inline tube bundles} \\ Hg_{\text{lam}} + Hg_{\text{turb},s} \left[1 - \exp \left(1 - \frac{Re_d + 200}{1000} \right) \right] & \text{staggered tube bundles} \end{cases} \quad (13.50)$$

where

$$Hg_{\text{lam}} = 140Re_d \frac{(X_\ell^{*0.5} - 0.6)^2 + 0.75}{X_t^{*1.6}(4X_t^*X_\ell^*/\pi - 1)} \quad (13.51)$$

Equation 13.51 is valid for all inline tube bundles. It is also valid for staggered tube bundles except that the term $X_t^{*1.6}$ needs to be changed to $X_d^{*1.6}$ when the minimum free flow area occurs in the diagonal planes of the staggered tube bundle, i.e., $X_\ell^* < 0.5(2X_t^* + 1)^{1/2}$.

$$Hg_{\text{turb},i} = \left[\left\{ 0.11 + \frac{0.6(1 - 0.94/X_\ell^*)^{0.6}}{(X_t^* - 0.85)^{1.3}} \right\} \times 10^{0.47(X_\ell^*/X_t^* - 1.5)} + 0.015(X_t^* - 1)(X_\ell^* - 1) \right] \times Re_d^2 - 0.1(X_t^*/X_\ell^*) + \phi_{t,n}Re_d^2 \quad (13.52)$$

$$Hg_{\text{turb},s} = \left[\left\{ 1.25 + \frac{0.6}{(X_t^* - 0.85)^{1.08}} \right\} + 0.2 \left(\frac{X_\ell^*}{X_t^*} - 1 \right)^3 - 0.005 \left(\frac{X_t^*}{X_\ell^*} - 1 \right)^3 \right] Re_d^{1.75} + \phi_{t,n}Re_d^2 \quad (13.53)$$

Equation 13.53 is valid for $Re_d \leq 250,000$. For higher Re_d , correct $Hg_{turb,s}$ of Equation 13.53 as follows.

$$Hg_{turb,s,corr} = Hg_{turb,s} \left(1 + \frac{Re_d - 250,000}{325,000} \right) \quad \text{for } Re_d > 250,000 \quad (13.54)$$

$$\phi_{t,n} = \begin{cases} \frac{1}{2X_t^{*2}} \left(\frac{1}{N_r} - \frac{1}{10} \right) & \text{for } 5 \leq N_r \leq 10 \quad \text{and} \quad X_\ell^* \geq 0.5(2X_t^* + 1)^{1/2} \\ 2 \left[\frac{(X_d^* - 1)}{X_t^*(X_t^* - 1)} \right]^2 \left(\frac{1}{N_r} - \frac{1}{10} \right) & \text{for } 5 \leq N_r \leq 10 \quad \text{and} \quad X_\ell^* < 0.5(2X_t^* + 1)^{1/2} \end{cases} \quad (13.55)$$

and $\phi_{t,n} = 0$ for $N_r > 10$ and N_r is the number of tube rows in the flow direction. It should be emphasized that $\phi_{t,n} Re_d^2$ takes into account the influence of tube bundle inlet and outlet pressure losses while the first bracketed [] terms on the right-hand sides of Equation 13.52 and Equation 13.53 take into account the frictional pressure loss in the tube bundle. For the total pressure loss of a tube bundle, the complete Equation 13.52 or Equation 13.53 should be used, i.e., both terms on the right-hand sides of these equations should be included.

The foregoing correlation of Equation 13.50 is valid for $1 < Re_d < 300,000$ and $N_r \geq 5$ for both inline and staggered tube bundles: $1.25 \leq X_t^* \leq 3.0$, and $1.2 \leq X_\ell^* \leq 3.0$ for inline tube bundle, and $1.25 \leq X_t^* \leq 3.0$, $0.6 \leq X_\ell^* \leq 3.0$ and $X_d^* \geq 1.25$ for staggered tube bundles. The experimental data for this correlation had $7.9 \leq d_0 \leq 73$ mm.

The pressure drop for the flow normal to the tube bundle is then computed from

$$\Delta p = \frac{\mu^2}{\rho g_c} \frac{N_r}{d_0^2} Hg \quad (13.56)$$

Note that only when the minimum flow area occurs in the diagonals for a staggered tube bundle, the term N_r should be replaced by $N_r - 1$ considering the number of flow resistances in the diagonal flow area.

In all correlations for heat transfer and pressure drop for tube bundles, $Re_d = \rho u_m d_0 / \mu$, where

$$u_m = \begin{cases} u_\infty \frac{X_t^*}{X_t^* - 1} & \text{inline tube bundles} \\ u_\infty \frac{X_t^*}{X_t^* - 1} & \text{staggered tube bundles with } X_\ell^* \geq 0.5(2X_t^* + 1)^{1/2} \\ u_\infty \frac{X_t^*}{2(X_d^* - 1)} & \text{staggered tube bundles with } X_\ell^* < 0.5(2X_t^* + 1)^{1/2} \end{cases} \quad (13.57)$$

Martin (2002) developed comprehensive correlations for heat transfer with flow normal to inline and staggered plain tube bundles as follows.

$$Nu = \begin{cases} 0.404 Lq^{1/3} \left(\frac{Re_d + 1}{Re_d + 1000} \right)^{0.1} & \text{inline tube bundles} \\ 0.404 Lq^{1/3} & \text{staggered tube bundles} \end{cases} \quad (13.58)$$

where

$$Lq = \begin{cases} 1.18 \text{ Hg Pr} \left(\frac{(4X_t^*/\pi) - 1}{X_\ell^*} \right) & \text{inline tube bundles} \\ 0.92 \text{ Hg Pr} \left(\frac{(4X_t^*/\pi) - 1}{X_d^*} \right) & \text{staggered tube bundles with } X_\ell^* \geq 1 \\ 0.92 \text{ Hg Pr} \left(\frac{(4X_t^* X_\ell^*/\pi) - 1}{X_\ell^* X_d^*} \right) & \text{staggered tube bundles with } X_\ell^* < 1 \end{cases} \quad (13.59)$$

where Hg is obtained from Equation 13.50. Note that no explicit definition of the Lévéque number Lq is required here. Refer to Shah and Sekulić (2003) for further details.

The foregoing heat transfer correlation of Equation 13.58 is valid for $1 < Re_d < 2,000,000$, $0.7 \leq Pr \leq 700$ (validity expected for $Pr > 700$, but not for $Pr < 0.6$) and $2 \leq N_r \leq 15$ for inline tube bundles (90° tube bundles) and $4 \leq N_r \leq 80$ for staggered tube bundles ($30, 45, 60^\circ$ tube bundles and other staggered tube bundles within the correlation tube pitch ranges); the tube pitch ratio ranged $1.02 \leq X_t^* \leq 3.0$ and $0.6 \leq X_\ell^* \leq 3.0$ for both inline and staggered tube bundles. The experimental data for this correlation had $7.9 \leq d_0 \leq 73$ mm. The Nusselt numbers are predicted accurately within $\pm 20\%$ for inline tube bundles and $\pm 14\%$ for staggered tube bundles using Equation 13.58 where the Hagen number Hg of Equation 13.59 is determined from the Gaddis and Gnielinski correlation of Equation 13.50. The Nusselt number prediction may be better if the experimental friction factors are used. Note that when the Gaddis and Gnielinski correlation is extrapolated outside their ranges of Re_d and N_r for Nu calculations, it has predicted Nu within the accuracy mentioned.

13.4.3.2 Plate-Fin Extended Surfaces

Offset Strip Fins. This is one of the most widely used enhanced fin geometries [Figure 13.9](#) in aircraft, cryogenics, and many other industries that do not require automotive type mass production. This surface has one of the highest heat transfer performance relative to the pressure drop. Extensive analytical, numerical, and experimental investigations have been conducted over the last 50 years. The most comprehensive correlations for j and f factors for the *offset* strip fin geometry are provided by Manglik and Bergles (1995) as follows:

$$j = 0.6522 \text{ Re}^{-0.5403} \left(\frac{s}{h'} \right)^{-0.1541} \left(\frac{\delta_f}{\ell_f} \right)^{0.1499} \left(\frac{\delta_f}{s} \right)^{-0.0678} \left[1 + 5.269 \times 10^{-5} \text{ Re}^{1.340} \left(\frac{s}{h'} \right)^{0.504} \left(\frac{\delta_f}{\ell_f} \right)^{0.456} \left(\frac{\delta_f}{s} \right)^{-1.055} \right]^{0.1} \quad (13.60)$$

$$f = 9.6243 \text{ Re}^{-0.7422} \left(\frac{s}{h'} \right)^{-0.1856} \left(\frac{\delta_f}{\ell_f} \right)^{0.3053} \left(\frac{\delta_f}{s} \right)^{-0.2659} \left[1 + 7.669 \times 10^{-8} \text{ Re}^{4.429} \left(\frac{s}{h'} \right)^{0.920} \left(\frac{\delta_f}{\ell_f} \right)^{3.767} \left(\frac{\delta_f}{s} \right)^{0.236} \right]^{0.1} \quad (13.61)$$

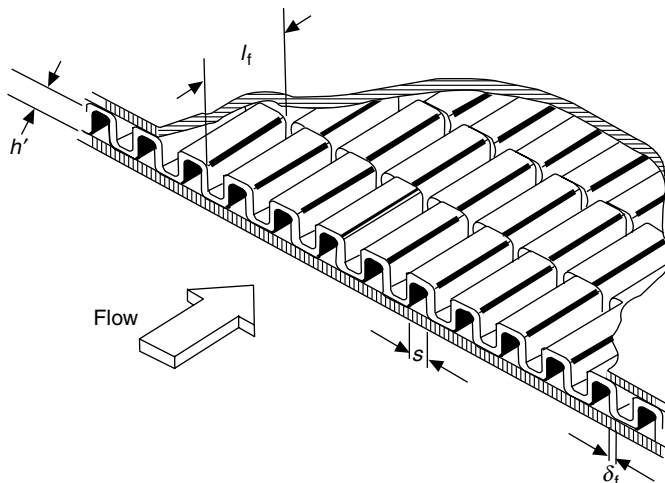


FIGURE 13.9 An offset strip fin geometry.

where

$$D_h = \frac{4A_{0,cell}}{A_{cell}/\ell_f} = \frac{4sh'\ell_f}{2(s\ell_f + h'\ell_f + h'\delta_f) + s\delta_f} \tag{13.62}$$

Geometrical symbols in Equation 13.62 are shown in Figure 13.9.

These correlations predict the experimental data of 18 test cores within $\pm 20\%$ for $120 \leq Re \leq 10^4$. Although all the experimental data for these correlations are obtained for air, the j factor takes into consideration minor variations in the Prandtl number, and the correlations should be valid for $0.5 < Pr < 15$.

Louver Fins. Louver or multilouver fins are extensively used in the auto industry due to their mass production manufacturability and hence lower cost. It has generally higher j and f factors than those for the offset strip fin geometry, and the increase in the friction factors is in general higher than the increase in the j factors. However, the exchanger can be designed for higher heat transfer and the same pressure drop compared to that with the offset strip fins by a proper selection of exchanger frontal area, core depth, and fin density. Published literature and correlations on the louver fins are summarized by Webb (1994); Cowell, Heikal, and Achaichia (1995), and the understanding of flow and heat transfer phenomena is summarized by Cowell, Heikal, and Achaichia (1995). The correlation for the Colburn factors for the corrugated louver fins (see Figure 13.10), based on an extensive database for *airflow* over louver fins, is obtained by Chang and Wang (1997) and Wang (2000) as follows.

$$j = Re_{\ell_p}^{-0.49} \left(\frac{\theta}{90}\right)^{0.27} \left(\frac{p_f}{\ell_p}\right)^{-0.14} \left(\frac{b}{\ell_p}\right)^{-0.29} \left(\frac{W_t}{\ell_p}\right)^{-0.23} \left(\frac{\ell_\ell}{\ell_p}\right)^{0.68} \left(\frac{p_t}{\ell_p}\right)^{-0.28} \left(\frac{\delta}{\ell_p}\right)^{-0.05} \tag{13.63}$$

where $Re_{\ell_p} = G\ell_p/\mu$ represents the Reynolds number based on the louver pitch ℓ_p . Also, θ is the louver angle, deg; p_f is the fin pitch, mm; b is the vertical fin height, mm; W_t is the tube outside width (= total fin length in the airflow direction if no overhangs), mm; ℓ_ℓ is the louver cut length, mm; p_t is the tube pitch, mm; δ is the fin thickness, mm. These symbols are shown in Figure 13.10.

Equation 13.63 and Equation 13.65 are valid for the following ranges of the parameters: $0.82 \leq D_h \leq 5.02$ mm, $0.51 \leq p_f \leq 3.33$ mm, $0.5 \leq \ell_p \leq 3$, $2.84 \leq b \leq 20$ mm, $15.6 \leq W_t \leq 57.4$ mm, $2.13 \leq \ell_\ell \leq 18.5$ mm, $7.51 \leq p_t \leq 25$ mm, $0.0254 \leq \delta \leq 0.16$ mm, $1 \leq N \leq 2$, and $8.4 \leq \theta \leq 35^\circ$. This

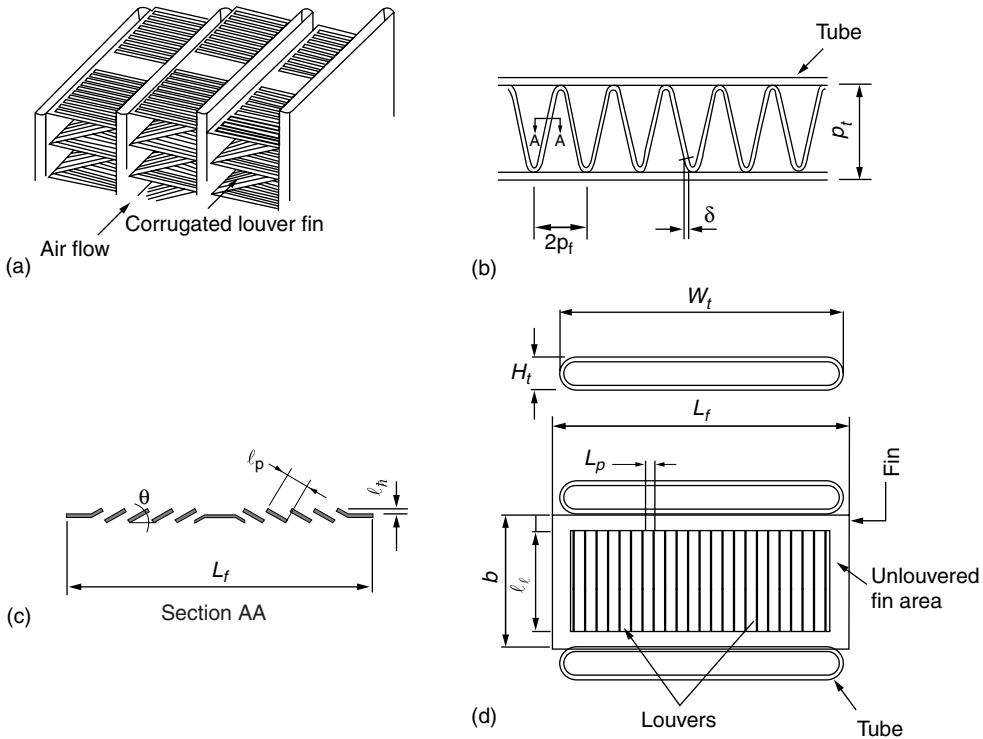


FIGURE 13.10 Definition of geometrical parameters of corrugated louver fins. (From Chang and Wang 1997. With permission.)

correlation predicts 89% of experimental j factors for 91 test cores within $\pm 15\%$ for $30 < Re_{\rho} < 5000$ with a mean deviation of 8%.

Chang and Wang (1997) also presented a simplified correlation for Equation 13.63 as

$$j = 0.425 Re_{\rho}^{-0.496} \tag{13.64}$$

They report that this correlation predicts 88% of data points within $\pm 25\%$ with the mean deviation of 13%.

The correlation for the Fanning friction factor based on the same database by Chang et al. (2000) as follows.

$$f = f_1 f_2 f_3 \tag{13.65}$$

where

$$f_1 = \begin{cases} 14.39 Re_{\rho}^{(-0.805 p_f/b)} \{ \ln [1.0 + (p_f/l_p)] \}^{3.04} & Re_{\rho} < 150 \\ 4.97 Re_{\rho}^{(0.6049 - 1.064/\theta^{0.2})} \{ \ln [(\delta/p_f)^{0.5} + 0.9] \}^{-0.527} & 150 < Re_{\rho} < 5000 \end{cases} \tag{13.66}$$

$$f_2 = \begin{cases} \left\{ \ln \left[(\delta/p_f)^{0.48} + 0.9 \right] \right\}^{-1.435} (D_h/\ell_p)^{-3.01} \left[\ln \left(0.5 \text{Re}_{\ell_p} \right) \right]^{-3.01} & \text{Re}_{\ell_p} < 150 \\ \left[(D_h/\ell_p) \ln(0.3 \text{Re}_{\ell_p}) \right]^{-2.966} (p_f/\ell_\ell)^{-0.7931} (p_t/b) & 150 < \text{Re}_{\ell_p} < 5000 \end{cases} \quad (13.67)$$

$$f_3 = \begin{cases} (p_f/\ell_\ell)^{-0.308} (L_f/\ell_\ell)^{-0.308} \left(e^{-0.1167 p_t/H_t} \right) \theta^{0.35} & \text{Re}_{\ell_p} < 150 \\ (p_t/H_t)^{-0.0446} \left\{ \ln \left[1.2 + (\ell_p/p_f)^{1.4} \right] \right\}^{-3.553} \theta^{-0.477} & 150 < \text{Re}_{\ell_p} < 5000 \end{cases} \quad (13.68)$$

Additional parameters for the friction factor correlations are: D_h is the hydraulic diameter of the fin geometry, mm; H_t is the tube outside height, mm; and L_f is the fin length in the airflow direction, mm. Note that θ in Equation 13.66 and Equation 13.68 are in degrees. The conventional definition of the hydraulic diameter ($D_h = 4A_0/\bar{P}$) is used in Equation 13.67 considering as if the louver fins were plain fins (without cuts) for the calculation of A_0 and A which is an excellent approximation considering the path of heat flow ideally not obstructed by the louvers; the effect of the braze fillets has also been neglected since no such information is available in the open literature. The correlation of Equation 13.65 predicts 83% of the experimental friction factor data points within $\pm 15\%$ with a mean deviation of 9% for the parameter ranges the same as those for Equation 13.63.

Note that the authors included the tube width W_t in the heat transfer correlation (to take into account the correct surface area). However, they used the fin length L_f for the friction factor correlation since the friction factor f of Equation 13.65 is for the fin friction component only (excluding entrance and exit pressure losses from the measured pressure drops).

13.4.3.3 Tube-Fin Extended Surfaces

Two major types of tube-fin extended surfaces are (1) individually finned tubes and (2) flat fins (also sometimes referred to as plate fins) with or without enhancements/interruptions on an array of tubes as shown in Figure 13.6. Extensive coverage of the published literature and correlations for these extended surfaces are provided by Webb (1994), Kays and London (1998), and Rozenman (1976). Empirical correlations for some important geometries are summarized next.

Individually Finned Tubes. This fin geometry, helically wrapped (or extruded) circular fins on a circular tube as shown in Figure 13.6a, is commonly used in process and waste heat recovery industries. The following correlation for j factors is recommended by Briggs and Young (see Webb 1994) for individually finned tubes on staggered tubebanks.

$$j = 0.134 \text{Re}_d^{-0.319} \left(\frac{s}{\ell_f} \right)^{0.2} \left(\frac{s}{\delta_f} \right)^{0.11} \quad (13.69)$$

where $\ell_f [= (d_e - d_0)/2]$ is the radial height of the fin, δ_f is the fin thickness, $s = p_f - \delta_f$ is the distance between adjacent fins, and p_f is the fin pitch. Equation 13.69 is valid for the following ranges: $1100 \leq \text{Re}_d \leq 18,000$, $0.13 \leq s/\ell_f \leq 0.63$, $1.01 \leq s/\delta_f \leq 7.62$, $0.09 \leq \ell_f/d_0 \leq 0.69$, $0.011 \leq \delta_f/d_0 \leq 0.15$, $1.54 \leq X_\lambda/d_0 \leq 8.23$, fin root diameter d_0 between 11.1 and 40.9 mm, and fin density $N_f (= 1/p_f)$ between 246 and 768 fins per meter. All data have been obtained on equilateral triangular tube bundle (Shah and Sekulić 2003). The standard deviation of Equation 13.69 with experimental results is 5.1%.

For friction factors, Robinson and Briggs (see Webb 1994) recommended the following correlation.

$$f_{tb} = 9.465 \text{Re}_d^{-0.316} \left(\frac{X_t}{d_0} \right)^{-0.927} \left(\frac{X_t}{X_\lambda} \right)^{0.515} \quad (13.70)$$

Here, $X_d = (X_t^2 + X_\lambda^2)^{1/2}$ is the diagonal pitch and X_t and X_λ are the transverse and longitudinal tube

itches, respectively. The correlation is valid for the following ranges: $2000 \leq Re_d \leq 50,000$, $0.15 \leq s/\ell_f \leq 0.19$, $3.75 \leq s/\delta_f \leq 6.03$, $0.35 \leq \ell_f/d_0 \leq 0.56$, $0.011 \leq \delta_f/d_0 \leq 0.025$, $1.86 \leq X_t/d_0 \leq 4.60$, $18.6 \leq d_0 \leq 40.9$ mm, and $311 \leq N_f \leq 431$ fins per meter. The standard deviation of Equation 13.44 with correlated data is 7.8%.

For crossflow over low-height finned tubes, Rabas and Taborek (1987); Ganguli and Yilmaz (1987), and Chai (1988) have assessed the pertinent literature. A simple but accurate correlation for heat transfer is given by Ganguli and Yilmaz (1987) as

$$j = 0.255 Re_d^{-0.3} \left(\frac{d_e}{s} \right)^{-0.3} \quad (13.71)$$

A more accurate correlation for heat transfer is given by Rabas and Taborek (1987). Chai (1988) provides the best correlation for friction factors:

$$f_{tb} = 1.748 Re_d^{-0.233} \left(\frac{\ell_f}{s} \right)^{0.552} \left(\frac{d_0}{x_t} \right)^{0.599} \left(\frac{d_0}{x_t} \right)^{0.1738} \quad (13.72)$$

This correlation is valid for $895 < Re_d < 713,000$, $20 < \theta < 40^\circ$, $X_t/d_0 < 4$, and $N \geq 4$, and θ is the tube layout angle. It predicts 89 literature data points within a mean absolute error of 6%; the range of actual error is from -16.7 to 19.9% . An alternative correlation for friction factor is given by Ganguli and Yilmaz (1987), and is summarized by Shah and Sekulić (2003).

Plain Flat Fins on a Staggered Tubebank. This geometry, as shown in Figure 13.6b, is used in the air-conditioning/refrigeration industry as well as where the pressure drop on the fin side prohibits the use of enhanced flat fins. An inline tubebank is generally not used unless fin side very low pressure drop is the essential requirement. Heat transfer correlation for Figure 13.6b flat plain fins on staggered tubebanks is provided by Wang and Chi (2000) and summarized by Wang (2000) as follows.

$$j = \begin{cases} 0.108 Re_{dc}^{-0.29} \left(\frac{X_t}{X_\ell} \right)^{c_1} \left(\frac{p_f}{d_c} \right)^{-1.084} \left(\frac{p_f}{D_h} \right)^{-0.786} \left(\frac{p_f}{X_t} \right)^{c_2} & \text{for } N_f = 1 \\ 0.086 Re_{dc}^{c_3} N_f^{c_4} \left(\frac{p_f}{d_c} \right)^{c_5} \left(\frac{p_f}{D_h} \right)^{c_6} \left(\frac{p_f}{X_t} \right)^{-0.93} & \text{for } N_f \geq 2 \end{cases} \quad (13.73)$$

where

$$c_1 = 1.9 - 0.23 \ln(Re_{dc}) \quad c_2 = -0.236 + 0.126 \ln(Re_{dc}) \quad (13.74a)$$

$$c_3 = -0.361 - \frac{0.042 N_f}{\ln(Re_{dc})} + 0.158 \ln \left[N_f \left(\frac{p_f}{d_c} \right)^{0.41} \right] \quad c_4 = -1.224 - \frac{0.076(X_\ell/D_h)^{1.42}}{\ln(Re_{dc})} \quad (13.74b)$$

$$c_5 = -0.083 + \frac{0.058 N_f}{\ln(Re_{dc})} \quad c_6 = -5.735 + 1.21 \ln \left(\frac{Re_{dc}}{N_f} \right) \quad (13.74c)$$

where p_f is the fin pitch, d_c is the collar diameter of the fin, and $Re_{dc} = \rho u_m d_c / \mu$. This j factor correlation predicts 89% of the test points of 74 cores within $\pm 15\%$ with a mean deviation of 8%. Wang and Chi (2000) also provided the following correlation for the friction factors.

$$f = 0.0267 \operatorname{Re}_{dc}^{c_7} \left(\frac{X_t}{X_\ell}\right)^{c_8} \left(\frac{p_f}{d_c}\right)^{c_9} \tag{13.75}$$

where

$$c_7 = -0.764 + 0.739 \left(\frac{X_t}{X_\ell}\right) + 0.177 \left(\frac{p_f}{d_c}\right) - \frac{0.00758}{N_r} \tag{13.76a}$$

$$c_8 = -15.689 + \frac{64.021}{\ln(\operatorname{Re}_{dc})} \quad c_9 = 1.696 - \frac{15.695}{\ln(\operatorname{Re}_{dc})} \tag{13.76b}$$

Equation 13.73 and Equation 13.75 are valid for the following ranges of the parameters: $300 \leq \operatorname{Re}_{dc} \leq 20,000$, $6.9 \leq d_c \leq 13.6$ mm, $1.30 \leq D_h \leq 9.37$ mm, $20.4 \leq X_t \leq 31.8$, $12.7 \leq X_\ell \leq 32$ mm, $1.0 \leq p_f \leq 8.7$ mm, and $1 \leq N_r \leq 6$. This friction factor correlation of Equation 13.75 predicts 85% of experimental friction factors of 74 test cores within $\pm 15\%$ with a mean deviation of 8%.

Corrugated Flat Fins on a Tube Array. There are a number of variations available for flat fins with a sharp vs. smooth wave. The specific flat-fin geometry shown in Figure 13.11 is designated as a corrugated (herringbone or sharp-wave) fin. The heat transfer and flow friction correlations are developed by Wang (2000) and presented separately for large and small diameter tubes as follows. For larger tube diameters ($d_0 = 12.7$ and 15.88 mm, before tube expansion), the following are the correlations.

$$j = 1.7910 \operatorname{Re}_{dc}^{c_1} \left(\frac{X_\ell}{\delta}\right)^{-0.456} N_r^{-0.27} \left(\frac{p_f}{d_c}\right)^{-1.343} \left(\frac{p_d}{x_f}\right)^{0.317} \tag{13.77}$$

$$f = 0.05273 \operatorname{Re}_{dc}^{c_2} \left(\frac{p_d}{x_f}\right)^{c_3} \left(\frac{p_f}{X_t}\right)^{c_4} \left[\ln\left(\frac{A}{A_{p,t}}\right)\right]^{-2.726} \left(\frac{D_h}{d_c}\right)^{0.1325} N_r^{0.02305} \tag{13.78}$$

where

$$c_1 = -0.1707 - 1.374 \left(\frac{X_\ell}{\delta}\right)^{-0.493} \left(\frac{p_f}{d_c}\right)^{-0.886} N_r^{-0.143} \left(\frac{p_d}{x_f}\right)^{-0.0296} \tag{13.79a}$$

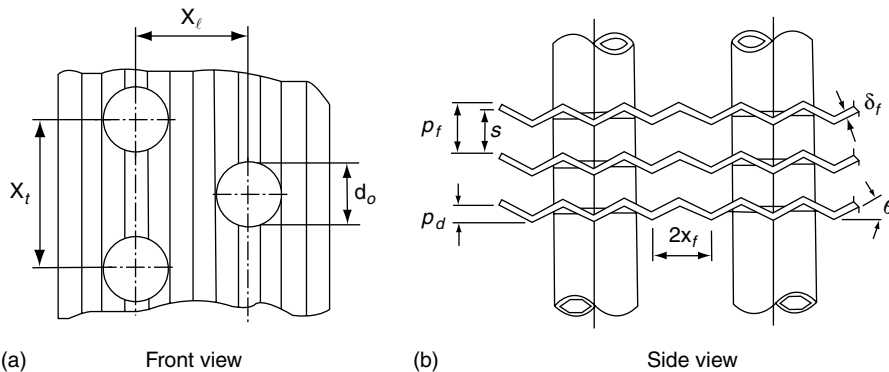


FIGURE 13.11 Corrugated fins on a staggered tube array.

$$c_2 = 0.1714 - 0.07372 \left(\frac{p_f}{X_\ell} \right)^{0.25} \left(\ln \frac{A}{A_{p,t}} \right) \left(\frac{p_d}{x_f} \right)^{-0.2} \quad (13.79b)$$

$$c_3 = 0.426 \left(\frac{p_f}{X_t} \right)^{0.3} \ln \left(\frac{A}{A_{p,t}} \right) \quad c_4 = -\frac{10.2192}{\ln(\text{Re}_{dc})} \quad (13.79c)$$

Here, x_f is the projected fin pattern length for one-half wave length, p_d is the fin pattern depth, peak-to-valley distance excluding fin thickness (as shown in Figure 13.11), and $A_{p,t}$ is the tube outside surface area when there are no fins. Equation 13.77 and Equation 13.78 are valid for the following ranges of the parameters: $500 \leq \text{Re}_{dc} \leq 10,000$, $3.63 \leq D_h \leq 7.23$ mm, $13.6 \leq d_c \leq 16.85$ mm, $31.75 \leq X_t \leq 38.1$, $27.5 \leq X_\ell \leq 33$ mm, $2.98 \leq p_f \leq 6.43$ mm, $1 \leq N_r \leq 6$, $12.3 \leq \theta \leq 14.7^\circ$, $6.87 \leq x_f \leq 8.25$ mm, and $p_d = 1.8$ mm. The correlation of Equation 13.77 predicts 93% of experimental Colburn factors for 18 test cores within $\pm 10\%$ with a mean deviation of 4%. Similarly, the correlation of Equation 13.78 predicts 92% of experimental friction factors for 18 test cores within $\pm 10\%$ with a mean deviation of 5%.

For smaller diameter tubes ($d_0 = 7.94$ and 9.53 mm before tube expansion), the following are the correlations for j and f factors.

$$j = 0.324 \text{Re}_{dc}^{c_1} \left(\frac{p_f}{X_\ell} \right)^{c_2} (\tan \theta)^{c_3} \left(\frac{X_\ell}{X_t} \right)^{c_4} N_r^{0.428} \quad (13.80)$$

$$f = 0.01915 \text{Re}_{dc}^{c_5} (\tan \theta)^{c_6} \left(\frac{p_f}{X_\ell} \right)^{c_7} \left[\ln \left(\frac{A}{A_{p,t}} \right) \right]^{-5.35} \left(\frac{D_h}{d_c} \right)^{1.3796} N_r^{-0.0916} \quad (13.81)$$

where

$$c_1 = -0.229 + 0.115 \left(\frac{p_f}{D_c} \right)^{0.6} \left(\frac{X_\ell}{D_h} \right)^{0.54} N_r^{-0.284} \ln(0.5 \tan \theta) \quad (13.82a)$$

$$c_2 = -0.251 + \frac{0.232 N_r^{1.37}}{\ln(\text{Re}_{dc}) - 2.303} \quad c_3 = -0.439 \left(\frac{p_f}{D_h} \right)^{0.09} \left(\frac{X_\ell}{X_t} \right)^{-1.75} N_r^{-0.93} \quad (13.82b)$$

$$c_4 = 0.502 [\ln(\text{Re}_{dc}) - 2.54] \quad c_5 = 0.4604 - 0.01336 \left(\frac{p_f}{X_\ell} \right)^{0.58} \left(\ln \frac{A}{A_{p,t}} \right) (\tan \theta)^{-1.5} \quad (13.82c)$$

$$c_6 = 3.247 \left(\frac{p_f}{X_t} \right)^{1.4} \ln \left(\frac{A}{A_{p,t}} \right) \quad c_7 = -\frac{20.113}{\ln(\text{Re}_{dc})} \quad (13.82d)$$

Equation 13.80 and Equation 13.81 are valid for the following ranges of the parameters: $300 \leq \text{Re}_{dc} \leq 8000$, $1.53 \leq D_h \leq 4.52$ mm, $8.58 \leq d_0 \leq 10.38$ mm, $X_t = 25.4$ mm, $19.05 \leq X_\ell \leq 25.04$ mm, $1.21 \leq p_f \leq 3.66$ mm, $1 \leq N_r \leq 6$, $14.5 \leq \theta \leq 18.5^\circ$, $4.76 \leq x_f \leq 6.35$ mm, and $1.18 \leq p_d \leq 1.68$ mm. The correlation of Equation 13.80 predicts 95% of experimental Colburn factors for 27 test cores within $\pm 15\%$ with a mean deviation of 6%. Similarly, the correlation of Equation 13.81 predicts 97% of experimental friction factors for data points of 27 test cores within $\pm 15\%$ with a mean deviation of 5%.

13.4.3.4 Regenerator Surfaces

Two most common types of regenerator surfaces are: (1) continuous cylindrical passages for rotary regenerators and some compact fixed-matrix regenerators and (2) randomly packed woven screens, crossed rods, and packed beds using a variety of materials.

For compact regenerators, the continuous cylindrical flow passages have simple geometries, such as triangular, rectangular, and hexagonal passages. The Nu and f factors of Table 13.6 are a valuable baseline for such passages. Due to the differences in the ideal geometries and boundary conditions compared to the actual ones, London, Young, and Stang (1970) presented the following correlations for air flow through triangular passages ($40 < Re < 800$).

$$f = \frac{14.0}{Re} \quad j = \frac{3.0}{Re} \quad (13.83)$$

London and Shah (1973) presented the following correlations for air flow through hexagonal passages ($80 < Re < 800$).

$$f = \frac{17.0}{Re} \quad j = \frac{4.0}{Re} \quad (13.84)$$

Refer to Shah and Sekulić (2003) for the correlations for crossed rod geometries.

13.5 Heat Transfer and Pressure Drop Correlations—Two-Phase Flows

13.5.1 Two-Phase Pressure Drop Correlations

In most compact heat exchanger applications, the pressure drop per unit length or pressure gradient along the flow length is practically constant in single-phase flows. Hence, we generally work directly with the pressure drop in single-phase flows. However, due to the phase change during condensation or vaporization, the pressure gradient within the fluid changes considerably along the flow path or axial length. The pressure drop in the phase-change fluid can then be computed by integrating the nonlinear pressure gradient along the flow path. Hence, the pressure drop computation is somewhat more complicated in two-phase flows.

The total local pressure gradient in two-phase flow through a constant cross-sectional duct can be calculated, based on a homogeneous model, as follows:

$$\frac{dp}{dz} = \frac{dp_{fr}}{dz} + \frac{dp_{mo}}{dz} + \frac{dp_{gr}}{dz} \quad (13.85)$$

where the three terms on the right-hand side correspond to the contributions by friction, momentum rate change, and gravity denoted by the subscripts fr , mo , and gr , respectively. The entrance and exit pressure loss terms of single-phase flow (see Equation 13.28) are lumped into the Δp_{fr} term since the information about these contributions is not available, due to the difficulty in measurements and small contribution. The in-tube two-phase frictional pressure drop is computed from the corresponding pressure drop for single-phase flow as follows using the two-phase friction multiplier denoted as ϕ^2 :

$$\left(\frac{dp}{dz}\right)_{fr} = \frac{4f_{lo}G^2}{2g_c\rho_l D_h} \phi_{lo}^2 \quad \text{where} \quad \phi_{lo}^2 = \frac{(dp/dz)_{fr}}{(dp/dz)_{fr,lo}} \quad (13.86)$$

where f_{lo} is the single-phase Fanning friction factor (see Table 13.6 and Table 13.7) based on the total mass flow rate as liquid and G is also based on the total mass flow rate as liquid; this means that the subscript “lo” indicates the two-phase flow considered as all liquid flow.

Alternatively, $(dp/dz)_{fr}$ is determined using the liquid or vapor-phase pressure drop multiplier as follows:

$$\left(\frac{dp}{dz}\right)_{fr} = \left(\frac{dp}{dz}\right)_{fr,l} \varphi_l^2 = \left(\frac{dp}{dz}\right)_{fr,g} \varphi_g^2 \tag{13.87}$$

where

$$\varphi_l^2 = \frac{(dp/dz)_{fr}}{(dp/dz)_{fr,l}} \quad \varphi_g^2 = \frac{(dp/dz)_{fr}}{(dp/dz)_{fr,g}} \quad \left(\frac{dp}{dz}\right)_{fr,l} = \frac{4f_l G^2}{2g_c \rho_l D_h} \quad \left(\frac{dp}{dz}\right)_{fr,g} = \frac{4f_g G^2}{2g_c \rho_g D_h} \tag{13.88}$$

where the subscripts l and g denote liquid and gas/vapor phases, respectively. φ_l^2 and φ_g^2 are functions of the parameter X (*Martinelli parameter*). φ_{go}^2 (defined similar to φ_{lo}^2 of Equation 13.86, with the subscript lo replaced by go) is a function of Y (*Chisholm parameter*). The X and Y are defined as follows:

$$X^2 = \frac{(dp/dz)_{fr,l}}{(dp/dz)_{fr,g}} \quad Y^2 = \frac{(dp/dz)_{fr,go}}{(dp/dz)_{fr,lo}} \tag{13.89}$$

Here, the subscript go means the total two-phase flow considered as all gas flow. The correlations to determine the two-phase frictional pressure gradient are presented in Table 13.8 for various ranges of G and μ_l/μ_g (Kandlikar, Shoji, and Dhir 1999, p. 228).

TABLE 13.8 Frictional Multiplier Correlations Used for Determining the Two-Phase Frictional Pressure Gradient in Equation 13.86

Correlation	Parameters
Friedel correlation (1979) for $\mu_l/\mu_g > 1000$ and all values of G: $\varphi_{go}^2 = E + \frac{3.24FH}{Fr^{0.045} We^{0.035}}$	$E = (1-x)^2 + x^2 \frac{\rho_l}{\rho_g} \frac{f_{go}}{f_{lo}}$ $F = x^{0.78}(1-x)^{0.24}$
Accuracy for annular flow: $\pm 21\%$ Ould Didi et al. (2002)	$H = \left(\frac{\rho_l}{\rho_g}\right)^{0.91} \left(\frac{\mu_g}{\mu_l}\right)^{0.19} \left(1 - \frac{\mu_g}{\mu_l}\right)^{0.7}$ $Fr = \frac{G^2}{g d_i \rho_{hom}^2}$ $We = \frac{G^2 d_i}{\rho_{hom} \sigma}$ $\frac{1}{\rho_{hom}} = \frac{x}{\rho_g} + \frac{1-x}{\rho_l}$ $\sigma =$ surface tension (N/m)
Chisholm correlation (1973) for $\mu_l/\mu_g > 1000$ and $G > 100$ kg/m ² s: Accuracy for annular flow: $\pm 38\%$ Ould Didi et al. (2002)	Y defined in Equation 13.89; n = 1/4 (exponent in $f = C Re^n$) G = total mass velocity, kg/m ² s $B = \begin{cases} 4.8 & G < 500 \\ 2400/G & 500 \leq G \leq 1900 \\ 55/G^{1/2} & G \geq 1900 \end{cases} \text{ for } 0 < Y < 9.5$ $B = \begin{cases} 520/YG^{1/2} & G \leq 600 \\ 21/G & G > 600 \end{cases} \text{ for } 9.5 < Y \leq 28$ B = 15,000/(Y ² G ^{1/2}) for Y > 28
Lockhart–Martinelli correlation (1949) for μ_l/μ_g (1000 and G < 100 kg/m ² s): $\varphi_l^2 = \frac{(dp/dz)_{fr}}{(dp/dz)_l} = 1 + \frac{c}{X} + \frac{1}{X^2}$ $\varphi_g^2 = \frac{(dp/dz)_{fr}}{(dp/dz)_g} = 1 + cX + X^2$	Correlation constant by Chisholm (1967): c = 20 for liquid and vapor both turbulent c = 10 for liquid-turbulent, vapor-laminar c = 12 for liquid-laminar, vapor-turbulent c = 5 for liquid and vapor both laminar
Accuracy for annular flow: $\pm 29\%$ Ould Didi et al. (2002)	

Source: From Shah, R. K. and Sekulić, D. P., *Fundamentals of Heat Exchanger Design*. Wiley, Hoboken, NJ, 2003.

The momentum pressure gradient can be calculated by integrating the momentum balance equation (Collier and Thome 1994), thus obtaining

$$\left(\frac{dp}{dz}\right)_{\text{mo}} = \frac{d}{dz} \left[\frac{G^2}{g_c} \left(\frac{x^2}{\alpha\rho_g} + \frac{(1-x)^2}{(1-\alpha)\rho_l} \right) \right] \quad (13.90)$$

where α represents the void fraction of the gas (vapor) phase (a ratio of volumetric flow rate of the gas/vapor phase divided by the total volumetric flow rate of the two-phase mixture) and x is the mass quality (a ratio of the mass flow rate of the vapor/gas phase divided by the total mass flow rate of the two-phase mixture). Equation 13.90 is valid for constant cross-sectional (flow) area along the flow length. For the homogeneous model, the two-phase flow behaves like a single phase and the vapor and liquid velocities are equal. A number of correlations for the void fraction α are given by Carey (1992); Kandlikar, Shoji, and Dhir (1999). An empirical correlation for the void fraction whose general form is valid for several frequently used models is given by Butterworth (Carey 1992) as

$$\alpha = \left[1 + A \left(\frac{1-x}{x} \right)^p \left(\frac{\rho_g}{\rho_l} \right)^q \left(\frac{\mu_l}{\mu_g} \right)^r \right]^{-1} \quad (13.91)$$

where the constants A , p , q , and r depend on the two-phase model and/or empirical data chosen. These constants for a nonhomogeneous model, based on steam-water data, are $A=1$, $p=1$, $q=0.89$, and $r=0.18$. For the homogeneous model, $A=p=q=1$ and $r=0$. For the Lockhart and Martinelli model, $A=0.28$, $p=0.64$, $q=0.36$, and $r=0.07$. For engineering design calculations, the homogeneous model yields the best results when the slip velocity between the gas and liquid phases is small (for bubbly or mist flows).

Finally, the pressure gradient due to the gravity (hydrostatic) effect is

$$\left(\frac{dp}{dz}\right)_{\text{gr}} = \pm \frac{g}{g_c} \sin \theta [\alpha\rho_g + (1-\alpha)\rho_l] \quad (13.92)$$

Note that the negative sign (i.e., the pressure recovery) stands for downward flow in inclined or vertical tubes/channels and the positive sign (i.e., pressure drop) represents upward flow in inclined or vertical tubes/channels. θ represents the angle of tube/channel inclination measured from the horizontal axis.

13.5.2 Heat Transfer Correlations for Condensation

Condensation represents a vapor–liquid phase-change phenomenon that usually takes place when vapor is cooled below its saturation temperature at a given pressure. The heat transfer rate per unit heat transfer surface area from the pure condensing fluid to the wall is given by

$$q'' = h_{\text{con}}(T_{\text{sat}} - T_w) \quad (13.93)$$

where h_{con} is the condensation heat transfer coefficient, T_{sat} is the saturation temperature of the condensing fluid at a given pressure, and T_w is the wall temperature. We summarize here the correlations for filmwise (convective) in-tube condensation, a common condensation mode in most industrial applications, for two most common flow patterns—annular film flow in horizontal and vertical tubes and stratified flow in horizontal tubes. For annular film flow, the correlation for the local heat transfer coefficient h_{loc} [$h_{\text{con}}=h_{\text{loc}}$ in Equation 13.93] is given in Table 13.9; and also for stratified flow, the correlation for mean condensation heat transfer coefficient $h_{\text{con}}=h_m$ is given in Table 13.9. Shah, Zhou, and Tagavi (1999) provide condensation correlations for a number of noncircular flow passage geometries.

TABLE 13.9 Heat Transfer Correlations for Internal Condensation in Horizontal Tubes

Stratification Conditions	Correlation
Annular flow ^a (film condensation) Shah (1979) Accuracy: ± 14.4% Kandlikar, Shoji, and Dhir 1999	$h_{loc} = 0.023 \frac{k_l}{d_i} Re_l^{0.8} Pr_l^{0.4} \left[(1-x)^{0.8} + \frac{3.8x^{0.76}(1-x)^{0.04}}{(p_{sat}/p_{cr})^{0.38}} \right]$ $Re_l = \frac{Gd_i}{\mu_l}, xG = \text{total mass velocity, kg/m}^2 \text{ s}$ $0.002 \leq p_{sat}/p_{cr} \leq 0.44 \quad 11 \leq G \leq 1599 \text{ kg/m}^2 \text{ s}$ $21 \leq T_{sat} \leq 310 \text{ }^\circ\text{C}, 0 \leq x \leq 1, Pr_l > 0.5$ $3 \leq u_{vap} \leq 300 \text{ m/s, no limit on } q$ $7 \leq d_i \leq 40 \text{ mm } Re_l > 350 \text{ for circular tubes}$
Stratified flow Carey (1992) Accuracy: ± 18% Ould Didi et al. (2002)	$h_m = 0.728 \left[1 + \frac{1-x}{x} \left(\frac{\rho_g}{\rho_l} \right)^{2/3} \right]^{-3/4} \left[\frac{k_l^3 \rho_l (\rho_l - \rho_g) g h'_{lg}}{\mu_l (T_{sat} - T_w) d_i} \right]^{1/4}$ <p>where $h'_{lg} = h_{lg} + 0.68c_{p,l}(T_{sat} - T_w)$</p>

13.5.3 Heat Transfer Correlations for Boiling

Vaporization (boiling and evaporation) phenomena have been investigated and reported extensively in the literature. In this case, the heat transfer rate per unit heat transfer surface area from the wall to the pure vaporizing fluid is given by

$$q'' = h_{tp}(T_w - T_{sat}) \tag{13.94}$$

where h_{tp} is the two-phase heat transfer coefficient during the vaporization process. We present here a general in-tube force convective boiling correlation proposed by Kandlikar (1991) and further modified by Kandlikar and Steinke (2003); Kandlikar and Balasubramanian (2004). It is based on empirical data for water, refrigerants, and cryogenes. The correlation consists of two parts, the convective and nucleate boiling terms and utilizes a fluid-surface parameter. The Kandlikar correlation for the two-phase heat transfer coefficient is as follows:

$$\frac{h_{tp}}{h_{io}} = \text{larger of } \begin{cases} [0.6683Co^{-0.2}f_2(Fr_{1o}) + 1058Bo^{0.7}F_{fl}](1-x)^{0.8} \\ [1.136Co^{-0.9}f_2(Fr_{1o}) + 667.2Bo^{0.7}F_{fl}](1-x)^{0.8} \end{cases} \tag{13.95}$$

where

$$h_{io} = \begin{cases} \frac{Re_{1o} Pr_1(f/2)(k_l/d_i)}{1.07 + 12.7(Pr^{2/3} - 1)(f/2)^{0.5}} & 10^4 \leq Re_{1o} \leq 5 \times 10^6 \\ \frac{(Re_{1o} - 1000)Pr_1(f/2)(k_l/d_i)}{1.00 + 12.7(Pr_1^{2/3} - 1)(f/2)^{0.5}} & 3000 \leq Re_{1o} \leq 10^4 \\ \frac{Nuk_l}{d_i} & 100 \leq Re_{1o} \leq 1600 \end{cases} \tag{13.96}$$

Use a linear interpolation for h_{io} for Re between 1600 and 3000 from h_{io} calculated from the last two equations of Equation 13.96. For Re_{1o} below 100, use Equation 13.95 where h_{io} is calculated from Equation 13.96. This is because for $Re \leq 100$, the nucleate boiling mechanism governs. Note that Nu in Equation 13.96 is calculated based on the appropriate boundary condition for the single-phase flow.

TABLE 13.10 F_{fl} Recommended by Kandlikar 1991

Fluid	F_{fl}	Fluid	F_{fl}
Water	1.00	R-114	1.24
R-11	1.30	R-134a	1.63
R-12	1.50	R-152a	1.10
R-13B1	1.31	R-32/R-132 (60%–40% wt.)	3.30
R-22	2.20	Kerosene	0.488
R-113	1.30		

$$f_2(\text{Fr}_{10}) = \begin{cases} (25 \text{Fr}_{10})^{0.3} & \text{for } \text{Fr}_{10} < 0.04 \text{ in horizontal tubes} \\ 1 & \text{for vertical tubes and for } \text{Fr}_{10} \geq 0.04 \text{ in horizontal tubes} \end{cases} \quad (13.97)$$

$$f = \frac{1}{[1.58 \ln(\text{Re}_{10}) - 3.28]^2} \quad (13.98)$$

Here, h_{10} is the single-phase heat transfer coefficient for the entire flow as liquid flow. Also, the convection number Co , the nucleate boiling number Bo , and the Froude number Fr for the entire flow as liquid are defined as follows:

$$\text{Co} = \left(\frac{\rho_g}{\rho_l}\right)^{0.5} \left(\frac{1-x}{x}\right)^{0.8} \quad \text{Bo} = \frac{ql}{Gh_{fg}} \quad \text{Fr} = \frac{G^2}{\rho_l^2 g d_i} \quad (13.99)$$

F_{fl} is a fluid-surface parameter and depends on the fluid and the heat transfer surface. F_{fl} values for several fluids in copper tubes are presented in Table 13.10. F_{fl} should be taken as 1.0 for stainless tubes. This correlation is valid for either vertical (upward and downward) or horizontal in-tube flow. A mean deviation of slightly less than 16% with water and 19% with refrigerants has been reported by Kandlikar (1991).

Note that being fluid specific, F_{fl} cannot be used for other fluids (new refrigerants) and mixtures. It is also not accurate for stratified wavy flows and at high vapor qualities since it is not based on the onset of dry out. The Thome model (Kattan, Thome, and Favrat 1998; Zrcher, Thome, and Favrat 1999), based on a flow pattern map, is recommended for those cases.

13.6 Exchanger Design Methodology

The problem of heat exchanger design is complex and multidisciplinary (Shah 1991b). The major design considerations for a new heat exchanger include process/design specifications, thermal and hydraulic design, mechanical design, manufacturing and cost considerations, and trade-offs and system-based optimization, as shown in Figure 13.12 (with possible strong interactions among these considerations as indicated by double-sided arrows). The thermal and hydraulic design has mainly analytical solutions; the structural design has also to some extent analytical/FEA solutions. Most of the other major design considerations involve qualitative and experience-based judgments, trade-offs, and compromises. Therefore, there is no unique solution to designing a heat exchanger for given process specifications. Further details on this design methodology are given by Shah and Sekulić (2003).

Two of the most important heat exchanger design problems are basic rating and sizing problems. Refer to Shah and Sekulić (2003) for a total of 21 rating and sizing problems. Determination of heat transfer and pressure drop performance of either an existing exchanger or an already sized exchanger is referred

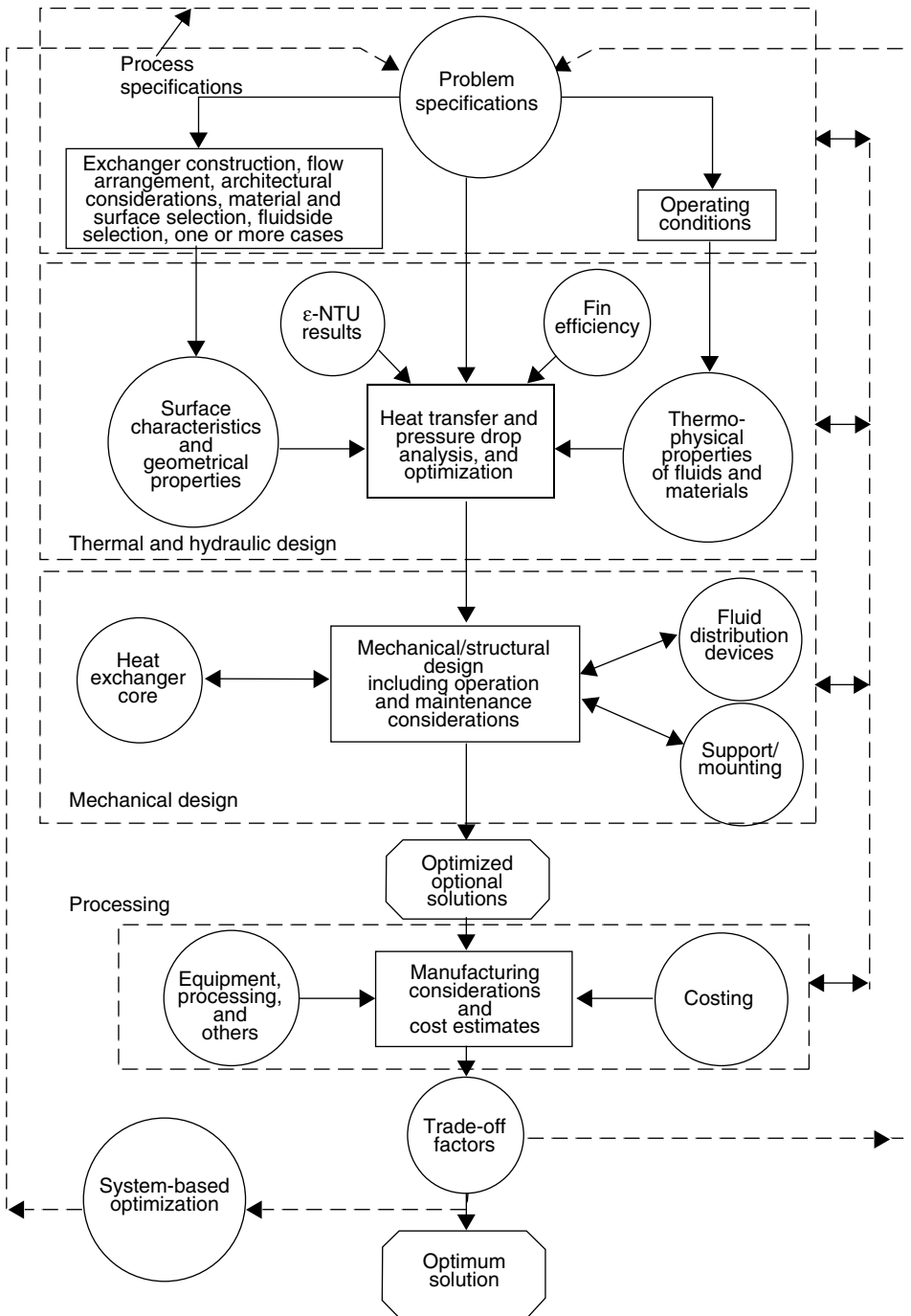


FIGURE 13.12 Heat exchanger design methodology.

to as the *rating problem*. The objective here is to verify the vendor’s specifications or to determine the performance at off-design conditions. The rating problem is also sometimes referred to as the *performance problem*. In contrast, the design of a new or existing type exchanger is referred to as the *sizing problem*. In a broad sense, this means the determination of the exchanger construction type, flow

arrangement, heat transfer surface geometries and materials, and physical size of an exchanger to meet the specified heat transfer and pressure drops. However, from the viewpoint of quantitative thermal–hydraulic analysis, we will consider that the selection of the exchanger construction type, flow arrangement, and materials has already been made. Thus in the sizing problem, we will determine the physical size (length, width, and height) and surface areas on each fluid side of the exchanger. The sizing problem is also sometimes referred to as the *design problem*.

The step-by-step solution procedures for the rating and sizing problems for counterflow and crossflow single-pass plate-fin heat exchangers have been presented with a detailed illustrative example by Shah (1981). Shah (1988a) presented further refinements in these procedures as well as step-by-step solution procedures for two-pass cross-counterflow plate-fin exchangers, and single-pass crossflow and two-pass cross-counterflow tube-fin exchangers. Also, step-by-step solution procedures for the rating and sizing problems for rotary regenerators (Shah 1988b), heat-pipe heat exchangers (Shah and Giovannelli 1988), and plate heat exchangers (Shah and Wanniarachchi 1991; Shah and Sekulić 2003) are available. As an illustration, the step-by-step solution procedures will be covered here for a single-pass crossflow plate-fin exchanger.

13.6.1 Rating Problem for a Single-Phase Crossflow Plate-Fin Exchanger

We will present here a step-by-step solution procedure for the rating problem for a crossflow plate-fin exchanger. Inputs to the rating problem for a two-fluid exchanger are the exchanger construction, flow arrangement and overall dimensions, complete details on the materials and surface geometries on both fluid sides including their nondimensional heat transfer and pressure drop characteristics (j and f vs. Re), fluid flow rates, inlet temperatures, and fouling factors. The fluid outlet temperatures, total heat transfer rate, and pressure drops on each fluid side of the exchanger are then determined as the rating problem solution.

1. Determine the surface geometrical properties on each fluid side. This includes the minimum free flow area A_0 , heat transfer surface area A (both primary and secondary), flow lengths L , hydraulic diameter D_h , heat transfer surface area density β , the ratio of minimum free flow area to frontal area σ , fin geometry (ℓ , δ , etc.) for fin efficiency determination, and any specialized dimensions used for heat transfer and pressure drop correlations.
2. Compute the fluid bulk mean temperature and fluid thermophysical properties on each fluid side. Since the outlet temperatures are not known for the rating problem, they are estimated initially. Unless it is known from the past experience, assume an exchanger effectiveness of 60%–75% for most single-pass crossflow exchangers or 80%–85% for single-pass counterflow and two-pass cross-counterflow exchangers. For the assumed effectiveness, calculate the fluid outlet temperatures.

$$T_{h,o} = T_{h,i} + \varepsilon(C_{\min}/C_c)(T_{h,i} - T_{c,i}) \quad (13.100)$$

$$T_{c,o} = T_{c,i} + \varepsilon(C_{\min}/C_c)(T_{h,i} - T_{c,i}) \quad (13.101)$$

Initially, assume $C_c/C_h \approx \dot{m}_c/\dot{m}_h$ for a gas-to-gas exchanger or $C_c/C_h \approx \dot{m}_c c_{p,c}/\dot{m}_h c_{p,h}$ for a gas-to-liquid exchanger with very approximate values of c_p s for the fluids in question. For exchangers with $C^* > 0.5$ (usually gas-to-gas exchangers), the bulk mean temperatures on each fluid side will be the arithmetic mean of the inlet and outlet temperatures on each fluid side (Shah 1981). For exchangers with $C^* < 0.5$ (usually gas-to-gas exchangers), the bulk mean temperature on the C_{\max} side will be the arithmetic mean of inlet and outlet temperatures; the bulk mean temperature on the C_{\min} side will be the log-mean average temperature obtained as follows.

$$T_{m,C_{\min}} = T_{m,C_{\max}} \pm \Delta T_{\ell m} \quad (13.102)$$

where ΔT_{lm} is the log-mean temperature difference based on the terminal temperatures (see Equation 13.19); use the plus sign if the C_{min} side is hot, otherwise use the negative sign. Once the bulk mean temperature is obtained on each fluid side, obtain the fluid properties from thermophysical property books or from handbooks. The properties needed for the rating problem are μ , c_p , k , Pr , and ρ . With this c_p , one more iteration may be carried out to determine $T_{h,0}$ or $T_{c,0}$ from Equation 13.100 or Equation 13.101 on the C_{max} side, and subsequently T_m on the C_{max} side, and refine fluid properties accordingly.

3. Calculate the Reynolds number $Re = GD_h/\mu$ and/or any other pertinent dimensionless groups (from the basic definitions) needed to determine the nondimensional heat transfer and flow friction characteristics (e.g., j or Nu and f) of heat transfer surfaces on each fluid side of the exchanger. Subsequently, compute j or Nu and f factors. Correct Nu (or j) for variable fluid property effects (Shah and Sekulić 2003) in the second and subsequent iterations from the following equations.

$$\text{For gases, } \frac{Nu}{Nu_{cp}} = \left[\frac{T_w}{T_m} \right]^{n'} \quad \frac{f}{f_{cp}} = \left[\frac{T_w}{T_m} \right]^{m'} \quad (13.103)$$

$$\text{For liquids, } \frac{Nu}{Nu_{cp}} = \left[\frac{\mu_w}{\mu_m} \right]^{n'} \quad \frac{f}{f_{cp}} = \left[\frac{\mu_w}{\mu_m} \right]^{m'} \quad (13.104)$$

where the subscript cp denotes constant fluid properties and m' and n' are empirical constants provided in Table 13.11. Note that T_w and T_m in Equation 13.103 and in Table 13.11a and Table 13.11b are absolute temperatures.

4. From Nu or j , compute the heat transfer coefficients for both fluid streams.

$$h = Nu k / D_h = j G_c Pr^{-2/3} \quad (13.105)$$

Subsequently, determine the fin efficiency η_f and the extended surface efficiency η_0 as follows.

$$\eta_f = \frac{\tanh m\ell}{m\ell} \quad \text{where} \quad m^2 = \frac{h\tilde{P}}{k_f A_k} \quad (13.106)$$

$$\eta_0 = 1 - (1 - \eta_f) \frac{A_f}{A} \quad (13.107)$$

where \tilde{P} is the wetted perimeter of the fin surface.

5. From the known heat capacity rates on each fluid side, compute $C^* = C_{min}/C_{max}$. From the known UA , determine $NTU = UA/C_{min}$. Also calculate the longitudinal conduction parameter λ . With the known NTU , C^* , λ , and flow arrangement determine the exchanger effectiveness ϵ from either closed-form equations of Table 13.3 or tabular/graphical results from Kays and London (1998).

TABLE 13.11a Property Ratio Method Exponents of Equation 13.103 and Equation 13.104 for Laminar Flow

Fluid	Heating	Cooling
Gases	$n' = 0.0, m' = 1.00$	$n' = 0.0, m' = 0.81$
	for $1 < T_w/T_m < 3$	for $0.5 < T_w/T_m < 1$
Liquids	$n' = -0.14, m' = 0.58$	$n' = -0.14, m' = 0.54$
	for $\mu_w/\mu_m < 1$	for $\mu_w/\mu_m > 1$

TABLE 13.11b Property Ratio Method Correlations or Exponents of Equation 13.103 and Equation 13.104 for Turbulent Flow

Fluid	Heating	Cooling
Gases	$Nu = 5 + 0.012 Re^{0.83} (Pr + 0.29) (T_w/T_m)^n$ $n = -[\log_{10} (T_w/T_m)]^{1/4} + 0.3$ for $1 < T_w/T_m < 5$, $0.6 < Pr < 0.9$, $10^4 < Re < 10^6$ and $L/D_h > 40$ $m' = -0.1$	$n' = 0$ $m' = -0.1$ (tentative)
Liquids	for $1 < T_w/T_m < 2.4$ $n' = -0.11^a$ for $0.08 < \mu_w/\mu_m < 1$ $ff_{cp} = (7 - \mu_m/\mu_w)/6^b$ or $m' \approx 0.25$ for $0.35 < \mu_w/\mu_m < 1$	$n' = -0.25^a$ for $1 < \mu_w/\mu_m < 40$ $m' = 0.24^b$ for $1 < \mu_w/\mu_m < 2$

^a Valid for $2 \leq Pr \leq 140$, $10^4 \leq Re \leq 1.25 \times 10^5$.

^b Valid for $1.3 \leq Pr \leq 10$, $10^4 \leq Re \leq 2.3 \times 10^5$.

Source: From Shah, 1981.

- With this ϵ , finally compute the outlet temperatures from Equation 13.100 and Equation 13.101. If these outlet temperatures are significantly different from those assumed in Step 2, use these outlet temperature in Step 2 [and do not use Equations (13.100) and (13.101)] and continue iterating Steps 2–6, until the assumed and computed outlet temperatures converge within the desired degree of accuracy. For a gas-to-gas exchanger, one iteration may be sufficient.
- Finally, compute the heat duty from

$$q = \epsilon C_{\min}(T_{h,i} - T_{c,i}) \tag{13.108}$$

- For the pressure drop calculations, we first need to determine the fluid densities at the exchanger inlet and outlet, ρ_i and ρ_o , for each fluid. The mean specific volume on each fluid side is then computed from Equation 13.29. Next, the entrance and exit loss coefficients, K_c and K_e , are obtained from Figure 13.9 for known σ , Re , and the flow passage entrance geometry. The friction factor on each fluid side is corrected for variable fluid properties using Equation 13.103 or Equation 13.104. Here, the wall temperature T_w is computed from

$$T_{w,h} = T_{m,h} - (R_h + R_{h,s})q \tag{13.109}$$

$$T_{w,c} = T_{m,c} + (R_c + R_{c,s})q \tag{13.110}$$

where the various resistance terms are defined by Equation 13.6. The core pressure drops on each fluid side are then calculated from Equation 13.28. This then completes the procedure for solving the rating problem.

13.6.2 Sizing Problem for a Single-Phase Crossflow Plate-Fin Exchangers

As defined earlier, we will concentrate here to determine the physical size (length, width, and height) of a single-pass counterflow and crossflow exchangers for specified heat duty and pressure drops. More specifically inputs to the sizing problem are surface geometries (including their nondimensional heat transfer and pressure drop characteristics), fluid flow rates, inlet and outlet fluid temperatures, fouling factors, and pressure drops on each fluid side.

For the solution to sizing of counterflow problem, there are four unknowns: two flow rates or Reynolds numbers (to determine correct heat transfer coefficients and friction factors) and two surface areas for the two-fluid crossflow exchanger. The following four equations (Equation 13.111, Equation 13.113 for hot and cold fluids, and Equation 13.115) are used to solve iteratively the surface areas on each fluid side: UA in Equation 13.111 is determined from NTU computed from the known heat duty or ϵ and C^* ; G in

Equation 13.113 represents two equations, for Fluid 1 and 2 (Shah 1988a); and the volume of the exchanger in Equation 13.115 is the same based on the surface area density of Fluid 1 and 2 sides.

$$\frac{1}{UA} \approx \frac{1}{(\eta_0 hA)_h} + \frac{1}{(\eta_0 hA)_c} \quad (13.111)$$

Here, we have neglected the wall and fouling thermal resistances. This equation in nondimensional form is given by

$$\frac{1}{NTU} = \frac{1}{ntu_h(C_h/C_{\min})} + \frac{1}{ntu_c(C_c/C_{\min})} \quad (13.112)$$

$$G = \left[\frac{2g_c \Delta p}{\text{Deno}} \right]^{1/2} \quad (13.113)$$

$$\text{Deno} = \frac{f}{j} \frac{ntu}{\eta_0} \text{Pr}^{2/3} \left(\frac{1}{\rho} \right)_m + 2 \left(\frac{1}{\rho_0} - \frac{1}{\rho_i} \right) + (1 - \sigma^2 + K_c) \frac{1}{\rho_i} - (1 - \sigma^2 - K_c) \frac{1}{\rho_0} \quad (13.114)$$

$$V = \frac{A_1}{\alpha_1} = \frac{A_2}{\alpha_2} \quad (13.115)$$

In the iterative solutions, the first time one needs ntu_h and ntu_c to start the iterations. These can be determined either from the past experience or by estimations. If both fluids are gases or liquids, one could consider that the design is “balanced,” that is, the thermal resistances are distributed approximately equally on the hot and cold fluid sides. In that case, $C_h = C_c$, and

$$ntu_h \approx ntu_c \approx 2NTU \quad (13.116)$$

Alternatively, if we have liquid on one fluid side and gas on the other fluid side, consider 10% thermal resistance on the liquid side; that is,

$$0.10 \left(\frac{1}{UA} \right) = \frac{1}{(\eta_0 hA)_{\text{liq}}} \quad (13.117)$$

Then from Equation 13.111 and Equation 13.112 with $C_{\text{gas}} = C_{\min}$, we can determine ntu on each fluid side as follows.

$$ntu_{\text{gas}} = 1.11NTU, \quad ntu_{\text{liq}} = 10C^*NTU \quad (13.118)$$

Also note that initial guesses of η_0 and j/f are needed for the first iteration to solve Equation 13.113. For a good design, consider $\eta_0 = 0.80$ and determine approximate value of j/f from the plot of j/f vs. Re curve for the known j and f vs. Re characteristics of each fluid side surface. The specific step-by-step design procedure is as follows.

1. To compute the fluid bulk mean temperature and the fluid thermophysical properties on each fluid side, determine the fluid outlet temperatures from the specified heat duty.

$$q = (\dot{m}c_p)_h(T_{h,i} - T_{h,o}) = (\dot{m}c_p)_c(T_{c,o} - T_{c,i}) \quad (13.119)$$

or from the specified exchanger effectiveness using Equation 13.100 and Equation 13.101. For the first time, estimate the values of c_p s. For exchangers with $C^* \geq 0.5$, the bulk mean temperature on each fluid side will be the arithmetic mean of inlet and outlet temperatures on each fluid side. For exchangers with $C^* < 0.5$, the bulk mean temperature on the C_{\max} side will be the arithmetic mean of the inlet and outlet temperatures on each fluid side, the bulk

mean temperature on the C_{\min} side will be the log-mean average as given by Equation 13.102. With these bulk mean temperatures, determine c_p and iterate one more time for the outlet temperatures if warranted. Subsequently, determine μ , c_p , k , Pr , and ρ on each fluid side.

2. Calculate C^* and ε (if q is given), and determine NTU from the ε -NTU expression, tabular or graphical results for the selected flow arrangement (in this case, it is unmixed–unmixed crossflow, Table 13.3). The influence of longitudinal heat conduction, if any, is ignored in the first iteration since we do not know the exchanger size yet.
3. Determine ntu on each fluid side by the approximations discussed with Equation 13.116 and Equation 13.118 unless it can be estimated from the past experience.
4. For the selected surfaces on each fluid side, plot j/f vs. Re curve from the given surface characteristics, and obtain an approximate mean value of j/f . If fins are employed, assume $\eta_o = 0.80$ unless a better value can be estimated.
5. Evaluate G from Equation 13.113 on each fluid side using the information from Steps 1 to 4 and the input value of Δp .
6. Calculate Reynolds number Re , and determine j and f on each fluid side from the given design data for each surface.
7. Compute h , η_b and η_o using Equation 13.105 through Equation 13.107. For the first iteration, determine U_1 on Fluid 1 side from the following equation derived from Equation 13.6 and Equation 13.115.

$$\frac{1}{U_1} = \frac{1}{(\eta_o h)_1} + \frac{1}{(\eta_o h_s)_1} + \frac{\alpha_1/\alpha_2}{(\eta_o h_s)_2} + \frac{\alpha_1/\alpha_2}{(\eta_o h)_2} \quad (13.120)$$

where $\alpha_1/\alpha_2 = A_1/A_2$, $\alpha = A/V$, V is the exchanger total volume, and subscripts 1 and 2 denote Fluid 1 and 2 sides. For a plate-fin exchanger, α_s are related to β_s as follows (Shah 1981; Kays and London 1998).

$$\alpha_1 = \frac{b_1 \beta_1}{b_1 + b_2 + 2\delta} \quad \alpha_2 = \frac{b_2 \beta_2}{b_1 + b_2 + 2\delta} \quad (13.121)$$

Here, β is the total surface area on one fluid side to the volume between plates on that fluid side. Note that the wall thermal resistance in Equation 13.120 is ignored in the first iteration. In second and subsequent iterations, compute U_1 from

$$\frac{1}{U_1} = \frac{1}{(\eta_o h)_1} + \frac{1}{(\eta_o h_s)_1} + \frac{\delta A_1}{k_w A_w} + \frac{A_1/A_2}{(\eta_o h_s)_2} + \frac{A_1/A_2}{(\eta_o h)_2} \quad (13.122)$$

where the necessary geometry information A_1/A_2 and A_1/A_w are determined from the geometry calculated in the previous iteration.

8. Now calculate the core dimensions. In the first iteration, use NTU computed in Step 2. For subsequent iterations, calculate longitudinal conduction parameter λ (and other dimensionless groups for a crossflow exchanger). With known ε , C^* , and λ , determine the correct value of NTU using either a closed-form equation or tabulated/graphical results (Shah and Mueller 1985). Determine A_1 from NTU using U_1 from the previous step and known C_{\min} ,

$$A_1 = \frac{NTUC_{\min}}{U_1} \quad (13.123)$$

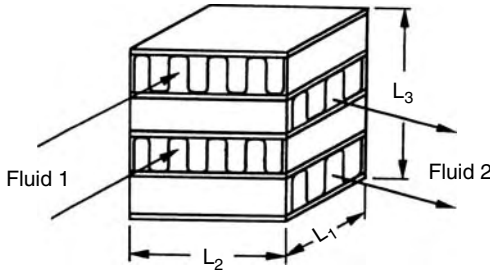


FIGURE 13.13 A single-pass crossflow exchanger.

and hence

$$A_2 = \frac{A_2}{A_1} A_1 = \frac{\alpha_2}{\alpha_1} A_1 \quad (13.124)$$

The free flow area A_0 from known \dot{m} and G is given by

$$A_{0,1} = \left(\frac{\dot{m}}{G}\right)_1 \quad A_{0,2} = \left(\frac{\dot{m}}{G}\right)_2 \quad (13.125)$$

so that

$$A_{fr,1} = \frac{A_{0,1}}{\sigma_1} \quad A_{fr,2} = \frac{A_{0,2}}{\sigma_2} \quad (13.126)$$

where σ_1 and σ_2 are generally specified for the surface or can be computed for plate-fin surfaces from (Kays and London 1998; Shah and Sekulić 2003):

$$\sigma_1 = \frac{b_1 \beta_1 D_{h,1} / 4}{b_1 + b_2 + 2\delta} = \frac{\alpha_1 D_{h,1}}{4} \quad \sigma_2 = \frac{b_2 \beta_2 D_{h,2} / 4}{b_1 + b_2 + 2\delta} = \frac{\alpha_2 D_{h,2}}{4} \quad (13.127)$$

Now compute the fluid flow lengths on each fluid side (see Figure 13.13) from the definition of the hydraulic diameter of the surface employed on each fluid side.

$$L_1 = \left(\frac{D_h A}{4A_0}\right)_1 \quad L_2 = \left(\frac{D_h A}{4A_0}\right)_2 \quad (13.128)$$

Since $A_{fr,1} = L_2 / L_3$ and $A_{fr,2} = L_1 / L_3$, we can obtain

$$L_3 = \frac{A_{fr,1}}{L_2} \quad \text{or} \quad L_3 = \frac{A_{fr,2}}{L_1} \quad (13.129)$$

Theoretically, L_3 s calculated from both expressions of Equation 13.129 should be identical. In reality, they may differ slightly due to the round-off error. In that case, consider an average value for L_3 .

9. Now compute the pressure drop on each fluid side, after correcting f factors for variable property effects, in a manner similar to Step 8 of the rating problem for a crossflow plate-fin exchanger.
10. If the values calculated for Δps are within input specifications and close to them, the solution to the sizing problem is completed. Finer refinements in the core dimensions, such as integer numbers of flow passages, may be carried out at this time. Otherwise, compute the new value of G on each fluid side using Equation 13.28 in which Δp is the input specified value, and f , K_c , K_e , and the geometrical dimensions are from the previous iteration.
11. Repeat (iterate) Steps 6–10 until both heat transfer and pressure drops are met as specified. It should be emphasized that since we have imposed no constraints on the exchanger dimensions, the procedure will yield L_1 , L_2 , and L_3 , for the selected surfaces such that the design will meet the heat duty and pressure drops on both fluid sides exactly.

Refer to Shah and Sekulić (2003) for taking into account the effect of longitudinal conduction in the exchanger as well as rating and sizing problem solution for other exchanger flow arrangements.

13.6.3 Rating and Sizing Problem for Condensers and Evaporators

Generally, the heat transfer coefficients and friction factors for two-phase flows are so much changing along the flow length that the lumped parameter approach for rating and sizing of the exchanger is not followed as is done for single-phase exchangers and discussed in the preceding section. The heat exchanger is divided into a large number of small elements and the mass, momentum, and energy equations are solved for each element along with the evaluation of quality of the phase-change fluid after each element. Because of complicated two-fluid flow arrangements for many phase-change exchangers, such calculations may not be possible even for the starting element since only one fluid side inlet conditions are known on that fluid side. Hence, for most phase-change exchangers, the conditions for the fluid side with unknown parameters are assumed and the finite difference calculations are pursued. After the first complete iteration for the exchanger, when the inlet conditions for the second fluid are computed and do not match, iterative calculations are done with the appropriate iterative scheme to get the converged solution. In the case of a sizing problem, first the exchanger size with the appropriate two-fluid flow arrangement is chosen and the rating calculations are done as mentioned earlier. If the converged solution does not provide the desired performance, a new exchanger size is chosen and iterative calculations are performed to get the new converged solution. This process of assuming the exchanger size is continued and iterative calculations are performed till the desired performance is achieved. Due to the complexity of the procedure and the length limitations for the article, the details on the rating and sizing of the two-fluid condensers and evaporators are not being covered here.

13.7 Flow Maldistribution

In previously presented heat transfer methods (ϵ -NTU, MTD, etc.) and pressure drop analyses, it is presumed that the fluid is uniformly distributed through the core. In practice, flow maldistribution occurs to some extent and often severely, and may result in a significant reduction in exchanger heat transfer performance and an increase in the pressure drop. Hence, it may be necessary for the designer to take into account the effect of flow maldistribution, causing undesirable performance deterioration upfront while designing a heat exchanger.

Some maldistributions are geometry induced (i.e., the result of exchanger fabrication conditions, such as header design or manufacturing tolerances, or the duct geometry/structure upstream of the exchanger); others are the result of exchanger operating conditions. Gross, passage-to-passage, and manifold-induced flow maldistributions are the examples of the former category; flow maldistributions induced by viscosity, natural convection, and density difference are of the latter category. Flow maldistributions associated with two-phase and multiphase flow are too complex and beyond the scope of this chapter. The analysis methods and results for some of these flow maldistributions for single-phase flows are summarized next.

13.7.1 Gross Flow Maldistribution

In gross flow maldistribution, the nonuniform distribution of the fluid flow is on the macroscopic level. It results due to the shape of the inlet header, upstream flow conditions, or gross blockage (caused by brazing, soldering, or other manufacturing considerations) of any part of the exchanger. Therefore, gross flow maldistribution is independent of the exchanger heat transfer surface geometry configuration and its microscopic nonuniformity. Gross flow maldistribution generally results in a *significant increase* in exchanger pressure drop and *some reduction* in exchanger heat transfer.

A design procedure for calculating the reduction in heat exchanger effectiveness due to one-dimensional nonuniform flow distribution on only one fluid side of the exchanger has been introduced by Shah (1981). The flow maldistribution in this procedure is characterized by an n -step velocity function

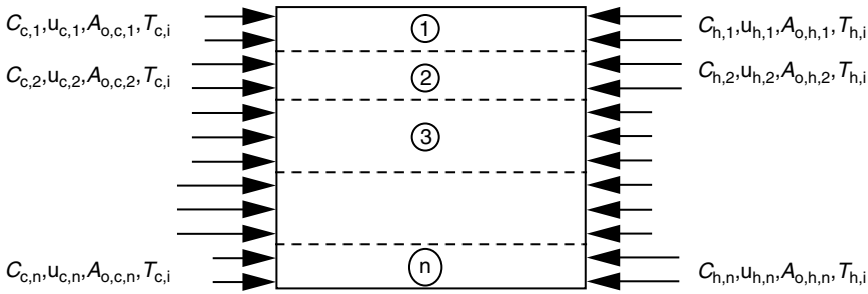


FIGURE 13.14 Idealized flow nonuniformity in a counterflow exchanger.

relating the flow nonuniformity as n adjacent subexchangers, each having a uniform flow distribution unique from the rest. This method has been applied to a counterflow, a parallel flow, and a single-pass unmixed–mixed crossflow exchanger (for the case where the nonuniform fluid side is the unmixed side) with the maldistributed fluid side having either the hot or cold fluid. For all other exchanger flow arrangements, a numerical analysis is essential.

In the case of a counterflow or parallel flow exchanger, the flow nonuniformity can be on hot or cold fluid sides as shown in Figure 13.14. The analysis for the exchanger of Figure 13.14 is straightforward, computing temperature effectiveness of individual subexchangers based on one fluid side only, and computing the total heat transfer rate by adding the qs of the subexchangers (Shah and Sekulić 2003).

A typical influence of gross flow maldistribution on the counterflow exchanger effectiveness is shown in Figure 13.15 (Shah 1985). The subject exchanger contains a two-step velocity maldistribution on the hot fluid side with $C^* = 1$, $u_{max}/u_m = 1.5$ and 2.0 , and $A_{0,1}/A_0 = 0.50, 0.35$, and 0.25 . It is idealized that the flows are fully-developed laminar; hence, h and U are constant. Otherwise, the variations in h should be evaluated at respective flow velocities (i.e., Reynolds numbers) and the subsequent new values of U

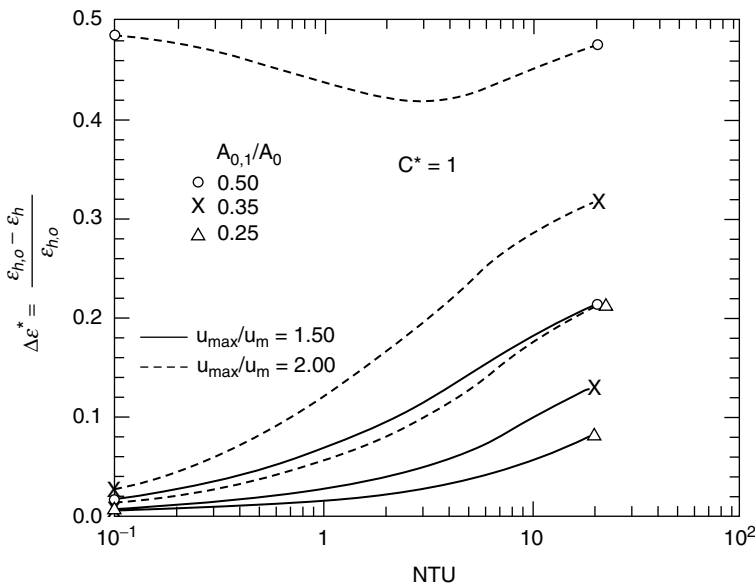


FIGURE 13.15 Influence of gross flow maldistribution on the counterflow exchanger effectiveness. (From Shah, R. K., *Handbook of Heat Transfer Applications*, 2nd Ed., Rohsenow, W. M. Hartnett, J. P. and Ganić, E. N. Part 3. McGraw-Hill, New York, Chap. 4, 1985. With permission.)

(or UA) should be calculated. From Figure 13.16, it can be seen that for particular values of u_{\max}/u_m and exchanger NTU, the greatest reduction in exchanger effectiveness occurs when the velocity function is equally distributed over flow area (e.g., $A_{0,1}/A_0 = A_{0,2}/A_0 = 0.5$). Also, as expected, the greater the maldistribution, the greater is the loss in the exchanger effectiveness.

Although not demonstrated here, it can be shown that an n -step ($n > 2$) velocity maldistribution results in less deterioration in ε compared to that for the two-step velocity maldistribution for the same u_{\max}/u_m ratio for the same exchanger (Shah 1981).

In a series of papers, Chiou investigated numerically the effect of various flow maldistributions on a single-pass unmixed–unmixed crossflow exchanger, and some of these results are summarized by Mueller and Chiou (1987). Chiou (1982) reported a lower reduction in the exchanger effectiveness for nonuniform inlet temperature than for nonuniform inlet velocity for a single-pass unmixed–unmixed crossflow exchanger. Cichelli and Boucher (1956); Fleming (1966), and Chowdhury and Sarangi (1985) analyzed the case of tube-side maldistribution in a counterflow shell-and-tube exchanger, while Mueller (1977) considered flow maldistributions on both tube and shell sides. For a rotary regenerator, Kutchev and Julien (1974) investigated gross flow maldistribution, while Kohler (1974) investigated the influence of flow path geometry and manufacturing tolerances.

No analysis is available for an increase in the pressure drop due to gross flow maldistribution. Since such nonuniform flow is associated with poor header design or gross core blockage, the static pressure distributions at the core inlet and outlet faces may not be uniform. Hence, no simple modeling for the pressure drop evaluation is possible. As a conservative approach, it is recommended that the core pressure drop on flow maldistributed side is evaluated based on the highest velocity component of that fluid side.

13.7.2 Passage-to-Passage Flow Maldistribution

Neighboring passages in a compact heat exchanger are geometrically never identical because of manufacturing tolerances. It is especially difficult to control precisely the passage size when small dimensions are involved (e.g., a rotary regenerator with $D_h = 0.5$ mm or 0.020 in.) in hundreds of neighboring passages. Since differently sized and shaped passages exhibit different flow resistances in laminar flow and the flow seeks a path of least resistance, a nonuniform flow results through the matrix. This passage-to-passage flow nonuniformity can result in a *significant penalty* in heat transfer performance with only a small compensating effect of *reduced* pressure drop. This effect is especially important for laminar flows in continuous cylindrical passages, but is of lesser importance for interrupted surfaces (where transverse flow mixing can occur) or for turbulent flow.

The theoretical analysis for this flow maldistribution for low- Re laminar flow surfaces has been carried out by London (1970) for a two-passage model and extended by Shah and London (1980) for an n -passage model. In the latter model, there are n different-size passages of the same basic shape, either rectangular or triangular. In Figure 13.16, a reduction in ntu for rectangular passages is shown when 50% of the flow passages are large ($c_2 > c_r$) and 50% of the passages are small ($c_1 < c_r$) compared to the reference or nominal passages. The results are presented for the passages having a nominal aspect ratio α^* of 1, 0.5, 0.25, and 0.125 for the (H) and (T) boundary conditions and for a reference ntu_r of 5.0. Here, ntu_{cost} , a percentage loss in ntu , and the channel deviation parameter δ_c are defined as:

$$ntu_{\text{cost}}^* = \left(1 - \frac{ntu_{\text{eff}}}{ntu_r} \right) \quad (13.130)$$

$$\delta_c = 1 - \frac{c_i}{c_r} \quad (13.131)$$

where ntu_{eff} is the effective ntu when two-passage model passage-to-passage nonuniformity is present, and ntu_r is the reference or nominal NTU. It can be seen from Figure 13.16 that a 10% channel deviation (which is common for a highly compact surface) results in 10 and 21% reduction in NTU_{H} and NTU_{T} , respectively, for $\alpha^* = 0.125$ and $ntu_r = 5.0$. In contrast, a gain in the pressure drop due to

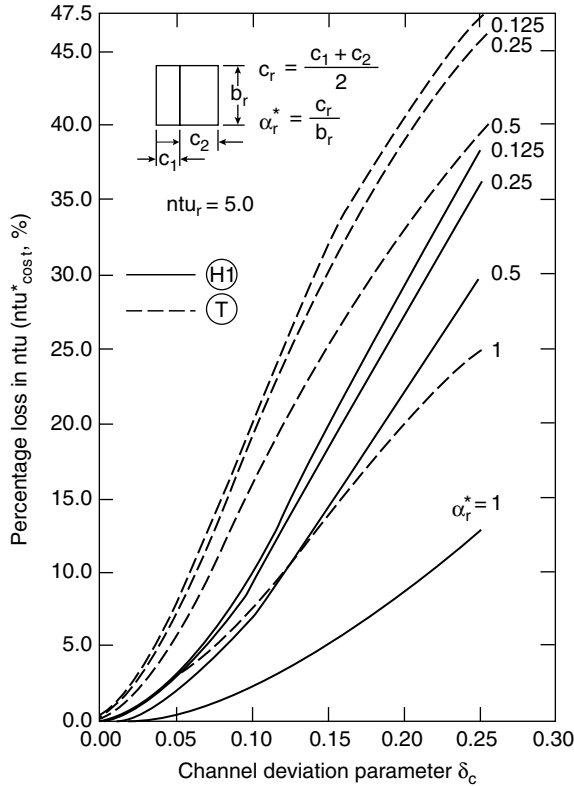


FIGURE 13.16 Percentage loss in NTU for two-passage nonuniformities in rectangular passages.

passage-to-passage nonuniformity is only 2.5% for $\delta_c=0.10$ and $\alpha_r^*=0.125$, as found from Figure 13.17. Here, Δp_{gain}^* is defined as:

$$\Delta p_{\text{gain}}^* = \left(1 - \frac{\Delta p_{\text{actual}}}{\Delta p_{\text{nominal}}} \right) \tag{13.132}$$

The results of Figure 13.16 and Figure 13.17 are also applicable to an n -passage model in which there are n different-size passages in a normal distribution about the nominal passage size. The channel deviation parameter needs to be modified for this case to

$$\delta_c = \left[\sum_{i=1}^n \chi_i \left(1 - \frac{c_i}{c_r} \right)^2 \right]^{1/2} \tag{13.133}$$

Here, χ_i is the fractional distribution of the i th shaped passage. For $n=2$, Equation 13.133 reduces to Equation 13.131. For triangular passages, c in Equation 13.133 is replaced by r_h . The following observations may be made from Figure 13.16 and additional results presented by Shah and London (1980): (1) the loss in NTU is more significant for the (T) boundary condition than for the (H1) boundary condition. (2) The loss in NTU increases with higher nominal NTU. (3) The loss in NTU is much more significant compared to the gain in Δp at a given δ_c . (4) The deterioration in performance is the highest for the two-passage model compared to the n -passage model with $n > 2$ for the same value of δ_c . Refer to Shah and Sekulić (2003) for details on additional analyses.

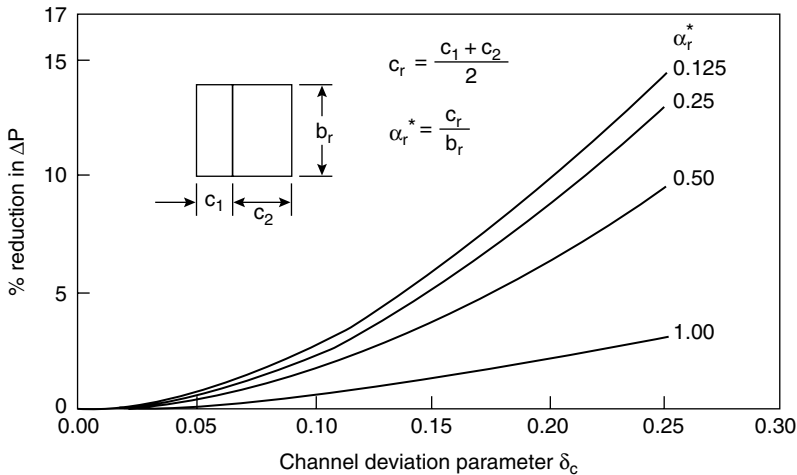


FIGURE 13.17 Percentage reduction in Δp for two-passage nonuniformities in rectangular passages.

13.7.3 Manifold-Induced Flow Maldistribution

Two of the most commonly used manifold systems connecting manifolds to the branches (particularly for plate heat exchangers) are the parallel flow (S or Z) and reverse-flow (U) systems as shown in Figure 13.18 for a single-pass exchanger. Since the flow length (and subsequently the flow resistance) is different for fluid particles going through different branches and inlet/outlet manifolds, and the imposed pressure drop (between inlet and outlet of the exchanger) is the same, it results in flow maldistribution regardless of perfect flow passages (branch geometry) and the type of the flow through the manifolds and branches (such as laminar, transition, or turbulent). Bajura and Jones (1976); Majumdar (1980); Shen (1992) have investigated this flow maldistribution, and qualitative conclusions of the first two investigators are summarized below due to space limitation; for some quantitative results, refer to Shah (1985).

1. A design rule of thumb is to limit the ratio of the flow area of lateral branches (exchanger core) to the flow area of the inlet header (area of pipe before lateral branches) A_0^* to less than unity to minimize flow maldistributions.
2. More uniform flow distribution through the core is achieved by a reverse-flow (U) manifold system in comparison to a parallel flow (S or Z) manifold system.
3. In a parallel flow (S or Z) manifold system, the maximum flow occurs through the last port, and in the reverse-flow (U) manifold system the first port.
4. The influence of the manifold pipe friction parameter F is less significant than that of the flow area ratio A_0^* .
5. Flow distribution becomes more uniform with a higher branch pressure loss coefficient K .
6. The flow area of a combining-flow manifold (outlet manifold/pipe in Figure 13.18a and b) should be larger than that for the dividing-flow manifold for a more uniform flow distribution through the core in the absence of heat transfer within the core. If there is heat transfer in the lateral branches (core), the fluid densities will be different in the inlet and outlet manifolds, the flow areas should be adjusted for this density change, and then the flow area of the combining manifold should be larger than that calculated previously.
7. Flow reversal is more likely to occur in parallel flow (S flow) systems that are subject to poor flow distribution.

Refer to Shah and Sekulić (2003) for further details.

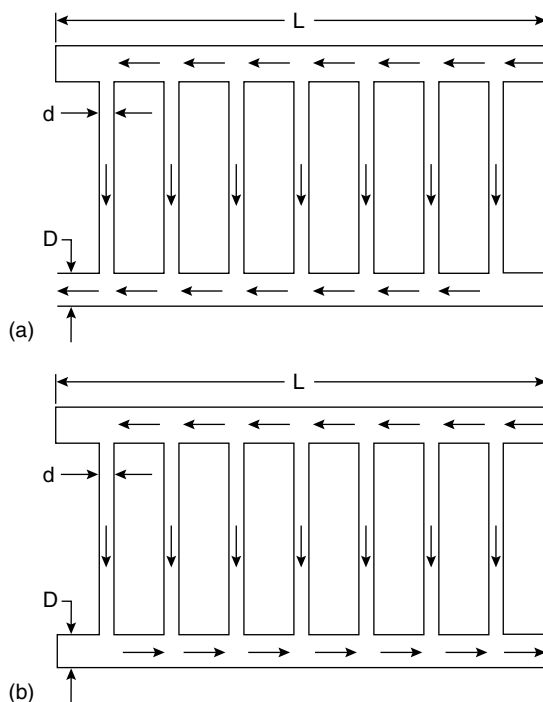


FIGURE 13.18 (a) Parallel flow or S or Z flow and (b) reverse-flow or U flow manifold systems.

13.7.4 Viscosity-Induced Flow Maldistribution

Whenever one or both fluids flowing in a heat exchanger are liquids and operate in the laminar flow region, there exists a possibility of viscosity-induced flow instability and maldistribution, and thus exchanger performance deterioration. The viscosity-induced flow instability is a result of large changes in fluid viscosity within the exchanger and is found to be present when the viscous liquid is being cooled; it is not present for the case of liquid being heated, although flow maldistribution will be present. For the case of liquid cooling, the liquid viscosity increases significantly with decreasing temperature. Thus, moderate temperature differences between parallel passages (or tubes) within an exchanger can result in large viscosity differences between these adjacently flowing streams. Because of the direct proportionality between the pressure drop and the product of flow rate and viscosity ($\Delta p \propto \dot{m}\mu$) in laminar flow, flow will be maldistributed in tubes having different heat transfer rates (and hence resultant different viscosities for the tube fluid), but will have the same pressure drop across each tube. The end result is that slower fluid streams are forced to flow slower and faster fluid streams to flow faster. This trend normally continues until a new equilibrium is reached, but unfortunately the resulting flow nonuniformity of this new exchanger condition will generally cause undesirable performance deterioration.

Mueller (1974); Putman and Rohsenow (1985) addressed the problem of viscosity-induced flow maldistribution from the flow instability point of view and not from the heat transfer performance deterioration point of view. Mueller (1974) provided a simple analysis of the pressure drop–mass flow rate relationship in a single tube laminar flow cooler. From an extension of this analysis, he proposed a method for determining a point (maximum pressure drop or flow rate) beyond which it would be safe to assume flow instability of this kind will not occur in a multitubular exchanger.

When the exchanger is operating outside the region of viscous instability, the deterioration in heat transfer performance and the pressure drop “gain” can be calculated using the same procedure as that for the passage-to-passage flow maldistribution. In this case, the flow rate ratio depends on the

viscosity ratio, whereas it depends on the ratios of the friction factor, hydraulic diameter, and flow area of two different flow passages in the case of passage-to-passage flow maldistribution (London 1970). Refer to Shah and Sekulić (2003) for more details and insight into this flow maldistribution.

13.8 Fouling in Heat Exchangers

13.8.1 Fouling, Its Effect and Mechanisms

Fouling refers to undesired accumulation of solid material (by-products of the heat transfer processes) on heat exchanger surfaces, which results in additional thermal resistance to heat transfer, thus reducing exchanger performance. The fouling layer also blocks the flow passage/area and increases surface roughness, which either reduces the flow rate in the exchanger or increases the pressure drop or both. The foulant deposits may be loose, such as magnetite particles, or hard and tenacious, such as calcium carbonate scale; other deposits may be sediment, polymers, cooking or corrosion products, inorganic salts, biological growth, and so on. Depending on the fluids, operating conditions, and heat exchanger construction, the maximum fouling layer thickness on the heat transfer surface may result in a few hours to a number of years.

Fouling in heat exchangers is a very complex phenomena and its negative impact translates into billions of dollars every year worldwide and is being investigated with considerable effort. Significant research activity in the fouling of heat exchanger equipment is going on worldwide. Some of the recent references for further studies are: Bott (1995); Panchal et al. (1997); Bott et al. (1999), and Müller-Steinhagen (2000), Bott (1995), Hewitt and Müller-Steinhagen (2000, 2003).

Fouling could be very costly depending on the nature of fouling and the applications. It increases capital costs: (a) oversurfacing the heat exchanger, (b) provisions for cleaning, and (c) use of special materials and constructions/surface features. It increases maintenance costs: (a) cleaning techniques, (b) chemical additives, and (c) troubleshooting. It may cause a loss of production: (a) reduced capacity, and (b) shutdown. It increases energy losses: (a) reduced heat transfer, (b) increased pressure drop, and (c) dumping dirty streams. Fouling promotes corrosion, severe plugging, and eventual failure of uncleaned heat exchangers. In a fossil-fired exhaust environment, gas-side fouling produces a potential fire hazard in heat exchangers.

The following are the major fouling mechanisms:

- *Crystallization or Precipitation Fouling.* This results from the deposition/formation of crystals of dissolved substances from the liquid onto the heat transfer surface due to solubility changes with temperatures beyond the saturation point. If the deposited layer is hard and tenacious, it is often referred to as scaling. If it is porous and mushy, it is called sludge.
- *Particulate Fouling.* This results from the accumulation of finely divided substances suspended in the fluid stream onto the heat transfer surface. If the settling occurs due to gravity, it is referred to as *sedimentation fouling*.
- *Chemical Reaction Fouling.* This is defined as the deposition of material produced by chemical reaction (between reactants contained in the fluid stream) in which the heat transfer surface material does not participate.
- *Corrosion Fouling.* This results from corrosion of the heat transfer surface that produces products fouling the surface and/or roughens the surface, promoting attachment of other foulants.
- *Biological Fouling.* This results from the deposition, attachment, and growth of biological organisms from liquid onto a heat transfer surface. Fouling due to microorganisms refers to *microbial fouling* and due to macroorganisms refers to *macrobial fouling*.
- *Freezing Fouling.* This results from the freezing of a single component liquid or higher-melting point constituents of a multicomponent liquid onto a subcooled heat transfer surface.

Biological fouling occurs only with liquids, since there are no nutrients in the gases. Also, crystallization fouling is not too common with gases, since most gases contain a few dissolved salts (mainly in mists) and even fewer inverse-solubility salts. All other types of fouling occur in both liquid and gas. More than one mechanism is usually present in many fouling situations, often with synergetic results. Liquid-side fouling generally occurs on the exchanger side where the liquid is being heated, and gas-side fouling occurs where the gas is being cooled; however, reverse examples can be found.

13.8.2 Importance of Fouling

Fouling in liquids and two-phase flows has a significant detrimental effect on heat transfer with some increase in pressure drop. In contrast, fouling in gases reduces heat transfer somewhat (5%–10% in general) in compact heat exchangers but increases pressure drop significantly (up to several hundred percent). For example, consider $U=1400 \text{ W/m}^2 \text{ K}$ as in a process plant liquid-to-liquid heat exchanger. Hence, $R=1/U=0.00072 \text{ m}^2 \text{ K/W}$. If the fouling factors ($r_{h,s}+r_{c,s}$) together amount to 0.00036 (considering a typical TEMA value of the fouling factor as 0.00018), 50% of the heat transfer area A requirement for given q is chargeable to fouling. However, for gas flows on both fluid sides of an exchanger, $U \approx 280 \text{ W/m}^2 \text{ K}$, and the same fouling factor of 0.00036 would represent only about 10% of the total surface area. Thus, one can see a significant impact on heat transfer surface area requirement due to fouling in heat exchangers having high U values (such as having liquids or phase-change flows).

Considering the core frictional pressure drop, Equation 13.31, as the main pressure drop component, the ratio of pressure drops of fouled and cleaned exchanger is given by

$$\frac{\Delta p_F}{\Delta p_C} = \frac{f_F}{f_C} \left(\frac{D_{h,C}}{D_{h,F}} \right) \left(\frac{u_{m,F}}{u_{m,C}} \right)^2 = \frac{f_F}{f_C} \left(\frac{D_{h,C}}{D_{h,F}} \right)^5 \quad (13.134)$$

where the term after the second equality sign is for a circular tube and the mass flow rates under fouled and clean conditions remain the same. Generally $f_F > f_C$ due to the fouled surface being rough. Thus although the effect of fouling on the pressure drop is usually neglected, it can be significant, particularly for compact heat exchangers with gas flows. If we consider $f_F = f_C$ and the reduction in the tube inside diameter due to fouling by only 10 and 20%, the resultant pressure drop increase will be 69 and 205%, respectively, according to Equation 13.134, regardless of whether the fluid is liquid or gas! However, such a significant increase in Δp will have a small effect on fluid pumping power for liquids compared to gases since $\mathcal{P} \propto \Delta p / \rho$ for a given flow rate and liquid density in general is considerably higher than the gas density.

13.8.3 Accounting of Fouling in Heat Exchangers

Fouling is an extremely complex phenomena characterized by a combined heat, mass, and momentum transfer under transient condition. Fouling is affected by a large number of variables related to heat exchanger surfaces, operating conditions, and fluids. Fouling is time (τ) dependent and zero at $\tau=0$. After the induction or delay period τ_d , the fouling resistance is pseudolinear, a falling rate, or asymptotic, as shown by the smooth lines in Figure 13.19, and the actual transient behavior is as represented by the dashed line for one asymptotic behavior.

Fouling is characterized by all or some of the following sequential events: initiation, transport, attachment, removal, and aging (Epstein 1983). Research efforts are concentrated on quantifying these events by semi-theoretical models (Epstein 1978) with a very limited success on specific fouling situations. Hence, the current heat exchanger design approach is to use a constant (supposedly an asymptotic) value of the fouling factor $r_s = 1/h_s$. Equation 13.6 presented earlier includes the fouling resistances on the hot and cold fluid sides for a nontubular extended surface exchanger. Here $1/h_s = r_s$,

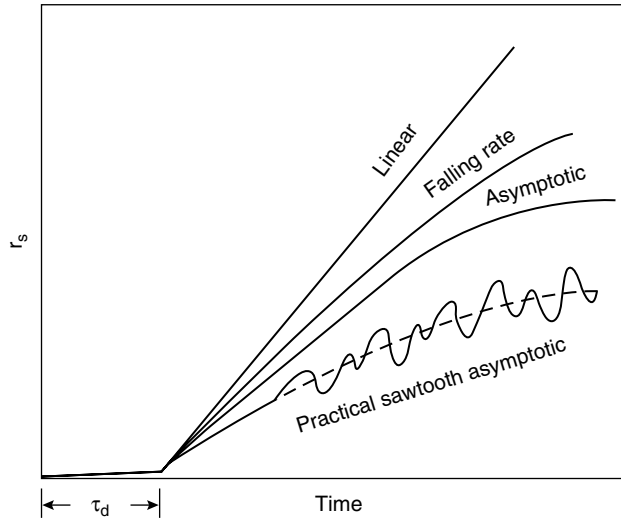


FIGURE 13.19 Characteristic fouling curves.

is generally referred to as the *fouling factor*. Fouling factors for some common fluids are presented in Table 13.12 and Table 13.13.

The specification of fouling effects in a process heat exchanger is usually represented in the following form, wherein the combined fouling factor $r_{s,t}$ is the sum of the fouling factors on the hot and cold fluid sides.

$$\text{Combined fouling factor } r_{s,t} = \frac{1}{U_F} - \frac{1}{U_C} \tag{13.135}$$

$$\text{Cleanliness factor CF} = \frac{U_F}{U_C} = \frac{1}{1 + r_{s,t} U_C} \tag{13.136}$$

$$\text{Percentage oversurface \%OS} = \left(\frac{A_F}{A_C} - 1 \right) 100 \tag{13.137}$$

Here, the subscripts F and C denote fouled and clean exchanger values, respectively. From Equation 13.6 with $A_h = A_c = A$, $\eta_o = 1$, $\Delta T_{m,F} = \Delta T_{m,C}$, it can be shown that

$$\frac{A_F}{A_C} = \frac{U_C}{U_F} = 1 + U_C r_{s,t} \tag{13.138}$$

where $r_{s,t} = r_{s,h} + r_{s,c}$. In heat exchanger design, constant (supposedly and asymptotic) values of $r_{s,h}$ and $r_{s,c}$ are used. Accordingly, extra heat transfer surface area is provided to take into account the deleterious effect of fouling. Thus, the heat exchanger will be “oversized” for the initial clean condition, “correctly sized” for asymptotic fouling (if it occurs in practice), and “undersized” just before the cleaning operation for nonasymptotic fouling.

13.8.4 Influence of Operating and Design Variables

Based on operational experience and research over the last several decades, many variables have been identified that influence fouling significantly. Most important variables are summarized as follows.

TABLE 13.12 Fouling Factors for Various Fluid Streams Used in Heat Exchangers

Fluid	Fouling Factors (m ² K/W)
Water Type	
Seawater (43°C maximum outlet)	0.000275–0.00035
Brackish water (43°C maximum outlet)	0.00035–0.00053
Treated cooling tower water (49°C maximum outlet)	0.000175–0.00035
Artificial spray pond (49°C maximum outlet)	0.000175–0.00035
Closed loop treated water	0.000175
River water	0.00035–0.00053
Engine jacket water	0.000175
Distilled water or closed cycle condensate	0.00009–0.000175
Treated boiler feedwater	0.00009
Boiler blowdown water	0.00035–0.00053
Liquids	
No. 2 fuel oil	0.00035
No. 6 fuel oil	0.0009
Transformer oil	0.000175
Engine lube oil	0.000175
Refrigerants	0.000175
Hydraulic fluid	0.000175
Industrial organic HT fluids	0.000175–0.00035
Ammonia	0.000175
Ammonia (oil bearing)	0.00053
Methanol solutions	0.00035
Ethanol solutions	0.00035
Ethylene glycol solutions	0.00035
MEA and DEA solutions	0.00035
DEG and TEG solutions	0.00035
Stable side draw and bottom products	0.000175–0.00035
Caustic solutions	0.00035
Gas or Vapor	
Steam (non-oil-bearing)	0.0009
Exhaust steam (oil-bearing)	0.00026–0.00035
Refrigerant (oil-bearing)	0.00035
Compressed air	0.000175
Ammonia	0.000175
Carbon dioxide	0.00035
Coal flue gas	0.00175
Natural gas flue gas	0.00090
Acid gas	0.00035–0.00053
Solvent vapor	0.000175
Stable overhead products	0.000175
Natural Gas & Petroleum Streams	
Natural gas	0.000175–0.00035
Overhead products	0.000175–0.00035
Lean oil	0.00035
Rich oil	0.000175–0.00035
Natural gasoline and liquefied petroleum gases	0.000175–0.00035
Oil Refinery Streams	
Crude and vacuum unit gases and vapors	
Atmospheric tower overhead vapors	0.00017
Light naphthas	0.00017
Vacuum overhead vapors	0.00035

(continued)

TABLE 13.12 (Continued)

Fluid	Fouling Factors (m ² K/W)
Crude and Vacuum Liquids	
Crude oil	
Gasoline	0.00035
Naphtha and light distillates	0.00035–0.00053
Kerosene	0.00035–0.00053
Light gas oil	0.00035–0.00053
Heavy gas oil	0.00053–0.0009
Heavy fuel oil	0.00053–0.00123
Vacuum tower bottoms	0.00176
Atmospheric tower bottoms	0.00123
Cracking and Coking Unit Streams	
Overhead vapors	0.00035
Light cycle oil	0.00035–0.00053
Heavy cycle oil	0.00053–0.0007
Light coker gas oil	0.00053–0.0007
Heavy coker gas oil	0.00070–0.0009
Bottoms slurry oil (1.5 m/s minimum)	0.00053
Light liquid products	0.00035
Catalytic Reforming, Hydrocracking, and Hydrodesulfurization Streams	
Reformer charge	0.00026
Reformer effluent	0.00026
Hydrocharger charge and effluent	0.00035
Recycle gas	0.000175
Liquid product over 50°C (API)	0.000175
Liquid product 30–50°C (API)	0.00035
Light Ends Processing Streams	
Overhead vapors and gases	0.000175
Liquid products	0.000175
Absorption oils	0.00035–0.00053
Alkylation trace acid streams	0.00035
Reboiler streams	0.00035–0.00053

Source: From Chenoweth, J. M. Final report, HTRI/TEMA joint committee to review the fouling section of TEMA standards. *Heat Transfer Eng.*, 11 (1), 73–107, 1988.

13.8.4.1 Flow Velocity

Flow velocity is one of the most important variables affecting fouling. Higher velocities increase fluid shear stress at the fouling deposit–fluid interface and increase the heat transfer coefficient, but at the same time increase pressure drop and fluid pumping power, may erode the surface, and may accelerate the corrosion of the surface by removing the protective oxide layer. The fouling build up in general is inversely proportional to flow velocity u . For water, the velocity should be kept above 2 m/s to suppress fouling, and the absolute minimum should be above 1 m/s to minimize fouling.

13.8.4.2 Surface Temperature

Higher surface temperatures promote chemical reaction, corrosion, crystal formation (with inverse solubility salts), and polymerization, but reduce biofouling for temperatures above the optimum growth, avoid potential freezing fouling, and avoid precipitation of normal solubility salts. It is highly recommended that the surface temperature is maintained below the reaction temperature; it should be kept below 60°C for cooling tower water.

TABLE 13.13 Fouling Factors and Design Parameters for Finned Tubes in Fossil-Fuel Exhaust Gases

Type of Flue Gas	Fouling Factor, m ² K/W	Minimum Spacing Between Fins, m	Maximum Gas Velocity to Avoid Erosion, m/s
Clean Gas (cleaning devices not required)			
Natural gas	0.000881–0.000528	0.00127–0.003	30.5–36.6
Propane	0.000176–0.000528	0.00178	
Butane	0.000176–0.000528	0.00178	
Gas turbine	0.000176		
Average Gas (provisions for future installation of cleaning devices)			
No. 2 oil	0.000352–0.000704	0.00305–0.00384	25.9–30.5
Gas turbine	0.000264		
Diesel engine	0.000528		
Dirty Gas (cleaning devices required)			
No. 6 oil	0.000528–0.00123	0.00457–0.00579	18.3–24.4
Crude oil	0.000704–0.00264	0.00508	
Residual oil	0.000881–0.00352	0.00508	
Coal	0.000881–0.00881	0.00587–0.00864	15.2–21.3

Source: From Weierman, R. C. In *Design of Heat Transfer Equipment for Gas-Side Fouling Service, Workshop on an Assessment of Gas-Side Fouling in Fossil Fuel Exhaust Environments*, Marner, W. J., and Webb, R. L., eds., pp. 853–861, 1982. Jet Propulsion Lab., Calif. Inst. of Technology, Pasadena, CA., JPL Publ. 82–67. 1982.

13.8.4.3 Tube Material

The selection of the tube material is important from the corrosion point of view, which in turn could increase crystallization and biological fouling. Copper alloys can reduce certain biofouling, but its use is limited by environmental concerns for river, ocean, and lake waters. Many other variables affect fouling. Discussing them is beyond our scope here, but the reader may refer to TEMA (1999).

13.8.5 Fouling Control and Cleaning Techniques

Control of fouling should be attempted first before any cleaning method is attempted. For gas-side fouling, one should verify that fouling exists, identify the sequential event that dominates the foulant accumulation, and characterize the deposit. For liquid-side fouling, fouling inhibitors/additives should be employed while the exchanger is in operation, such as using antidispersant polymers to prevent sedimentation fouling, “stabilizing” compounds to prevent polymerization and chemical reaction fouling, corrosion inhibitors to prevent corrosion fouling, biocide/germicides to prevent biofouling, and softeners, acids, and polyphosphates to prevent crystallization fouling.

If the foulant control is not effective, the exchanger must be cleaned either on-line or off-line. On-line cleaning includes: flow-driven brushes/sponge balls inside tubes, power-driven rotating brushes inside tubes, acoustic horns/mechanical vibrations for tube banks with gases, sootblowers, and shutting the cold gas supply, flowing hot gas, or reversing the fluids. Off-line cleaning methods without dismantling the exchanger include chemical cleaning (circulate acid/detergent solutions), circulating particulate slurry (such as sand and water), and thermal cleaning to melt frost layers. Off-line cleaning with a heat exchanger opened includes high-pressure steam or water cleaning, thermal baking of an exchanger, and rinsing of small heat exchanger modules removed from the container of modular exchangers.

13.9 Concluding Remarks

Heat exchangers play a critical and dominant role in energy conservation, conversion, recovery, and utilization, and in the economic development of new energy sources as well as in many solutions to

environmental problems. Compact heat exchangers have the major advantages of having high heat fluxes, small volumes and packaging, and total lower cost. With the advancement of manufacturing technologies, many innovative and new designs of compact heat exchangers have emerged in recent years that are capable of withstanding either extreme high pressures or high temperatures, but generally cannot handle heavy fouling due to small flow passages that cannot be cleaned mechanically. Hence, compact heat exchangers are used for relatively clean gas flows, refrigerant flows and some liquid flows in many mass production, and niche applications replacing shell-and-tube and other heat exchangers. In this article, a comprehensive review is made of thermal and hydraulic design aspects of single-phase compact heat exchangers. A good number of references are also provided for further study of many types of heat exchangers. Refer to Shah (2006) for comprehensive review on compact heat exchangers that includes CHEs for fuel cell systems and microturbines as well as other topics not covered here.

13.10 Nomenclature

- A total heat transfer area (primary + fin) on one fluid side of a heat exchanger— A_p , primary surface area; A_f , fin surface area (m^2)
- A_f fin or extended surface area on one fluid side of the exchanger (m^2)
- A_{fr} frontal area on one fluid side of an exchanger (m^2)
- A_k total wall cross-sectional area for heat conduction in fin or for longitudinal conduction in the exchanger (m^2)
- A_0 minimum free flow area on one fluid side of a heat exchanger (m^2)
- A_p primary surface area on one fluid side of an exchanger (m^2)
- A_w total wall area for heat conduction from the hot fluid to the cold fluid, or total wall area for transverse heat conduction (in the matrix wall thickness direction) (m^2)
- Bi Biot number, $Bi = h(\delta_w/2)/k_w$ for the regenerator analysis, dimensionless
- b plate spacing, $h' + \delta_f$ (m)
- C flow stream heat capacity rate with a subscript c or h , $\dot{m}c_p$ ($W/^\circ C$)
- C^* heat capacity rate ratio, C_{min}/C_{max} , dimensionless
- C_r heat capacity rate of a regenerator, $M_w c_w N$ ($W/^\circ C$)
- C_r^* total matrix heat capacity rate ratio, C_r/C_{min} , $C_{r,h}^* = C_{r,h}/C_h$, $= C_{r,c}/C_c$, dimensionless
- c_p specific heat of fluid at constant pressure ($J/kg K$)
- c_w specific heat of wall material ($J/kg K$)
- D_h hydraulic diameter of flow passages, $4A_0/L$ (m)
- d_e fin tip diameter of an individually finned tube (m)
- d_i, d_o tube inside and outside diameters, respectively (m)
- Eu N-row average Euler number, $\Delta p/(\rho u_m^2 N/2g_c)$, $\Delta p/(G^2 N/2g_c \rho)$, dimensionless
- F log-mean temperature difference correction factor, dimensionless
- f Fanning friction factor, $\rho \Delta p g_c D_h / (2LG^2)$, dimensionless
- f_{tb} average Fanning friction factor per tube row for crossflow over a tube bank outside, $\Delta p / (4G^2 N / 2g_c \rho)$, $Eu/4$, dimensionless
- G mass velocity based on the minimum free flow area, \dot{m}/A_0 ($kg/m^2 s$)
- g gravitational acceleration (m^2/s)
- g_c proportionality constant in Newton's Second Law of Motion, $g_c = 1$ and dimensionless in SI units, $g_c = 32.174 \text{ lbf} \cdot \text{ft} / \text{lbf} \cdot \text{s}^2$
- Hg Hagen number, defined by Equation 13.56, dimensionless
- (H) thermal boundary condition referring to constant axial as well as peripheral wall heat flux, also constant peripheral wall temperature; boundary condition valid only for the circular tube, parallel plates, and concentric annular ducts when symmetrically heated
- (H1) thermal boundary condition referring to constant axial wall heat flux with constant peripheral wall temperature

- (H2) thermal boundary condition referring to constant axial wall heat flux with constant peripheral wall heat flux
- h heat transfer coefficient (W/m² K)
- h' height of the offset strip fin (see Figure 13.9) (m)
- h_{fg} specific enthalpy of phase change (see Table 13.9) (J/kg)
- j Colburn factor, $NuPr^{-1/3}/Re, StPr^{2/3}$, dimensionless
- K_c contraction loss coefficient for flow at heat exchanger entrance, dimensionless
- K_e expansion loss coefficient for flow at heat exchanger exit, dimensionless
- k fluid thermal conductivity (W/m K)
- k_f thermal conductivity of the fin material (W/m K)
- k_w thermal conductivity of the matrix (wall) material (W/m K)
- L fluid flow (core or tube) length on one fluid side of an exchanger (m)
- ℓ fin length for heat conduction from primary surface to the midpoint between plates for symmetric heating, see Table 13.4 for other definitions of ℓ (m)
- ℓ_f offset strip fin length or fin height for individually finned tubes, ℓ_f represents the fin length in the fluid flow direction for an uninterrupted fin with $\ell_f=L$ in most cases (m)
- M_w mass of the regenerator (kg)
- m fin parameter, $[2h(1 + \delta_f/\ell_f)/k_f\delta_f]^{1/2} \approx [2h/k_f\delta_f]^{1/2}$ (1/m)
- \dot{m} fluid mass flow rate, $\rho u_m A_o$ (kg/s, 1 bm/h)
- N number of tube rows
- N regenerator rotational speed (rev/s)
- N_f number of fins per meter (1/m)
- N_r number of tube rows in the flow direction
- N_t total number of tubes in an exchanger
- NTU number of heat transfer units, UA/C_{min} , it represents the total number of transfer units in a multipass unit, $NTU_s = UA/C_{shell}$, dimensionless
- Nu Nusselt number, hD_h/k , dimensionless
- ntu_c number of heat transfer units based on the cold fluid side, $(\eta_0 hA)_c/C_c$, dimensionless
- ntu_h number of heat transfer units based on the hot fluid side, $(\eta_0 hA)_h/C_h$, dimensionless
- \dot{m} mass flow rate (kg/s)
- \tilde{P} temperature effectiveness of one fluid, dimensionless
- P wetted perimeter of exchanger passages on one fluid side, $\tilde{P} = A/L$ (m)
- \mathcal{P} fluid pumping power (W)
- Pr fluid Prandtl number, $\mu c_p/k$, dimensionless
- p fluid static pressure (Pa)
- Δp fluid static pressure drop on one fluid side of heat exchanger core (Pa)
- p_f fin pitch (m)
- q exchanger heat transfer rate or heat duty (W)
- q_e heat transfer rate (leakage) at the fin tip (W)
- q' heat flux, q/A (W/m²)
- R heat capacity rate ratio used in the P -NTU method, $R_1 = C_1/C_2, R_2 = C_2/C_1$, dimensionless
- R thermal resistance based on the surface area A , compare Equation 13.5 and Equation 13.6 for definitions of specific thermal resistances, generally with the subscript noted in Eq. (13.5) (K/W)
- Re Reynolds number, GD_h/μ , dimensionless
- Re_d Reynolds number, $\rho u_m d_o/\mu$, dimensionless
- r_h hydraulic radius, $D_h/4, A_o L/A$ (m)
- r_s fouling factor, $1/h_s$ (m² K/W)
- St Stanton number, h/Gc_p , dimensionless
- s distance between adjacent fins, $p_f - \delta_f$ (m)
- T fluid static temperature to a specified arbitrary datum (°C)
- T_s ambient temperature (°C)

- T_o fin base temperature ($^{\circ}\text{C}$)
 T_{λ} fin tip temperature ($^{\circ}\text{C}$)
 U overall heat transfer coefficient ($\text{W}/\text{m}^2 \text{K}$)
 u_m fluid mean axial velocity in the exchanger minimum free flow area on one fluid side (m/s)
 V heat exchanger total volume (m^3)
 X Martinelli parameter defined by Equation 13.89, dimensionless
 X_d diagonal tube pitch (m)
 X_l longitudinal tube pitch (m)
 X_t transverse tube pitch (m)
 X_l^* a ratio of the longitudinal pitch to the tube outside diameter in a circular tube bank, X_l/d_o , dimensionless
 X_t^* a ratio of the transverse pitch to the tube diameter in a circular tube bank, X_t/d_o , dimensionless
 x mass quality (a ratio of mass flow rate of the vapor (or gas) phase divided by the total mass flow rate of two-phase mixture, dimensionless)
 Y Chisholm parameter, defined by Equation 13.89, dimensionless
 z axial coordinate in Section 13.5 (m)
 α void fraction of the vapor phase in Section 13.5, dimensionless
 α ratio of total heat transfer area on one fluid side of an exchanger to the total volume of an exchanger, A/V (m^2/m^3)
 β heat transfer surface area density, a ratio of total transfer area on one fluid side of a plate-fin heat exchanger to the volume between the plates on that fluid side (m^2/m^3)
 ε heat exchanger effectiveness, represents an overall exchanger effectiveness for a multipass unit, dimensionless
 δ wall thickness (m)
 δ_f fin thickness (m)
 η_f fin efficiency, dimensionless
 η_o extended surface efficiency, dimensionless
 η_p pump/fan efficiency, dimensionless
 λ longitudinal wall heat conduction parameter based on the total conduction area, $\lambda = k_w A_{k,t}/C_{\min} L$,
 $\lambda_c = k_w A_{k,c}/C_c L$, $\lambda_h = k_w A_{k,h}/C_h L$, dimensionless
 μ fluid dynamic viscosity (Pa s)
 ρ fluid density (kg/m^3)
 σ ratio of free flow area within the core to frontal area A_o/A_{fr} , dimensionless
 θ, ϕ angular coordinate shown in Figure 13.7 (rad)

13.10.1 Subscripts

- C clean surface value
 c cold fluid side
 con condensation
 F fouled surface value
 f fin
 fr friction
 g gas
 go gas only
 h hot fluid side
 i inlet to the exchanger
 l liquid
 lam laminar
 lo liquid only

loc local

- o outlet to the exchanger or overall
- s scale or fouling, or staggered tubebank

sat saturated

tp two phase

turb turbulent

w wall or properties at the wall temperature

- 1 one section (inlet or outlet) of the exchanger
- 2 other section (outlet or inlet) of the exchanger

References

- Bačić, B. S., Romie, P. E., and Herman, C. Y. 1988. The galerkin method for two-pass crossflow heat exchanger problem. *Chem. Eng. Comm.*, 70 177–198.
- Bajara, R. A. and Jones, E. H. 1976. Flow distribution manifolds. *J. Fluid Eng.-Trans. ASME*, 98 654–666.
- Bhatti, M. S. and Shah, R. K. 1987. Turbulent and transition flow convective heat transfer in ducts. In *Handbook of Single-Phase Convective Heat Transfer*, S. Kakaç, R.K. Shah, and W. Aung, eds., pp. 95–101. Wiley, New York. Chap. 4.
- Bott, T. R. 1995. *Fouling of Heat Exchangers*. Elsevier Science Publishers Ltd., Amsterdam, The Netherlands.
- Bott, T. R., Melo, L. F., Panchal, C. B., and Somerscales, E. F. C. 1999. *Understanding Heat Exchanger Fouling and Its Mitigation*. Begell House, Inc., New York.
- Carey, V. P. 1992. *Liquid-Vapor Phase Change Phenomena*. Taylor & Francis, Bristol, PA.
- Chai, H. C. 1988. A simple pressure drop correlation equation for low finned tube crossflow heat exchangers. *Int. Commun. Heat Mass Transfer*, 15 95–101.
- Chang, Y. J., and Wang, C. C. 1997. A generalized heat transfer correlation for louver fin geometry. *Int. J. heat and Mass Transfer*, Vol. 40, 533–544.
- Chang, Y. J., Hsu, K. C., Lin, Y. T., and Wang, C. C. 2000. A generalized friction correlation for louver fin geometry. *Int. J. Heat Mass Transfer*, Vol. 43, 2237–2243.
- Chenoweth, J. M. 1988. Final report, HTRI/TEMA joint committee to review the fouling section of TEMA standards. *Heat Transfer Eng.*, 11 (1), 73–107.
- Chiou, J. P. 1982. The effect of nonuniformities of inlet temperatures of both fluids on the thermal performance of crossflow heat exchanger. *Heat Transfer 1982. 7th International Heat Transfer Conference*, pp. 179–184.
- Chowdhury, K. and Sarangi, S. 1985. The effect of flow maldistribution on multipassage heat exchanger performance. *Heat Transfer Eng.*, 6 (4), 45–54.
- Churchill, S. W. 1977. Friction-factor equation spans all fluid flow regimes. *Chem. Eng.*, 84 (24), 91–92.
- Cichelli, M. T. and Boucher, D. E. 1956. Design of heat exchanger heads for low holdup. *AIChE Chem. Eng. Prog.*, 52 (5), 213–218.
- Collier, J. G. and Thome, J. R. 1994. *Convective Boiling and Condensation. 3rd Ed.* McGraw-Hill, New York.
- Cowell, T. A., Heikal, M. R., and Achaichia, A. 1995. Flow and heat transfer in compact louvered fin surfaces. *Exp. Therm. Fluid Sci.*, 10 192–199.
- Epstein, N. 1978. Fouling in heat exchangers. In *Heat Transfer 1978, Vol. 6*, pp. 235–254. Hemisphere, New York.
- Epstein, N. 1983. Thinking about heat transfer fouling: a 5 x 5 matrix. *Heat Transfer Eng.*, 4 (1), 43–56.
- Fleming, R. B. 1966. The effect of flow distribution in parallel channels of counterflow heat exchangers. *Adv. Cryogenic Eng.* 352–362.
- Friedel, L. 1979. Improved friction pressure drop correlations for horizontal and vertical two-phase pipe flow. European Two-Phase Flow Group Meeting, Ispra, Italy, Paper E2.
- Gaddis, E. S. and Gnielinski, V. 1985. Pressure drop in cross flow across the tube bundles. *Int. Chem. Eng.*, 25 1–15.

- Ganguli, A. and Yilmaz, S. B. 1987. New heat transfer and pressure drop correlations for crossflow over low-finned tube banks. *AIChE Symp. Ser.*, 83 9–14.
- Ghajar, A. J. and Tam, L. M. 1994. Heat transfer measurements and correlations in the transition region for a circular tube with three different inlet configurations. *Exp. Therm. Fluid Sci.*, 8 79–90.
- Hesselgreaves, J. G. 2001. *Compact Heat Exchangers-Selection Design, and Operation*, Elsevier Science, Ltd., Oxford, UK.
- Hewitt, G. E. 1989. *Hemisphere Handbook of Heat Exchanger Design. Hemisphere Handbook of Heat Exchanger Design*. Hemisphere, New York.
- Hewitt, G. and Müller-Steinhagen, H., 2000. *Heat Exchanger Fouling in the Pre-heat Train of a Crude Oil Distillation Units*. ESDU Data Item 00016, International Ltd., London, U.K.
- Hewitt, G. and Müller-Steinhagen, H. 2003. *Fouling in Cooling Water Systems Using Seawater*. ESDU Data Item 03004, International Ltd., London, U.K.
- Hewitt, G. E., Shires, G. L., and Bott, T. R. 1994. *Process Heat Transfer*. CRC Press, Boca Raton, Florida.
- Huang, L. J. and Shah, R. K. 1992. Assessment of calculation methods for efficiency of straight fins of rectangular profiles. *Int. J. Heat Fluid Fl.*, 13 282–293.
- Idelchik, I. E. 1994. *Handbook of Hydraulic Resistance. 3rd Ed.* CRC Press, Boca Raton, FL.
- Kakaç, S., and Liu, H., 1998, *Heat Exchangers: Selection, Rating and Thermal Design*, CRC Press Boca Raton, FL.
- Kandlikar, S. G. 1991. Development of a flow boiling map for subcooled and saturated flow boiling of different fluids in circular tubes. *ASME J. Heat Transfer*, 113 190–200.
- Kandlikar, S. G. and Steinke, M. E. 2003. Predicting heat transfer during flow boiling in minichannels and microchannels. *ASHRAE Trans.*, 109 (1), 1–9.
- Kandlikar, S. G. and Balasubramanian, P. 2004. An extension of the flow boiling correlation to transition, laminar and deep laminar flows in minichannels and microchannels. *Heat Transfer Eng.*, 25 (3), 86–93.
- Kandlikar, S. G., Shoji, M., and Dhir, V. K. eds. 1999. *Handbook of Phase Change: Boiling and Condensation*, pp. 395–401. Taylor & Francis, New York.
- Kattan, N., Thome, J. R., and Favrat, D. 1998. Flow boiling in horizontal tubes, Part I; Development of diabatic two-phase flow pattern map. *ASME J. Heat Transfer*, 120, 140–147; Part 2; New heat transfer data for five refrigerants. *ASME J. Heat Transfer*, 120, 148–155; Part 3; Development of a new heat transfer model based on flow patterns. *ASME J. Heat Transfer*, 120, 156–165.
- Kays, W. M. and London, A. L. 1998. *Compact Heat Exchangers. Reprint 3rd Ed.* Krieger Publishing, Malabar, Fl.
- Kohler, M. 1974. *The Influence of Flow Path Geometry and Manufacturing Tolerances on Gas Turbine Regenerator Efficiency*, SAE Paper No. 740183.
- Kundu, B. and Das, P. K. 2000. Performance of symmetric polygonal fins with and without tip loss—a comparison of different methods of prediction. *Can. J. Chem. Eng.*, 78 395–401.
- Kutchev, J. A. and Julien, H. L. 1974. The measured influence of flow distribution on regenerator performance, *SAE Trans.*, 83, SAE Paper No. 740164.
- London, A. L. 1970. Laminar flow gas turbine regenerators—the influence of manufacturing tolerances. *ASME J. Eng. Power*, 92A 45–56.
- London, A. L. and Shah, R. K. 1973. Glass-ceramic hexagonal and circular passage surfaces—heat transfer and flow friction design characteristics. *SAE Trans.*, 82 (Sec. 1), 425–434.
- London, A. L., Young, M. B. O., and Stang, J. H. 1970. Glass ceramic surfaces, straight triangular passages—heat transfer and flow friction characteristics. *ASME J. Eng. Power*, 92A 381–389.
- Majumdar, A. K. 1980. Mathematical modeling of flows in dividing and combining flow manifold. *Appl. Math. Model.*, 4 424–432.
- Manglik, R. M. and Bergles, A. E. 1995. Heat transfer and pressure drop correlations for the rectangular offset-strip-fin compact heat exchanger. *Exp. Therm. Fluid Sci.*, 10 171–180.
- Martin, H. 2002. The generalized Lévêque equation and its practical use for the prediction of heat and mass transfer rates from pressure drop. *Chem. Eng. Sci.*, 57 3217–3223.

- Miller, D. S. 1990. *Internal Flow Systems. 2nd Ed. BHRA Fluids Engineering Series., Vol. 5*, British Hydromechanics Research Association, Cranfield, United Kingdom.
- Mueller, A. C. 1974. Criteria for maldistribution in viscous flow coolers. *Heat Transfer* 1974, 5 170–174.
- Mueller, A. C. 1977. An inquiry of selected topics on heat exchanger design. *AIChE Symp. Ser.* 164, 73 273–287.
- Mueller, A. C. and Chiou, J. P. 1987. Review of various types of flow maldistribution in heat exchangers. Book No. H00394, *HTD-Vol. 75*, pp. 3–16. ASME, New York.
- Müller-Steinhagen, H. ed. 2000. *Heat Exchanger Fouling—Mitigation and Cleaning Technologies*, pp. 935–947. Publico Publications, Essen, Germany.
- Ould Didi, M. B., Kattan, N., and Thome, J. R. 2002. Predication of two-phase pressure gradients of refrigerants in horizontal tubes. *Int. J. Refrig.*, 25 935–947.
- Palen, J. W. ed. 1987. *Heat Exchanger Sourcebook*, pp. 1031–1038. Hemisphere Publishing Corp., Washington, DC.
- Panchal, C. B., Bott, T. R., Somerscales, E. F. C., and Toyama, S. 1997. *Fouling Mitigation of Industrial Heat Exchange Equipment*. Begell House, New York.
- Putnam, G. R. and Rohsenow, W. M. 1985. Viscosity induced nonuniform flow in laminar flow heat exchangers. *Int. J. Heat Mass Tran.*, 28 1031–1038.
- Rabas, T. J. and Taborek, J. 1987. Survey of turbulent forced-convection heat transfer and pressure drop characteristics of low-finned tube banks in cross flow. *Heat Transfer Eng.*, 8 (2), 49–62.
- Razelos, P. 1980. *Personal Communication, Department of Applied Science*. City University of New York, Staten Island, NY.
- Reay, D. A. 1979. *Heat Recovery Systems*. E. & EN. Spon, London; UK.
- Roetzel, W. and Spang, B. 1987. Analytisches verfahren zur thermisen berechnung mehrgängiger rohrbündelwreübertrager. *Fortschr-Ber. VDI, Reihe. 19, Nr. 18*.
- Roetzel, W. and Spang, B. 1989. Thermal calculation of multipass shell and tube heat exchangers. *Chem. Eng. Res. Des.*, 67 115–120.
- Rozenman, T. 1976. Heat transfer and pressure drop characteristics of dry cooling tower extended surfaces. Part I: Heat Transfer and Pressure Drop Data, Report BNWL-PFR 7–100; Part II: Data Analysis and Correlation, Report BNWL-PFR 7–102, Battelle Pacific Northwest Laboratories, Richland, WA.
- Saunders, E. A. D. 1988. *Heat Exchangers: Selection, Design & Construction*. Longman Scientific & Technical, Essex, UK.
- Shah, M. M. 1977. A general correlation for heat transfer during subcooled boiling in pipes and annuli. *ASHRAE Trans.*, 83 (1), 205–215; also, Shah, M. M. 1982. Chart correlation for saturated boiling heat transfer: equations and further study. *ASHRAE Trans.*, 88 (1), 185–196.
- Shah, M. M. 1979. A general correlation for heat energy during film condensation inside pipe, *Int. J. Heat Mass Transfer*, Vol. 22, pp. 547–556.
- Shah, R. K. 1981. Compact heat exchangers. In *Heat Exchangers: Thermal-Hydraulic Fundamentals and Design*, Kakaç, S., Bergles, A. E., and Mayinger, E., eds., pp. 111–151. Hemisphere Publishing Corp., Washington, DC.
- Shah, R. K. 1983. Heat exchanger basic design methods. In *Low Reynolds Number Flow Heat Exchangers*, Kakaç, S., Shah R. K., and Bergles, A. E., eds., pp. 21–72. Hemisphere Publishing Corp., Washington, DC.
- Shah, R. K. 1985. Compact heat exchangers. In *Handbook of Heat Transfer Applications, 2nd Ed.*, Rohsenow, W. M., Hartnett, J. P., and Ganić, E. N., eds., Chap. 4, Part 3, pp. 255–266. McGraw-Hill, New York.
- Shah, R. K. 1988. Plate-fin and tube-fin heat exchanger design procedures. In *Heat Transfer Equipment Design*, Shah, R. K., Subbarao, E. C., and Mashelkar, R. A., eds., pp. 255–266. Hemisphere Publishing Corp., Washington, DC.
- Shah, R. K. 1988. Counterflow rotary regenerator thermal design procedures. In *Heat Transfer Equipment Design*, Shah, R. K., Subbarao, E. C., and Mashelkar R. A., eds., pp. 267–296. Hemisphere Publishing Corp., Washington, DC.

- Shah, R. K. 1991a. Industrial heat exchangers—functions and types. In *Industrial Heat Exchangers*, Buchlin, J.-M., ed., von Kármán Institute for Fluid Dynamics, Belgium. Lecture Series No. 1991-04.
- Shah, R. K. 1991b. Multidisciplinary approach to heat exchanger design. In *Industrial Heat Exchangers*, Buchlin, J.-M., ed., von Kármán Institute for Fluid Dynamics, Belgium. Lecture Series No. 1991-04.
- Shah, R. K. 1993. Nonuniform heat transfer coefficients for heat exchanger thermal design. In *Aerospace Heat Exchanger Technology*, Shah, R. K. and Hashemi, A., eds., pp. 417–445. Elsevier Science, Amsterdam, Netherlands.
- Shah, R. K. and Bhatti, M. S. 1987. Laminar convective heat transfer in ducts. In *Handbook of Single-Phase Convective Heat Transfer*, Kakaç, S., Shah, R. K., and Aung, W., eds., pp. 81–122. Wiley, New York, Chap. 3.
- Shah, R. K. and Bhatti, M. S. 1988. Assessment of correlations for single-phase heat exchangers. In *Two-Phase Flow Heat Exchangers: Thermal-Hydraulic Fundamentals and Design*, Kakaç, S., Bergles, A. E., and Fernandes, E. O., eds., pp. 81–122. Kluwer Academic Publishers, Dordrecht, The Netherlands.
- Shah, R. K. and Giovannelli, A. D. 1988. Heat pipe heat exchanger design theory. In *Heat Transfer Equipment Design*, Shah, R. K., Subbarao, E. C., and Mashelkar, R. A., eds., pp. 609–653. Hemisphere Publishing Corp., Washington, DC.
- Shah, R. K. and London, A. L. 1978. *Laminar Flow Forced Convection in Ducts*. Supplement 1 to Advances in Heat Transfer. Academic Press, New York.
- Shah, R. K. and London, A. L. 1980. Effects of nonuniform passages on compact heat exchanger performance. *ASME J. Eng. Power*, 102A, 653–659.
- Shah, R. K. and Mueller, A. C. 1985. Heat exchanger basic thermal design methods. In *Handbook of Heat Transfer and Applications, 2nd Ed.*, Rohsenow, W. M. Hartnett, J. P., and Ganić, E. N., eds., pp. 4-1–4-77. McGraw-Hill, New York. Chap. 4, Part I.
- Shah, R. K. and Muller, A. C. 1988. Heat exchange. In *Ullmann's Encyclopedia of Industrial Chemistry, Unit Operations II, Vol. B3*. VCH Publishers, Weinheim, Germany, Chap. 2.
- Shah, R. K. and Pignotti, A. 1997. The influence of a finite number of baffles on the shell-and-tube heat exchanger performance. *Heat Transfer Eng.*, 18 (1), 82–94.
- Shah, R. K., and Sekulic, D. P. 1998. Heat Exchangers, In *Handbook of Heat Transfer, 3rd Ed.*, Rohsenow, W. M., Hartnett, J. P., and Cho, Y. I., eds., Chap. 17, 169 pages, McGraw-Hill, New York.
- Shah, R. K. and Sekulić, D. P. 2003. *Fundamentals of Heat Exchanger Design*. Wiley, Hoboken, NJ.
- Shah, R. K. and Wanniarachchi, A. S. 1991. Plate heat exchanger design theory. In *Industrial Heat Exchangers*, J. M. Buchlin, ed., pp. 179–216. von Kármán Institute for Fluid Dynamics, Belgium., Lecture Series No. 1991-04.
- Shah, R. K., Zhou, S. Q., and Tagavi, K. 1999. The role of surface tension in film condensation in extended surface passages. *J. Enhanc. Heat Transf.*, 6 179–216.
- Shah, R. K., 2006. Advances in science and Technology of compact heat exchangers, *Heat Transfer Engineering*, Vol. 27, No. 5, pp. 3–22.
- Shen, P. I. 1992. The effect of friction on flow distribution in dividing and combining flow manifolds. *ASME J. Fluids Eng.*, 114 121–123.
- Singh, K. P. and Soler, A. I. 1984. *Mechanical Design of Heat Exchangers and Pressure Vessel Components*. Arcturus Publishers, Cherry Hill, NJ.
- Spang, B., Xuan, Y., and Roetzel, W. 1991. Thermal performance of split-flow heat exchangers. *Int. J. Heat Mass Trans.*, 34 863–874.
- Srinivasan, V. and Shah, R. K. 1995. Fin Efficiency of Extended Surfaces in Two-Phase Flow, Celata, G. P., and Shah, R. K., eds., In *Two Phase Flow Modeling and Experimentation 1995*, Vol. 2, pp. 1107–1118. Edizioni ETS, Pisa, Italy.
- TEMA 1999. *Standards of the Tubular Exchanger Manufacturers Association. 8th Ed.* Tubular Exchanger Manufacturers Association, New York.
- Walker, G. 1990. *Industrial Heat Exchangers-A Basic Guide. 2nd Ed.* Hemisphere, Washington, DC.
- Wang, C. C. 2000. Recent progress on the air-side performance of fin-and-tube heat exchangers. *Int. J. Heat Exchangers*, 1 49–76.

- Wang, C. C. and Chi, K. U. 2000. Heat transfer and friction characteristics of plain fin-and-tube heat exchangers: part 2: correlation. *Int. J. Heat Mass Tran.*, 43 2692–2700.
- Webb, R. L. 1994. *Principles of Enhanced Heat Transfer*. Wiley, New York.
- Weierman, R. C. 1982. In *Design of Heat Transfer Equipment for Gas-Side Fouling Service, Workshop on an Assessment of Gas-side Fouling in Fossil Fuel Exhaust Environments*, Marner, W. J., and Webb, R. L., eds., pp. 853–861. Jet Propulsion Lab., Calif. Inst. of Technology, Pasadena, CA., JPL Publ. 82-67.
- Xuan, Y., Spang, B., and Roetzel, W. 1991. Thermal analysis of shell and tube exchangers with divided-flow pattern. *Int. J. Heat Mass Trans.*, 34 853–861.
- Yokell, S. 1990. *A Working Guide to Shell-and-Tube Heat Exchangers*. McGraw-Hill, New York.
- Zrcher, O., Thome, J. R., and Favrat, D. 1999. Evaporation of ammonia in a smooth horizontal tube: heat transfer measurements and predictions. *ASME J. Heat Transfer*, 121 89–101.
- Zukauskas, A. 1987. Convective heat transfer in cross flow. In *Handbook of Single-Phase Convective Heat Transfer*, Kakaç, S., Shah, R. K., and Aung, W., eds., Wiley, New York, Chap. 6.